# Grid homology for knots and links

Peter S. Ozsváth, András I. Stipsicz and Zoltán Szabó

*To the memory of our fathers,*
*Ozsváth István, Stipsicz István, and Dr. Szabó István*

# Contents

CHAPTER 2

# Knots and links in $S^3$

In this chapter we collect the notions and results from classical knot theory most relevant to our subsequent discussions. In Section 2.1 we provide some basic definitions and describe some families of knots that will serve as guiding examples in the further chapters. We discuss Seifert surfaces in Section 2.2, and we define the Seifert form in Section 2.3. Based on this notion, we define the signature of a knot and use it to bound the unknotting number. We devote Section 2.4 to the definition and basic properties of the Alexander polynomial (returning to its multi-variable generalization in Section 11.5). Extending ideas from Section 2.3, in Section 2.6 we give a proof of the lower bound of the slice genus provided by the signature. Finally, in Section 2.7 we use the Goeritz matrix associated to a diagram to derive a simple formula for the signature of a knot. This material is standard; for a more detailed treatment see [**28, 119, 199**]. Further basic theorems of knot theory are collected in Appendix B.

## 2.1. Knots and links

DEFINITION 2.1.1. An $\ell$–component ***link*** $L$ in $S^3$ is a collection of $\ell$ disjoint smoothly embedded simple closed curves. A 1–component link $K$ is a ***knot***. The links we consider in this book will typically be oriented. If we want to emphasize the choice of an orientation, we write $\vec{L}$ for a link, equipped with its orientation. The links $\vec{L}_1, \vec{L}_2$ are ***equivalent*** if they are ***ambiently isotopic***, that is, there is a smooth map $H\colon S^3 \times [0,1] \to S^3$ such that $H_t = H|_{S^3\times\{t\}}$ is a diffeomorphism for each $t \in [0,1]$, $H_0 = \mathrm{id}_{S^3}$, $H_1(\vec{L}_1) = \vec{L}_2$ and $H_1$ preserves the orientation on the components. An equivalence class of links under this equivalence relation is called a ***link*** (or ***knot***) ***type***.

The above definition can be made with $\mathbb{R}^3 = S^3 \setminus \{p\}$ instead of $S^3$, but the theory is the same: two knots in $\mathbb{R}^3$ are equivalent if and only if they are equivalent when viewed in $S^3$. For this reason, we think of links as embedded in $\mathbb{R}^3$ or $S^3$ interchangeably.

Two $\ell$-component links $\vec{L}_i$ $(i = 0, 1)$ are *isotopic* if the two smooth maps $f_i\colon \cup_{j=1}^{\ell} S^1 \to S^3$ defining the links are isotopic, that is, there is a smooth map $F\colon (\cup_{j=1}^{\ell} S^1)\times [0,1] \to S^3$ which has the property that $F_t = F|_{(\cup_{j=1}^{\ell} S^1)\times\{t\}}$ are $n$-component links with $F_i = f_i$ $(i = 0, 1)$. By the isotopy extension theorem [**87**, Section 8, Theorem 1.6], two links are ambiently isotopic if and only if they are isotopic.

Reflecting $L$ through a plane in $\mathbb{R}^3$ gives the *mirror image* $m(L)$ of $L$. Reversing orientations of all the components of $\vec{L}$ gives $-\vec{L}$.

REMARK 2.1.2. Another way to define equivalence of links is to say that $\vec{L}_1$ and $\vec{L}_2$ are equivalent if there is an orientation-preserving diffeomorphism $f\colon S^3 \to S^3$ so that $f(\vec{L}_1) = \vec{L}_2$. In fact, this gives the same equivalence relation since the group of orientation-preserving diffeomorphisms of $S^3$ is connected [**22**].

REMARK 2.1.3. It is not hard to see that the smoothness condition in the above definition can be replaced by requiring the maps to be $PL$ (piecewise linear). For basic notions of $PL$ topology, see [**202**]. The PL condition provides an equivalent theory of knots and links, cf. [**18**]. (Assuming only continuity would allow wild knots, which we want to avoid.)

The complements of equivalent links are homeomorphic; therefore the fundamental group of the complement, also called the *link group* (or the *knot group* for a knot), is an invariant of the link type. The first homology group of an $\ell$-component link $L = (L_1, \dots, L_\ell)$ is given by

$$H_1(S^3 \setminus L; \mathbb{Z}) \cong \mathbb{Z}^\ell. \tag{2.1}$$

An isomorphism $\phi\colon H_1(S^3 \setminus L; \mathbb{Z}) \to \mathbb{Z}^\ell$ is specified by an orientation and a labeling of the components of $L$: $\phi$ sends the homology class of the positively oriented meridian $\mu_i \in H_1(S^3 \setminus L; \mathbb{Z})$ of the $i^{th}$ component $L_i$ to the vector $(0, \dots, 0, 1, 0, \dots, 0) \in \mathbb{Z}^\ell$ (where 1 occurs at the $i^{th}$ position). For the orientation convention on the meridian, see Figure 2.1. Suppose that $L$ is a link in

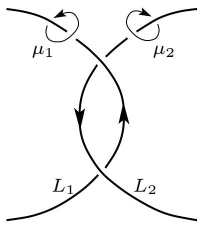


FIGURE 2.1. **Meridians of the components of a link.** The oriented link $\vec{L}$ of the diagram has two components $\vec{L}_1, \vec{L}_2$, with oriented meridians $\mu_1$ and $\mu_2$.

$\mathbb{R}^3$ and $pr_P\colon \mathbb{R}^3 \to P$ is the orthogonal projection to an oriented plane $P \subset \mathbb{R}^3$. For a generic choice of $P$ the projection $pr_P$ restricted to $L$ is an immersion with finitely many double points. At the double points, we illustrate the strand passing under as an interrupted curve segment. If $L$ is oriented, the orientation is specified by placing an arrow on the diagram tangent to each component of $L$. The resulting diagram $\mathcal{D}$ is called a *knot* or *link diagram* of $\vec{L}$. Obviously, a link diagram determines a link type.

The local modifications of a link diagram indicated in Figure 2.2 are the *Reidemeister moves*; there are three types of these moves, denoted $R_1$, $R_2$ and $R_3$. When thinking of oriented link diagrams, the strands in the local picture can be oriented in any way. The figures indicate changes to the diagram within a small disk; the rest of the diagram is left alone. The Reidemeister moves obviously preserve the link type. The importance of the Reidemeister moves is underscored by the following theorem. (For a proof of this fundamental result, see Section B.1.)

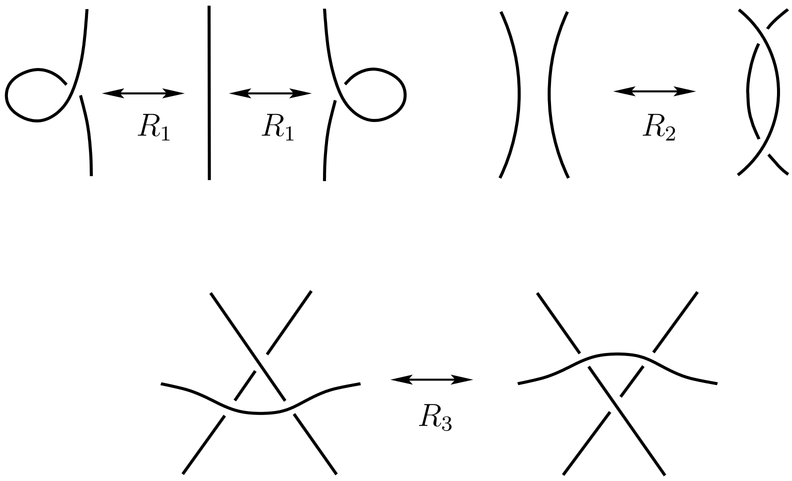


FIGURE 2.2. **The Reidemeister moves $R_1, R_2, R_3$.**

THEOREM 2.1.4 (Reidemeister, [**197**]). *The link diagrams $\mathcal{D}_1$ and $\mathcal{D}_2$ correspond to equivalent links if and only if these diagrams can be transformed into each other by a finite sequence of Reidemeister moves and planar isotopies.* □

The following examples will appear throughout the text.

EXAMPLES 2.1.5.

- Let $p, q > 1$ be relatively prime integers. The $(p, q)$ ***torus knot*** $T_{p,q}$ is defined as the set of points

$$\{(z_1, z_2) \in \mathbb{C}^2 \mid z_1\overline{z}_1 + z_2\overline{z}_2 = 1,\ z_1^p + z_2^q = 0\} \subset S^3. \tag{2.2}$$

This knot can be drawn on a standard, unknotted torus in three-space, so that it meets a longitudinal curve $q$ times (each with local intersection number $+1$) and a meridional curve $p$ times (again, each with local intersection number $+1$). A diagram for $T_{p,q}$ is shown in Figure 2.3. It is easy

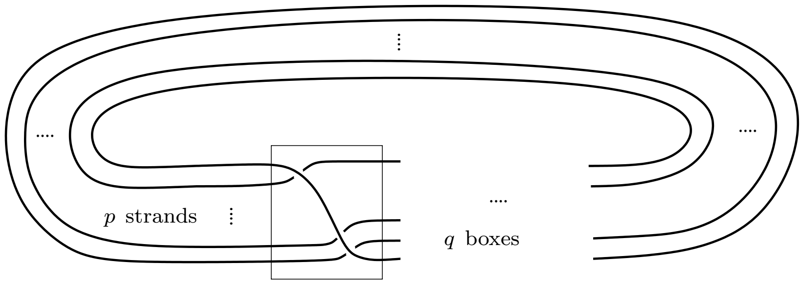


FIGURE 2.3. **Diagram of the torus link $T_{p,q}$.** The result is a knot if $\gcd(p, q) = 1$; in general the torus link has $\gcd(p, q)$ components.

to see that $T_{p,q}$ and $T_{q,p}$ are isotopic knots. The mirror image $m(T_{p,q})$ of $T_{p,q}$ is called the ***negative torus knot*** $T_{-p,q}$. For general choices of $p$ and $q$, the definition of Equation 2.2 produces a link, the ***torus link***

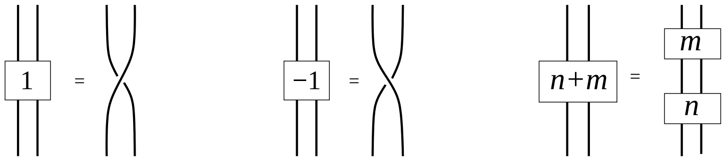


FIGURE 2.4. **Convention for twists.**

$T_{p,q}$, a link with $\gcd(p,q)$ components. $T_{2,3}$ is the ***right-handed trefoil*** knot, and $T_{-2,3}$ is the ***left-handed trefoil*** knot.
- For $a_1,\ldots,a_n \in \mathbb{Z}$ the diagram of Figure 2.5 defines the $(a_1,\ldots,a_n)$ ***pretzel knot*** (or ***pretzel link***) $P(a_1,\ldots a_n)$ on $n$ strands. Informally,

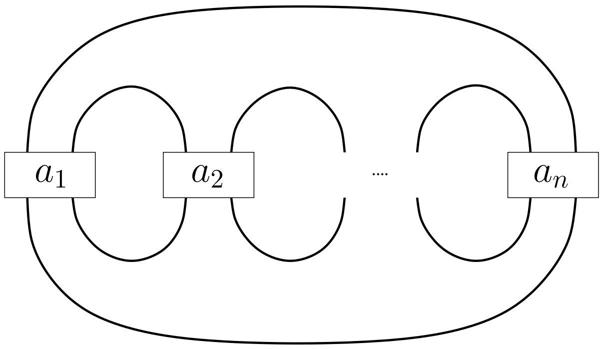


FIGURE 2.5. **Diagram of the pretzel link** $P(a_1,\ldots,a_n)$**.** A box with an integer $a_i$ means $a_i$ right half-twists for $a_i \geq 0$ and $-a_i$ left half-twists for $a_i < 0$, cf. Figure 2.4.

the pretzel link is constructed by taking $2n$ strands $s_1, s_2, \ldots, s_{2n-1}, s_{2n}$, introducing $|a_i|$ half-twists (right half-twists when $a_i \geq 0$ and left half-twists when $a_i < 0$) on the two strands $s_{2i-1}, s_{2i}$ and then closing up the strands as shown in Figure 2.5. (The conventions on the half-twists are indicated in Figure 2.4.)
- For $n \in \mathbb{Z}$ we define the ***twist knot*** $W_n$ by Figure 2.6. Notice that we fix the clasp, and allow the twist in the box to have arbitrary sign and parity. Informally, a twist knot is constructed by considering two strands, adding $|n|$ half-twists (right if $n \geq 0$ and left if $n < 0$) to them and then closing up with the clasp shown by Figure 2.6.
- A diagram of the ***Kinoshita-Terasaka knot*** $KT$ is shown in the left of Figure 2.7; the knot diagram on the right of Figure 2.7 represents the ***Conway knot*** $C$. These two knots are ***mutants*** of each other, that is, if we cut out the dashed disk from the left diagram of Figure 2.7 and glue it back after a $180°$ rotation, we get the Conway knot.

REMARK 2.1.6. If we equip the torus knot $T_{p,q}$ with its two possible orientations, we get isotopic knots. Similarly, the twist knots $W_n$ are isotopic when equipped with the two possible orientations. When $p$ and $q$ are not relatively prime, we define the oriented link $\vec{T}_{p,q}$ by orienting all the parallel strands in Figure 2.3 in the same direction.

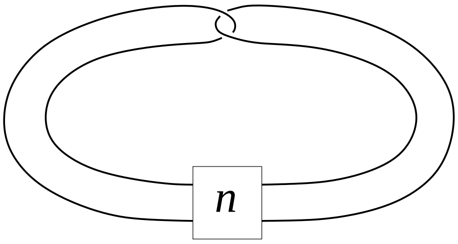


FIGURE 2.6. **Diagram of the twist knot $W_n$.** Clearly, $W_{-1}$ and $W_0$ are both unknots, $W_{-2}$ is the right-handed trefoil knot $T_{2,3}$, and $W_1$ is the left-handed trefoil knot $m(T_{2,3}) = T_{-2,3}$. The knot $W_2$ is also called the *figure-eight knot*.

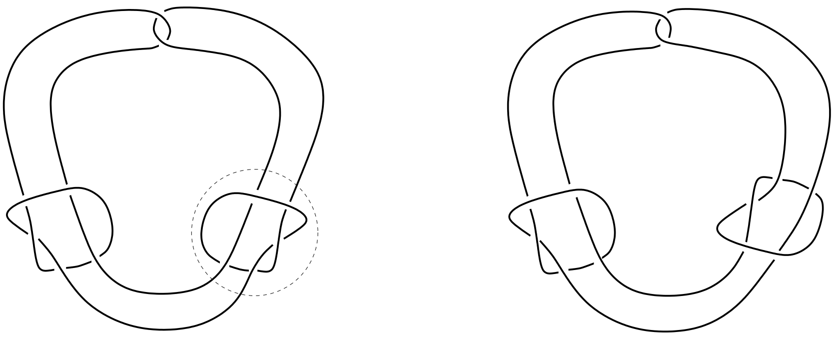

FIGURE 2.7. **The Kinoshita-Terasaka knot $KT$ (on the left) and its Conway mutant, the Conway knot $C$ (on the right).** The two knots are mutants of each other, as the dashed circle on the Kinoshita-Terasaka knot shows.

EXERCISE 2.1.7. **(a)** The above families are not disjoint. Find knots that appear in more than one family.
**(b)** Using the Seifert-Van Kampen theorem [**83**, Theorem 1.20] show that for $(p, q) = 1$, the knot group of the torus knot $T_{p,q}$ is isomorphic to $\langle x, y \mid x^p = y^q \rangle$.
**(c)** Compute the link group of $T_{3,6}$.
**(d)** Verify the claim of Remark 2.1.6 for the right-handed trefoil and for the figure-eight knots.
**(e)** Show that the figure-eight knot $W_2$ and its mirror $m(W_2)$ are isotopic.

The oriented link $\vec{T}_{2,2}$ is also called the *positive Hopf link* $H_+$. Reversing the orientation on one component of $\vec{T}_{2,2}$, we get the *negative Hopf link* $H_-$; see Figure 2.8. A simple three-component link is the *Borromean rings*; see Figure 2.9.

An interesting property of knots and links is related to the existence of a fibration on their complement.

DEFINITION 2.1.8. A link $\vec{L}$ is ***fibered*** if the complement $S^3 \setminus \vec{L}$ admits a fibration $\varphi\colon S^3 \setminus \vec{L} \to S^1$ over the circle with the property that for each $t \in S^1$ the closure $\overline{\varphi^{-1}(t)}$ of the fiber $\varphi^{-1}(t)$ is equal to $\varphi^{-1}(t) \cup \vec{L}$ and is a compact, oriented surface with oriented boundary $\vec{L}$. (For more on fibered knots, see [**18**, Chapter 5].)

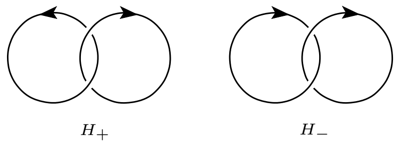


FIGURE 2.8. **The two Hopf links $H_+$ and $H_-$.**

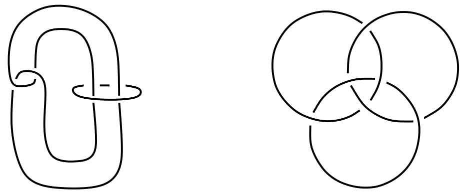

FIGURE 2.9. **The Whitehead link (on the left) and the Borromean rings (on the right).**

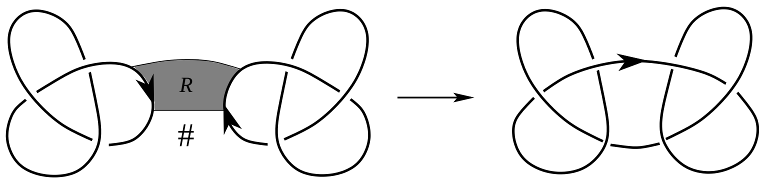


FIGURE 2.10. **The connected sum operation.** The band $R$ is shown by the shaded rectangle.

EXERCISE 2.1.9. Verify that the torus knot $T_{p,q}$ is fibered. (*Hint:* Refer to Example 2.1.5 and consider the map $f/|f|$ for $f(z_1, z_2) = z_1^p + z_2^q$.)

A well-studied and interesting class of knots are defined as follows.

DEFINITION 2.1.10. A link diagram $\mathcal{D}$ is called ***alternating*** if the crossings alternate between over-crossings and under-crossings, as we traverse each component of the link. A link admitting an alternating diagram is called an ***alternating link***.

EXAMPLES 2.1.11. The twist knots $W_n$ are alternating for all $n$. More generally, consider the pretzel links $P(a_1, \ldots, a_n)$ where the signs of the $a_i$ are all the same; these pretzel links are also alternating. The Borromean rings is an alternating link.

Suppose that $\vec{K}_1, \vec{K}_2$ are two oriented knots in $S^3$ that are separated by an embedded sphere. Form the *connected sum* $\vec{K}_1 \# \vec{K}_2$ of $\vec{K}_1$ and $\vec{K}_2$ as follows. First choose an oriented rectangular disk $R$ with boundary $\partial R$ composed of four oriented arcs $\{e_1, e_2, e_3, e_4\}$ such that $\vec{K}_1 \cap R = -e_1 \subset \vec{K}_1$ and $\vec{K}_2 \cap R = -e_3 \subset \vec{K}_2$, and the separating sphere intersects $R$ in a single arc and intersects $e_2$ and $e_4$ in a single point each. Then define $\vec{K}_1 \# \vec{K}_2$ as

$$\vec{K}_1 \# \vec{K}_2 = (\vec{K}_1 \setminus e_1) \cup e_2 \cup e_4 \cup (\vec{K}_2 \setminus e_3).$$

The resulting knot type is independent of the chosen band $R$. For a pictorial presentation of the connected sum of two knots, see Figure 2.10.

The connected sum operation for knots is reminiscent to the product of integers: every knot decomposes (in an essentially unique way) as the connected sum of basic knots (called *prime knots*). For more on prime decompositions see [**119**, Theorem 2.12]. As it turns out, fiberedness of the connected sum is determined by the same property of the components: by a result of Gabai [**64**], the connected sum of two knots is fibered if and only if the two knots are both fibered.

We define now a numerical obstruction to pulling arbitrarily far apart two disjoint, oriented knots $\vec{K}_1$ and $\vec{K}_2$.

DEFINITION 2.1.12. Suppose that $\vec{K}_1, \vec{K}_2 \subset S^3$ are two disjoint, oriented knots. Let $\mathcal{D}$ be a diagram for the oriented link $\vec{K}_1 \cup \vec{K}_2$. The ***linking number*** $\ell k(\vec{K}_1, \vec{K}_2)$ of $\vec{K}_1$ with $\vec{K}_2$ is half the sum of the signs of those crossings (in the sense of Figure 2.11) where one strand comes from $\vec{K}_1$ and the other from $\vec{K}_2$.

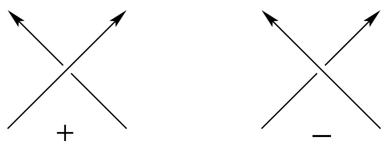


FIGURE 2.11. **Signs of crossings.** The crossing shown on the left is positive, while the one on the right is negative.

PROPOSITION 2.1.13. *The linking number $\ell k(\vec{K}_1, \vec{K}_2)$ has the following properties:*

- *it is independent of the diagram used in its definition;*
- *if $\vec{K}_1$ and $\vec{K}_2$ can be separated by a two-sphere, then $\ell k(\vec{K}_1, \vec{K}_2) = 0$;*
- *it is integral valued;*
- *it is symmetric; i.e. $\ell k(\vec{K}_1, \vec{K}_2) = \ell k(\vec{K}_2, \vec{K}_1)$.*

**Proof.** The fact that $\ell k(\vec{K}_1, \vec{K}_2)$ is independent of the diagram is a straightforward verification using the Reidemeister moves. It follows immediately that if $\vec{K}_1$ and $\vec{K}_2$ can be separated by a two-sphere, then $\ell k(\vec{K}_1, \vec{K}_2) = 0$.

Let $\vec{K}_1'$ be obtained from $\vec{K}_1$ by changing a single crossing with $\vec{K}_2$ (with respect to some fixed diagram $\mathcal{D}$). It is straightforward to see that $\ell k(\vec{K}_1', \vec{K}_2)$ differs from $\ell k(\vec{K}_1, \vec{K}_2)$ by $\pm 1$. Continue to change crossings of $\vec{K}_1$ with $\vec{K}_2$ to obtain a new link $\vec{K}_1'' \cup \vec{K}_2$ (and a diagram of $\vec{K}_1'' \cup \vec{K}_2$) with the property that at any crossings between $\vec{K}_1''$ and $\vec{K}_2$, the strand in $\vec{K}_1''$ is above the strand in $\vec{K}_2$. It follows that the difference between $\ell k(\vec{K}_1'', \vec{K}_2)$ and $\ell k(\vec{K}_1, \vec{K}_2)$ is an integer. Since $\vec{K}_1''$ can be lifted above $\vec{K}_2$, and then separated from it by a two-sphere, $\ell k(\vec{K}_1'', \vec{K}_2) = 0$. We conclude that $\ell k(\vec{K}_1, \vec{K}_2)$ is integral valued. Finally, the definition of linking number is manifestly symmetric in the roles of $\vec{K}_1$ and $\vec{K}_2$. □

The linking number has a straightforward generalization to pairs $\vec{L}_1$ and $\vec{L}_2$ of oriented links. Clearly, the linking number is not the only obstruction to pulling apart the link $\vec{L}_1 \cup \vec{L}_2$. For instance, the two components of the Whitehead link of Figure 2.9 have zero linking number, but cannot be separated by a sphere (cf. Exercise 2.4.12(f)). Similarly, for any two components of the Borromean rings the linking number is zero; but no component can be separated from the other two.

DEFINITION 2.1.14. Let $\mathcal{D}$ be a diagram of the link $\vec{L}$. The ***writhe*** $\mathrm{wr}(\mathcal{D})$ of the diagram $\mathcal{D}$ is defined to be the number of positive crossings in $\mathcal{D}$ minus the number of negative ones. Notice that if $\mathcal{D}$ is the diagram of a knot, then the chosen orientation does not influence the value of the writhe $\mathrm{wr}(\mathcal{D})$.

EXERCISE 2.1.15. **(a)** Consider the homology element $[\vec{K}_2] \in H_1(S^3 \setminus \vec{K}_1; \mathbb{Z}) \cong \mathbb{Z}$ given by $\vec{K}_2 \subset S^3 \setminus \vec{K}_1$. If $\mu_1$ is the homology class of an oriented normal circle of $\vec{K}_1$, then show that $[\vec{K}_2] = \ell k(\vec{K}_1, \vec{K}_2) \cdot \mu_1$.
**(b)** Show that the Reidemeister moves $R_2$ and $R_3$ do not change the writhe of a projection. Determine the change of the writhe under the two versions of $R_1$.
**(c)** Suppose that $\mathcal{D}$ is the diagram of the link $\vec{L} = \vec{L}_1 \cup \vec{L}_2$. Reverse the orientation on all components of $\vec{L}_2$ (while keeping the orientations of the components of $\vec{L}_1$ fixed). Let $\mathcal{D}'$ denote the resulting diagram. Show that

$$\mathrm{wr}(\mathcal{D}) = \mathrm{wr}(\mathcal{D}') + 4\ell k(\vec{L}_1, \vec{L}_2).$$

## 2.2. Seifert surfaces

Knots and links can be studied via the surfaces they bound. More formally:

DEFINITION 2.2.1. A smoothly embedded, compact, connected, oriented surface-with-boundary in $\mathbb{R}^3$ is a ***Seifert surface*** of the oriented link $\vec{L}$ if $\partial\Sigma = L$, and the orientation induced on $\partial\Sigma$ agrees with the orientation specified by $\vec{L}$.

Recall that a connected, compact, orientable surface $\Sigma$ is classified (up to diffeomorphism) by its number of boundary components $b(\Sigma)$, and an additional numerical invariant $g$, called the *genus*; see [**137**, Theorem 11.1]. This quantity can be most conveniently described through the Euler characteristic $\chi(\Sigma)$ of the surface, since

$$\chi(\Sigma) = 2 - 2g(\Sigma) - b(\Sigma).$$

From a given Seifert surface $\Sigma$ of $\vec{L}$ further Seifert surfaces can be obtained by *stabilizing* (or *tubing*) $\Sigma$: connect two distinct points $p, q \in \mathrm{Int}\,\Sigma$ by an arc $\gamma$ in $S^3 \setminus \Sigma$ that approaches $\Sigma$ at $p$ and $q$ from the same side of $\Sigma$. Deleting small disk neighborhoods of $p$ and $q$ from $\Sigma$ and adding an annulus around $\gamma$, we get a new surface, which (by our assumption on $\gamma$ approaching $\Sigma$) inherits a natural orientation from $\Sigma$, and has genus $g(\Sigma) + 1$, cf. Figure 2.12. According to the following result, any two Seifert surfaces of a given link can be transformed into each other by this operation (and isotopy). For a proof of the following result, see [**9**] or Section B.3.

THEOREM 2.2.2 (Reidemeister-Singer, [**213**]). *Any two Seifert surfaces $\Sigma_1$ and $\Sigma_2$ of a fixed oriented link $\vec{L}$ can be stabilized sufficiently many times to obtain Seifert surfaces $\Sigma_1'$ and $\Sigma_2'$ that are ambient isotopic.* □

EXERCISE 2.2.3. **(a)** Show that any knot or link in $S^3$ admits a Seifert surface. (*Hint:* Using the orientation, resolve all crossings in a diagram to get a disjoint

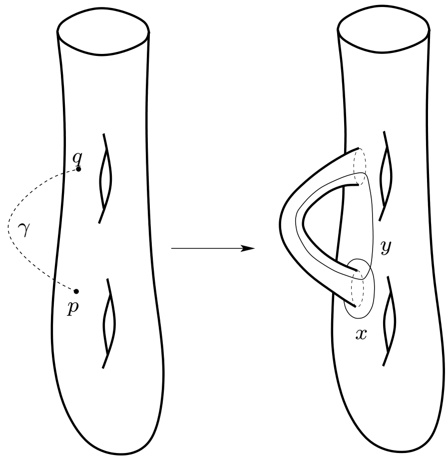


FIGURE 2.12. **Schematic picture of a stabilization of a Seifert surface.** The arc $\gamma$ in the complement of the surface is assumed to approach $\Sigma$ from the same side at $p$ and $q$, so the result of the stabilization admits a natural orientation. Although the diagram shows an unknotted arc, $\gamma$ is allowed to be knotted.

union of oriented circles in the plane, and consider disks bounded by the resulting unknots. Move these disks appropriately to different heights and restore the crossings by adding bands to the disks. Connectedness can be achieved by tubing together various components. For further details, see Section B.3 or [**119**, Chapter 8].)
**(b)** Find a Seifert surface with genus equal to one for $W_n$.
**(c)** Find a Seifert surface with genus equal to one for the 3-stranded pretzel knot $P(a_1, a_2, a_3)$ with $a_i$ odd for $i = 1, 2, 3$.
**(d)** Find a Seifert surface of genus $n$ for the $(2, 2n+1)$ torus knot $T_{2,2n+1}$.

DEFINITION 2.2.4. The ***genus*** (or Seifert genus) $g(\vec{L})$ of a link $\vec{L}$ is the minimal genus of any Seifert surface for $\vec{L}$.

EXERCISE 2.2.5. Show that the unique knot with $g(K) = 0$ is the unknot $\mathcal{O}$.

REMARK 2.2.6. The linking number from Definition 2.1.12 has the following alternative definition using Seifert surfaces: $\ell k(\vec{K}_1, \vec{K}_2)$ is the algebraic intersection number of a Seifert surface for $\vec{K}_1$ with the oriented knot $\vec{K}_2$; see [**199**, Chapter 5].

Unlike the case of knots, the Seifert genus of a link in general depends on the orientations of the various components of $L$.

EXAMPLE 2.2.7. Let $\vec{L}_1$ denote the torus link $\vec{T}_{2,4}$, and let $\vec{L}_2$ be the same link with the orientation reversed on one component. It is easy to see that $\vec{L}_2$ bounds an annulus, hence $g(\vec{L}_2) = 0$, while $g(\vec{L}_1) = 1$.

It is proved in [**119**, Theorem 2.4] that the Seifert genus is additive under connected sum of oriented knots.

## 2.3. Signature and the unknotting number

A Seifert surface $\Sigma$ for an oriented link $\vec{L}$ determines a bilinear form on $H_1(\Sigma;\mathbb{Z})$ as follows. Consider two elements $x, y \in H_1(\Sigma;\mathbb{Z})$ and represent them by oriented, embedded one-manifolds. More precisely, $x$ can be represented by a collection $\gamma_x$ of pairwise disjoint, oriented, simple closed curves, and $y$ can be represented by a similar $\gamma_y$. (Note that $\gamma_x$ and $\gamma_y$ might have non-empty intersection, though.) Let $\gamma_y^+$ denote the push-off of $\gamma_y$ in the positive normal direction of $\Sigma$.

Definition 2.3.1. The ***Seifert form*** $S$ for the Seifert surface $\Sigma$ of the link $\vec{L}$ is defined for $x, y \in H_1(\Sigma;\mathbb{Z})$ by

$$S(x,y) = \ell k(\gamma_x, \gamma_y^+).$$

It is easy to see that the resulting form is independent of the chosen representatives of the homology classes, and it is a bilinear form on $H_1(\Sigma;\mathbb{Z})$. By choosing a basis $\{a_1,\dots,a_n\}$ of $H_1(\Sigma;\mathbb{Z})$ (represented by embedded circles $\alpha_1,\dots,\alpha_n$), the form is represented by a ***Seifert matrix*** $(S_{i,j}) = (\ell k(\alpha_i, \alpha_j^+))$.

The Seifert form gives rise to various invariants of knots and links. In the following we will concentrate on the *signature* and the *Alexander polynomial* (in Section 2.4). The reason for this choice is that these two invariants have analogues in grid homology: the $\tau$-invariant (to be defined in Chapter 6 and further explored in Chapters 7 and 8) shares a number of formal properties with the signature, while the Poincaré polynomial of grid homology can be regarded as a generalization of the Alexander polynomial.

Before proceeding with these definitions, we recall some simple facts from linear algebra. The signature of a symmetric, bilinear form $Q$ on a finite dimensional real vector space $V$ is defined as follows. Let $V^+$ resp. $V^-$ be any maximal positive resp. negative definite subspace of $V$. The dimensions of $V^+$ and $V^-$ are invariants of $Q$, and the signature $\sigma(V)$ of $V$ is given by $\sigma(V) = \dim(V^+) - \dim(V^-)$. We define the signature of a symmetric $n \times n$ matrix $M$ as the signature of the corresponding symmetric bilinear form $Q_M$ on $\mathbb{R}^n$.

Exercise 2.3.2. **(a)** Let $V$ be a vector space equipped with a symmetric, bilinear form $Q$. Let $W \subset V$ be a codimension one subspace. Show that

$$|\sigma(Q|_W) - \sigma(Q)| \leq 1.$$

**(b)** Suppose that $Q$ on $V$ is specified by a symmetric matrix $M$. Let $Q'$ be represented by a matrix $M'$ which differs from $M$ by adding 1 to one of the diagonal entries. Show that $\sigma(Q) \leq \sigma(Q') \leq \sigma(Q) + 2$.

Definition 2.3.3. Suppose that $\Sigma$ is a Seifert surface for the oriented link $\vec{L}$ and $S$ is a Seifert matrix of $\Sigma$. The ***signature*** $\sigma(\vec{L})$ of $\vec{L}$ is defined as the signature of the symmetrized Seifert matrix $S + S^T$. The ***determinant*** $\det(\vec{L})$ of the link $\vec{L}$ is $|\det(S+S^T)|$. The ***unnormalized determinant*** $\mathrm{Det}(\vec{L})$ of $\vec{L}$ is defined as $i^n \cdot \det(S+S^T) = \det(iS + iS^T)$, where $S+S^T$ is an $n \times n$ matrix. Note that if $\vec{L}$ has an odd number of components (hence $n$ is even) then $\mathrm{Det}(\vec{L}) \in \mathbb{Z}$.

We wish to show that $\sigma(\vec{L})$, $\det(\vec{L})$, and $\mathrm{Det}(\vec{L})$ are independent of the chosen Seifert matrix of $\vec{L}$. A key step is the following:

LEMMA 2.3.4. *If $\Sigma$ is a Seifert surface for $\vec{L}$ and $\Sigma'$ is a stabilization of $\Sigma$, then there is a basis for $H_1(\Sigma';\mathbb{Z})$ whose Seifert matrix has the form*

$$\begin{pmatrix} S & \xi & 0 \\ 0 & 0 & 1 \\ 0 & 0 & 0 \end{pmatrix} \quad or \quad \begin{pmatrix} S & 0 & 0 \\ \xi^T & 0 & 0 \\ 0 & 1 & 0 \end{pmatrix}$$

*where $S$ is a Seifert matrix for $\Sigma$ and $\xi$ is some vector.*

**Proof.** Suppose that $\{a_1, \ldots, a_n\}$ is a basis for $H_1(\Sigma;\mathbb{Z})$, giving the Seifert matrix $S$. Adding the two new homology classes $y$ and $x$ of the stabilized surface $\Sigma'$ (as shown by Figure 2.12), we add two columns and two rows to the Seifert matrix. Clearly, $\ell k(a_i, x^+) = \ell k(x, a_i^+) = 0$ for all $i = 1, \ldots, n$, and $\ell k(x, x^+) = 0$. Furthermore, according to which side the stabilizing curve $\gamma$ approaches $\Sigma$, either $\ell k(x, y^+) = 0$ and $\ell k(x^+, y) = 1$ or $\ell k(x, y^+) = 1$ and $\ell k(x^+, y) = 0$ (after replacing $y$ by $-y$, if needed). Now, changing the basis by adding multiples of $x$ if necessary to the $a_i$'s and $y$, we get a Seifert matrix of the desired form. □

THEOREM 2.3.5. *The quantities $\sigma(\vec{L})$, $\det(\vec{L})$ and $\operatorname{Det}(\vec{L})$ are independent of the chosen Seifert matrix of $\vec{L}$ giving invariants of the link $\vec{L}$.*

**Proof.** This follows immediately from Theorem 2.2.2 and Lemma 2.3.4. □

The signature, the determinant, and the unnormalized determinant are constrained by the following identity:

PROPOSITION 2.3.6. *For an oriented link $\vec{L}$,*

$$\operatorname{Det}(\vec{L}) = i^{\sigma(\vec{L})} \det(\vec{L}).$$

**Proof.** If $A$ is a symmetric matrix over $\mathbb{R}$, then it is elementary to verify that $\det(iA) = i^{\operatorname{sgn}(A)}|\det(A)|$, where $\operatorname{sgn}(A)$ denotes the signature of $A$. This is obvious if $A$ is singular. If $A$ is a non-singular $n \times n$ matrix, and $n_+$ and $n_-$ are the dimensions of the maximal positive definite resp. negative definite subspaces of $A$, then $n = n_+ + n_-$ and

$$\det(iA) = i^{n-2n_-}|\det(A)| = i^{n_+-n_-}|\det(A)| = i^{\operatorname{sgn}(A)}|\det(A)|.$$

Applying this to the symmetric matrix $S + S^T$, where $S$ is a Seifert matrix for the link, we get the desired statement. □

EXERCISE 2.3.7. **(a)** Show that for a knot we have $\det(S - S^T) = 1$, and for a link with more than one component $\det(S - S^T) = 0$ holds.
**(b)** Show that the signature of a knot is an even integer, and for the unknot $\mathcal{O}$ we have $\sigma(\mathcal{O}) = 0$. Compute $\det(\mathcal{O})$ using a genus one Seifert surface.
**(c)** Prove that $\sigma(m(K)) = -\sigma(K)$ and $\sigma(-K) = \sigma(K)$.
**(d)** Show that for $n \geq 0$, the signature of $T_{2,2n+1}$ is $-2n$.
**(e)** Compute the signature of the three-stranded pretzel knots $P(a_1, a_2, a_3)$ with $a_1$, $a_2$, and $a_3$ odd.

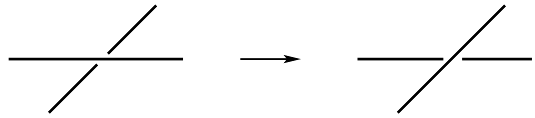

FIGURE 2.13. **A strand passes through another one in unknotting a knot.**


FIGURE 2.14. **Changing the knot at a crossing.**

**(f)** Show that the signature is additive under connected sum, that is, $\sigma(K_1\#K_2) = \sigma(K_1) + \sigma(K_2)$.
**(g)** Suppose that $L$ is a *split link*, that is, $L$ can be written as $L = L_1 \cup L_2$ with $L_i$ non-empty in such a way that there is an embedded sphere $S^2 \subset S^3 \setminus L$ separating $L_1$ and $L_2$. Show that $\det(L) = 0$.
**(h)** Compute $\sigma(T_{3,4})$ and $\sigma(T_{3,7})$. (Cf. Exercise 2.7.9.)

Imagine modifying a knot in the following manner: allow the knot to move around in three-space, so that at one moment, two different strands are allowed to pass through one another transversely. These two knots are said to be related by a *crossing change*. Alternatively, take a suitable diagram of the initial knot, and modify it at exactly one crossing, as indicated in Figure 2.13. Any knot can be turned into the unknot after a finite sequence of such crossing changes. The minimal number of crossing changes required to unknot $K$ is called the *unknotting number* or *Gordian number* $u(K)$ of the knot. Clearly, $u(K) = u(m(K))$.

EXERCISE 2.3.8. **(a)** Suppose that the diagram $\mathcal{D}$ of a knot $K$ has the following property: there is a point $p$ on $\mathcal{D}$ such that starting from $p$ and traversing through the knot, when we reach a crossing for the first time, we traverse on the overcrossing strand. Show that in this case $K$ is the unknot.
**(b)** Verify that for any diagram of a knot $K$ half of the number of crossings provides an upper bound for $u(K)$.
**(c)** Suppose that $\mathcal{D}$ is a diagram of the knot $K$ with $c(\mathcal{D})$ crossings, and it contains an arc $\alpha$ with $c(\alpha)$ overcrossings and no undercrossings. Improving the result of (b) above, show that $u(K) \leq \frac{1}{2}(c(\mathcal{D}) - c(\alpha))$. Using the diagram of Example 2.1.5, show that $u(T_{p,q}) \leq \frac{1}{2}(p-1)(q-1)$.

Computing the unknotting number of a knot is a difficult task. There is no general algorithm to determine $u(K)$, since $u(K)$ is difficult to bound from below effectively. The signature provides a lower bound for $u(K)$, as we shall see below. (See Chapter 6 for an analogous bound using grid homology.)

PROPOSITION 2.3.9. ([**156**, Theorem 6.4.7]) *Let $K_+$ and $K_-$ be two knots before and after a crossing change, as shown in Figure 2.14. Then, the signatures of $K_+$ and $K_-$ are related by the following:*
$$-2 \leq \sigma(K_+) - \sigma(K_-) \leq 0.$$

**Proof.** Consider the oriented resolution $K_0$ of $K_+$ at its distinguished crossing. This is a two-component oriented link, where the crossing is locally removed, in a manner consistent with the orientation on $K_+$ (compare Figure 2.15). Fix a Seifert surface $\Sigma_0$ for $K_0$. Adding a band $B$ to $\Sigma_0$ gives a Seifert surface $\Sigma_+$ for $K_+$, while adding $B$ after introducing an appropriate twist, we get a Seifert surface $\Sigma_-$ for $K_-$. Fix a basis for $H_1(\Sigma_0;\mathbb{Z})$ and extend it to a basis for $H_1(\Sigma_\pm;\mathbb{Z})$ by adding the homology element $\gamma_\pm$, obtained as the union of some fixed path in $\Sigma_0$ and an arc which passes through the band $B$. The two resulting Seifert matrixes differ only at the diagonal entry corresponding to $\gamma_\pm$, which is the linking number $\ell k(\gamma_\pm, (\gamma_\pm)^+)$. When we change the band from the Seifert surface of $K_+$ to the Seifert surface of $K_-$ this linking number increases by one. When relating the symmetrized Seifert matrices of the two surfaces, this fact implies that the signature of the symmetrized Seifert matrix either does not change or it increases by two (cf. Exercise 2.3.2(b)), proving the lemma. □

COROLLARY 2.3.10. *For a knot $K \subset S^3$ we have the inequality $\frac{1}{2}|\sigma(K)| \leq u(K)$.*

**Proof.** This follows immediately from Proposition 2.3.9 and the fact that the unknot $\mathcal{O}$ has vanishing signature. □

EXERCISE 2.3.11. Prove that for $n \geq 0$ the unknotting number of $T_{2,2n+1}$ is $n$.

REMARK 2.3.12. By Proposition 2.3.6, the parity of half the signature is determined by the sign of $\mathrm{Det}(L)$. Knowing this parity alone leads to the following method for determining the signature of an arbitrary knot $K$. Start from an unknotting sequence for $K$, and look at it in reverse order; i.e. starting at the unknot, which has vanishing signature. Observe that at each step in the sequence, $\frac{1}{2}\sigma$ can change by zero or $\pm 1$. The parity of half the signature determines whether or not the change is non-zero, and in that case, Proposition 2.3.9 shows that the change in signature is determined by the type of the crossing change.

Note that, Proposition 2.3.9 gives a bound on $u(K)$ which is slightly stronger than the one stated in Corollary 2.3.10: if the signature of the knot $K$ is positive, then in any unknotting sequence for $K$ at least $\frac{1}{2}\sigma(K)$ moves must change a negative crossing to a positive one. Sometimes this stronger bound is referred to as a *signed unknotting bound*.

## 2.4. The Alexander polynomial

Beyond the signature and the determinant, further knot and link invariants can be derived from the Seifert matrix. Suppose that $\vec{L} \subset S^3$ is a given link in $S^3$ with a Seifert surface $\Sigma$ and a corresponding Seifert matrix $S$. Consider the matrix $t^{-\frac{1}{2}}S - t^{\frac{1}{2}}S^T$ and define the *(symmetrized) Alexander polynomial* $\Delta_{\vec{L}}(t)$ by

$$\Delta_{\vec{L}}(t) = \det(t^{-\frac{1}{2}}S - t^{\frac{1}{2}}S^T). \tag{2.3}$$

Although the Seifert matrix $S$ in the formula depends on certain choices, the above determinant (as the notation suggests) is an invariant of $\vec{L}$:

THEOREM 2.4.1. *The Laurent polynomial* $\Delta_{\vec{L}}(t) \in \mathbb{Z}[t^{\frac{1}{2}}, t^{-\frac{1}{2}}]$ *is independent from the chosen Seifert surface and Seifert matrix of* $\vec{L}$ *and hence is an invariant of the oriented link* $\vec{L}$.

**Proof.** The independence of $\Delta_{\vec{L}}(t)$ from the chosen basis of $H_1(\Sigma;\mathbb{Z})$ is a simple exercise in linear algebra. Indeed, a base change replaces $S$ with $PSP^T$ for a matrix with $\det P = \pm 1$, hence the Alexander polynomial is the same for the two bases. The theorem now follows from Theorem 2.2.2 and Lemma 2.3.4. □

EXAMPLE 2.4.2. The Alexander polynomial of the torus knot $T_{p,q}$ is equal to

$$\Delta_{T_{p,q}}(t) = t^k \frac{(t^{pq}-1)(t-1)}{(t^p-1)(t^q-1)} \tag{2.4}$$

with $k = -\frac{(p-1)(q-1)}{2}$, cf. Exercise 2.4.15.

It follows immediately from the definitions that

$$\mathrm{Det}(\vec{L}) = \Delta_{\vec{L}}(-1),$$

where the value of $\Delta_{\vec{L}}$ at $-1$ is to be interpreted as substituting $-i$ for $t^{\frac{1}{2}}$.

LEMMA 2.4.3. *For a knot* $K$ *the Alexander polynomial* $\Delta_K(t)$ *is a symmetric Laurent polynomial, that is,*

$$\Delta_K(t^{-1}) = \Delta_K(t). \tag{2.5}$$

**Proof.** Let $\Sigma$ be a genus $g$ Seifert surface for $K$. Since $H_1(\Sigma;\mathbb{Z}) \cong \mathbb{Z}^{2g}$, $S$ is a $2g \times 2g$ matrix, hence we have $\Delta_K(t^{-1}) = (-1)^{2g}\det(t^{-\frac{1}{2}}S^T - t^{\frac{1}{2}}S) = \Delta_K(t)$, concluding the proof. □

More generally, if $\vec{L}$ is an oriented link, then $\Delta_{\vec{L}}(t^{-1}) = (-1)^{|L|-1}\Delta_{\vec{L}}(t)$, where $|L|$ denotes the number of components of $L$.

EXERCISE 2.4.4. **(a)** Show that for a knot $K$ the Alexander polynomial is in $\mathbb{Z}[t, t^{-1}]$. Verify the same for any link with an odd number of components.
**(b)** Show that for a knot $K$ the Alexander polynomials of $K$, $-K$, and $m(K)$ are all equal.
**(c)** Show that the Alexander polynomial of the twist knot $W_k$ is given by the formulas

$$\Delta_{W_{2n}}(t) = -nt + (2n+1) - nt^{-1}$$
$$\Delta_{W_{2n-1}}(t) = nt - (2n-1) + nt^{-1}.$$

**(d)** Compute the Alexander polynomial of the $(2, 2n+1)$ torus knot $T_{2,2n+1}$.
**(e)** Let $P$ denote the 3-stranded pretzel knot $P(2b_1+1, 2b_2+1, 2b_3+1)$ with integers $b_i$ $(i = 1, 2, 3)$. Compute the Seifert form corresponding to a Seifert surface of genus equal to one. Show that the Alexander polynomial of $P$ is

$$\Delta_P(t) = Bt + (1-2B) + Bt^{-1},$$

where $B = b_1b_2 + b_1b_3 + b_2b_3 + b_1 + b_2 + b_3 + 1$.

Note that there are infinitely many pretzel knots with Alexander polynomial $\Delta_K(t) \equiv 1$; the smallest non-trivial one is the pretzel knot $P(-3, 5, 7)$.

The following exercise demonstrates that the Alexander polynomial depends on the orientation of a link:

EXERCISE 2.4.5. Consider the $(2, 2n)$ torus link $T_{2,2n}$ for $n \geq 1$. Orient the two strands so that the linking number of the two components is $n$, and compute the Alexander polynomial. Now reverse the orientation on one of the components, and compute the Alexander polynomial of this new oriented link.

Some important properties of the Alexander polynomial $\Delta_K(t)$ for knots are collected in the next result. Since the Alexander polynomial $\Delta_K(t)$ of the knot $K \subset S^3$ is symmetric in $t$, we can write it as

$$\Delta_K(t) = a_0 + \sum_{i=1}^{n} a_i(t^i + t^{-i}). \tag{2.6}$$

We define the *degree* $d(K)$ of $\Delta_K(t)$ as the maximal $d$ for which $a_d \neq 0$.

THEOREM 2.4.6 ([**119, 199**]). *Suppose that the knot $K \subset S^3$ has Alexander polynomial $\Delta_K(t)$ of degree $d(K)$. Then*

*(1) For the Seifert genus $g(K)$ of $K$ we have $g(K) \geq d(K)$.*
*(2) For any two knots $K_1$ and $K_2$, $\Delta_{K_1 \# K_2}(t) = \Delta_{K_1}(t) \cdot \Delta_{K_2}(t)$.*
*(3) For any knot $K$, $\Delta_K(1) = 1$.*

**Proof.** For the first claim, choose a Seifert surface for $K$ with genus $g(K)$, and use its associated Seifert form to compute the Alexander polynomial. The inequality $g(K) \geq d(K)$ follows at once.

The second property is clear by choosing Seifert surfaces $\Sigma_1$ and $\Sigma_2$ for $K_1$ and $K_2$ and taking their boundary connected sum.

Given any two curves $\gamma_1$ and $\gamma_2$ in $\Sigma$, $\ell k(\gamma_1^+, \gamma_2) - \ell k(\gamma_2^+, \gamma_1)$ is the algebraic intersection number of $\gamma_1$ and $\gamma_2$. To prove the third property, choose a basis $\{\alpha_i, \beta_j\}_{i,j=1}^g$ for $H_1(\Sigma)$ so that $\#(\alpha_i \cap \beta_i) = 1$ and all other pairs of curves are disjoint. If $S$ is the Seifert matrix with respect to this basis, then the matrix $S^T - S$ decomposes as blocks of $\begin{pmatrix} 0 & 1 \\ -1 & 0 \end{pmatrix}$; and since this matrix has determinant 1, the claim follows at once. □

An argument using a $\mathbb{Z}$-fold covering of $S^3 \backslash K$ shows that the Alexander polynomial provides an obstruction for a knot being fibered.

THEOREM 2.4.7. ([**199**, page 326]) *If $K$ is fibered, then $g(K) = d(K)$ and $a_{d(K)} = \pm 1$.* □

EXAMPLE 2.4.8. The computation of the Alexander polynomials for twist knots (given in Exercise 2.4.4(c)) together with the above result shows that $W_{2n}$ and $W_{2n-1}$ are not fibered once $|n| > 1$.

An important computational tool for the symmetrized Alexander polynomial $\Delta_{\vec{L}}$ is provided by the *skein relation*.

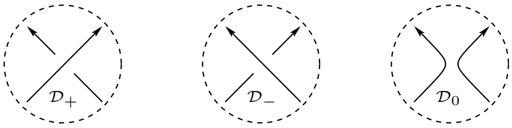


FIGURE 2.15. **Diagrams for the skein relation.** Three diagrams differ only inside the indicated disk.

DEFINITION 2.4.9. Three oriented links $(\vec{L}_+, \vec{L}_-, \vec{L}_0)$ are said to form an ***oriented skein triple*** if they can be specified by diagrams $\mathcal{D}_+$, $\mathcal{D}_-$, $\mathcal{D}_0$ that are identical outside of a small disk, in which they are as illustrated in Figure 2.15. In this case, $\mathcal{D}_0$ is called the *oriented resolution* of $\mathcal{D}_+$ (or $\mathcal{D}_-$) at the distinguished crossing.

THEOREM 2.4.10. *Let $(\vec{L}_+, \vec{L}_-, \vec{L}_0)$ be an oriented skein triple. Then,*

$$\Delta_{\vec{L}_+}(t) - \Delta_{\vec{L}_-}(t) = (t^{\frac{1}{2}} - t^{-\frac{1}{2}})\Delta_{\vec{L}_0}(t). \tag{2.7}$$

**Proof.** Fix a Seifert surface $\Sigma_0$ for $\vec{L}_0$ as in the proof of Proposition 2.3.9, and consider the Seifert surfaces $\Sigma_+$ and $\Sigma_-$ for $\vec{L}_+$ and $\vec{L}_-$ obtained from $\Sigma_0$ by adding the appropriate bands around the crossing. Let $S_0$ denote the Seifert form corresponding to a chosen basis of $H_1(\Sigma_0;\mathbb{Z})$. As in the proof of Proposition 2.3.9, such a basis can be extended to bases of $H_1(\Sigma_\pm;\mathbb{Z})$ by adding one further basis element $\gamma_\pm$ that passes through the band.

When computing the determinants defining the terms in the skein relation (2.7), on the left-hand-side all terms cancel except the ones involving the diagonal entries given by $\ell k(\gamma_\pm, (\gamma_\pm)^+)$ in the Seifert form. In the computation of the determinant, this entry gives rise to a factor $(t^{\frac{1}{2}} - t^{-\frac{1}{2}})$, which is multiplied with the determinant of the corresponding minor. Since that minor is $t^{-\frac{1}{2}}S_0 - t^{\frac{1}{2}}S_0^T$, whose determinant is $\Delta_{\vec{L}_0}(t)$, the statement of the theorem follows at once. $\square$

EXAMPLE 2.4.11. Using the skein relation, it follows immediately that the Alexander polynomial of the Hopf link $H_\pm$ is equal to $\pm(t^{\frac{1}{2}} - t^{-\frac{1}{2}})$. A slightly longer computation shows that the Alexander polynomial $\Delta_B(t)$ of the Borromean rings $B$ is equal to $(t^{\frac{1}{2}} - t^{-\frac{1}{2}})^4$.

EXERCISE 2.4.12. **(a)** Show that for a split link $\vec{L}$ we have $\Delta_{\vec{L}}(t) \equiv 0$.
**(b)** Show that the skein relation, together with the normalization $\Delta_{\mathcal{O}}(t) = 1$ on the unknot $\mathcal{O}$, determines the Alexander polynomial for all oriented links.
**(c)** Using the skein relation, determine the Alexander polynomial of $W_n$ for all $n$. Determine the Seifert genus of $W_n$.
**(d)** Verify that the Kinoshita-Terasaka and the Conway knots both have Alexander polynomial equal to $1$.
**(e)** Given a knot $K$, consider the 2-component link $L$ we get by adding a meridian to $K$. Depending on the orientation of the meridian we get $L(+)$ and $L(-)$ (in the first case the linking number of the two components is $1$, while in the second case it is $-1$). Show that $\Delta_{L(\pm)}(t) = \pm(t^{\frac{1}{2}} - t^{-\frac{1}{2}})\Delta_K$.
**(f)** Determine the Alexander polynomial of the Whitehead link of Figure 2.9.

The Alexander polynomial is an effective tool for studying alternating knots. (Compare the results below with Theorems 2.4.6 and 2.4.7.)

THEOREM 2.4.13 ([**156, 153**]). *Suppose that $K$ is an alternating knot with Alexander polynomial $\Delta_K(t) = a_0 + \sum_{i=1}^{d} a_i(t^i + t^{-i})$ and with degree $d(K)$.*

- *The genus $g(K)$ of the knot $K$ is equal to $d(K)$. In particular, if the Alexander polynomial of $K$ is trivial, then $K$ is the unknot.*
- *For $i = 0, \dots, d(K)-1$ the product $a_i a_{i+1}$ is negative, that is, none of the coefficients (of index between $0$ and $d(K)$) of the Alexander polynomial of $K$ vanish, and these coefficients alternate in sign.*
- *The knot $K$ is fibered if and only if $a_{d(K)} = \pm 1$.* □

EXERCISE 2.4.14. Identify the torus knots that are alternating.

**2.4.1. The Alexander polynomial via Fox calculus.** There is an algebraic way to compute the Alexander polynomial of a link through *Fox's free differential calculus.* For this construction, fix a presentation of the fundamental group of the link complement

$$\pi_1(S^3 \setminus L) = \langle g_1, \dots, g_n \mid r_1, \dots, r_m \rangle.$$

(By possibly adding trivial relations, we can always assume that $m \geq n-1$.) We associate to the presentation its $n \times m$ *Jacobi matrix* $J = (J_{i,j})$ over $\mathbb{Z}[t, t^{-1}]$, which is defined as follows. The presentation gives a surjective homomorphism of groups $F_n \to \pi_1(S^3 \setminus L)$, where $F_n$ denotes the free group generated by the letters $g_1, \dots, g_n$. Consider the induced map $\mathbb{Z}[F_n] \to \mathbb{Z}[\pi_1(S^3 \setminus L)]$ on the group algebras. Composing this map with the abelianization, we get a map $\mathbb{Z}[F_n] \to \mathbb{Z}[H_1(S^3 \setminus L; \mathbb{Z})]$. Recall that the orientation of the link $L$ provides a further map $H_1(S^3 \setminus L; \mathbb{Z}) \to \mathbb{Z}$, sending the oriented meridians of the components to $1$. Hence, after identifying the group algebra $\mathbb{Z}[\mathbb{Z}]$ with $\mathbb{Z}[t, t^{-1}]$, we get a map

$$\phi\colon \mathbb{Z}[F_n] \to \mathbb{Z}[t, t^{-1}]. \tag{2.8}$$

For a word $w \in F_n$ define the *free derivative*

$$\frac{\partial w}{\partial g_j} \in \mathbb{Z}[F_n]$$

by the rules

$$\frac{\partial uv}{\partial x} = \frac{\partial u}{\partial x} + u\frac{\partial v}{\partial x}, \qquad \frac{\partial g_i}{\partial g_i} = 1, \qquad \frac{\partial g_i}{\partial g_j} = 0 \quad (i \neq j).$$

EXERCISE 2.4.15. **(a)** Show that for $n \in \mathbb{N}$ $\frac{\partial x^n}{\partial x} = \frac{x^n - 1}{x-1}$ and $\frac{\partial x^{-n}}{\partial x} = -x^{-1}\frac{x^{-n}-1}{x^{-1}-1}$.
**(b)** Suppose that for $p, q \in \mathbb{N}$ relatively prime integers the group $G$ is presented as $\langle x, y \mid x^p y^{-q} \rangle$. Determine $\frac{\partial (x^p y^{-q})}{\partial x}$ and $\frac{\partial (x^p y^{-q})}{\partial y}$.

Applying the map $\phi$ of Equation (2.8) on the free derivative $\frac{\partial r_i}{\partial g_j}$ we get a polynomial $J_{i,j}$, the $(i,j)$-term of the Jacobi matrix $J$ of the presentation. Consider the ideal $\epsilon_1$ generated by the determinants of the $(n-1) \times (n-1)$-minors of the Jacobian $J$. For the proof of the following theorem, see [**119**, Chapters 6 and 11].

THEOREM 2.4.16. *The ideal $\epsilon_1$ is a principal ideal, and its generator $P(t)$ is $\pm t^{\frac{k}{2}}$ times the Alexander polynomial $\Delta_{\vec{L}}(t)$, for some $k \in \mathbb{Z}$.* □

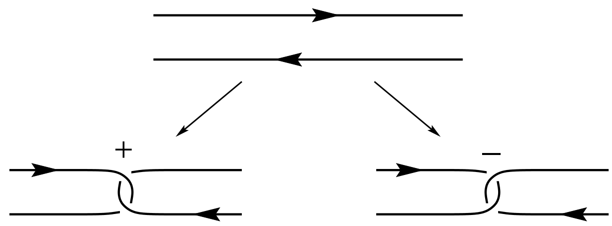


FIGURE 2.16. **By introducing a clasp we construct the Whitehead double of $K$.** Notice that there are two different ways for introducing the clasp, providing a further parameter $\pm$ besides the chosen framing.

EXERCISE 2.4.17. **(a)** Using Fox calculus, verify Equation (2.4), and compute the Alexander polynomial of the $(p,q)$ torus knot. (*Hint:* Recall Exercise 2.1.7(b) and apply Exercise 2.4.15(b)).
**(b)** Using the Alexander polynomial (and the result of Theorem 2.4.6), show that the Seifert genus of the torus knot $T_{p,q}$ is given by $g(T_{p,q}) = \frac{1}{2}(p-1)(q-1)$.
**(c)** Find a presentation of $\pi_1(S^3 \setminus B)$ for the Borromean rings $B$, and compute $\pm\Delta_B(t)$ with the aid of Fox calculus.

## 2.5. Further constructions of knots and links

The normal bundle $\nu(K) \to K$ of a knot $K \subset S^3$ is an oriented $D^2$-bundle over $S^1$, hence it is trivial. A trivialization of this bundle is called a *framing* of $K$. Thought of as a complex line bundle, the normal bundle can be trivialized by a single (nowhere zero) section, hence by a push-off $K'$ of $K$. The linking number $\ell k(K,K')$ of the knot $K$ with the push-off $K'$ determines the framing up to isotopy. With this identification, the push-off along a Seifert surface, providing the *Seifert framing*, corresponds to $0$.

EXERCISE 2.5.1. Suppose that the knot $K$ is given by the diagram $\mathcal{D}$. The diagram provides a framing by pushing off the arcs of $\mathcal{D}$ within the plane. Show that the resulting framing corresponds to the writhe $\mathrm{wr}(\mathcal{D}) \in \mathbb{Z}$.

Knots with interesting properties can be constructed as follows. For a given knot $K$ consider the push-off $K'$ of $K$ corresponding to the framing $k \in \mathbb{Z}$, and orient $K'$ opposite to $K$. Then the resulting two-component link $L_k(K)$ bounds an annulus between $K$ and $K'$, and it is easy to see from the definition that for the given framing $k$, the link will have Alexander polynomial equal to $\Delta_{L_k(K)}(t) = k(t^{-\frac{1}{2}} - t^{\frac{1}{2}})$. (The annulus provides a Seifert surface with corresponding $1 \times 1$ Seifert matrix $(k)$.) In particular, for $k=0$ the resulting link $L_0(K)$ has vanishing Alexander polynomial.

Modify now the link $L_k(K)$ constructed above by replacing the two close parallel segments near a chosen point $p$ with a clasp as shown in Figure 2.16. The resulting knot is called a *Whitehead double* of $K$. Notice that since the clasp can be positive or negative, for each framing $k$ we actually have two doubles, $W_k^+(K)$ and $W_k^-(K)$;

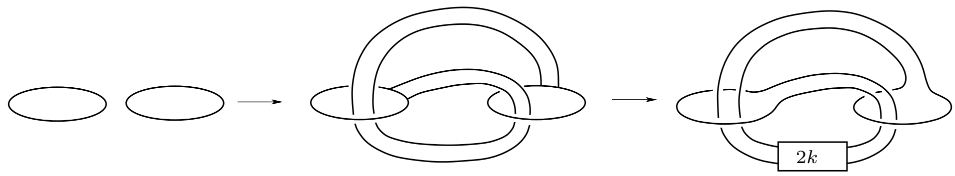


(a) (b) (c)

FIGURE 2.17. **Adding a band.** Start from the two-component unlink of (a) and add the band $B$ (an example shown in (b)) to get the knot $K(B)$. Adding $k$ full twists to $B$ we get the family $K(B,K)$ of knots, shown by (c).

the *$k$-framed positive resp. negative Whitehead double of $K$*. Observe that the $k$-twisted Whitehead double of the unknot is a twist knot; more precisely, $W_k^+(\mathcal{O}) = W_{2k}$ and $W_k^-(\mathcal{O}) = W_{2k-1}$.

LEMMA 2.5.2. *The 0-framed Whitehead doubles $W_0^{\pm}(K)$ for any knot $K$ have Alexander polynomial $\Delta_{W_0^{\pm}(K)}(t) = 1$.*

**Proof.** Use the skein relation at a crossing of the clasp, and note that the oriented resolution has vanishing Alexander polynomial, as shown above, while the knot obtained by a crossing change is the unknot. □

EXERCISE 2.5.3. Compute $\mathrm{Det}(W_0^{\pm}(K))$ and show that $\sigma(W_0^{\pm}(K)) = 0$.

Another class of examples is provided by the two-component unlink, equipped with an embedded band $B$ added to the unlink which turns it into a knot $K(B)$, cf. Figure 2.17. In this construction $B$ can be any band whose interior is disjoint from the unlink, and whose ends are contained in different components of the unlink. A band $B$ gives rise to further bands by adding twists to it: by adding $k$ full twists to $B$, we get $K(B,k)$.

LEMMA 2.5.4. *The Alexander polynomial of $K(B,k)$ is independent of $k$:*

$$\Delta_{K(B,k)}(t) = \Delta_{K(B)}(t).$$

**Proof.** Applying the skein relation to a crossing coming from the twist on the band $B$, the three links in the skein triple are $K(B,k)$, $K(B,k-1)$ and the two-component unlink. Since the two-component unlink has vanishing Alexander polynomial, induction on $k$ verifes the statement of the lemma. □

REMARK 2.5.5. Using other knot invariants, it is not hard to see that $K(B,k)$ for various $k$ can be distinct. For example, if $K(B)$ has non-trivial Jones polynomial (cf. [**119**]), then the Jones polynomials distinguish the $K(B,k)$ for various values of $k$.

For a variation on this theme, consider the *Kanenobu knots* $K(p,q)$ shown in Figure 2.18. These knots are constructed from the two-component unlink by a

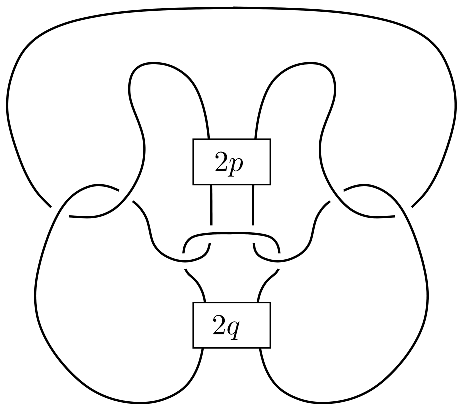


FIGURE 2.18. **The Kanenobu knot** $K(p,q)$**.** The boxes represent $2p$ and $2q$ half twists; that is $p$ and $q$ full twists.

similar procedure as our previous examples $K(B,k)$ in two different ways: we could regard the region with the $p$ full twists as a band added to the two-component unlink (cf. Figure 2.19(a)), or we can do the same with the region of the $q$ full twists, as shown in Figure 2.19(b). It follows that all of them have the same Alexander polynomial.

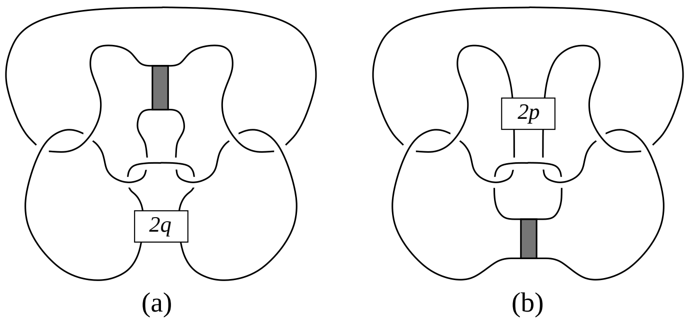


FIGURE 2.19. **Two ribbon representations of** $K(p,q)$**.**

If we allow both parameters to change so that $p+q$ stays fixed, then not only the Alexander polynomials, but also the HOMFLY (and hence the Jones) polynomials and Khovanov (and Khovanov-Rozansky) homologies of the resulting knots stay equal. For these latter computations see [**225**], cf. also [**85**].

REMARK 2.5.6. The definition of the Alexander polynomial through Fox calculus provides further invariants by considering the $k^{th}$ elementary ideals $\epsilon_k$ generated by the determinants of the $(n-k)\times(n-k)$ minors of a Jacobi matrix $J$ for $k>1$. Indeed, the Kanenobu knots (of Figure 2.18) can be distinguished by the Jones polynomial together with the second elementary ideal $\epsilon_2$: for $K(p,q)$ it is generated by the two polynomials $t^2-3t+1$ and $p-q$, hence for fixed $p+q$ this ideal determines $p$ and $q$. For this computation and further related results see [**99**].

EXERCISE 2.5.7. Determine $\Delta_{K(p,q)}(t)$. (*Hint:* Pick $p=q=0$ and identify $K(0,0)$ with the connected sum of two copies of the figure-eight knot.)

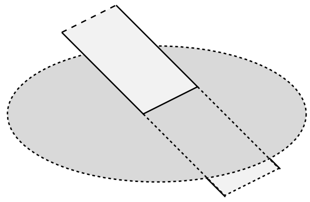

FIGURE 2.20. **Ribbon singularity.**

The construction of the knots $K(B)$ naturally generalizes by considering the $n$-component unlink and adding $(n-1)$ disjoint bands to it in such a way that the result is connected. A knot presented in this way is called a *ribbon knot*.

EXERCISE 2.5.8. Show that $K \subset S^3$ is ribbon if and only if it bounds an immersed disk in $S^3$, where the double points of the immersion, that is, the self-intersections of the disk locally look like the picture of Figure 2.20.

## 2.6. The slice genus

A further basic knot invariant is the *(smooth) slice genus* (or *four-ball genus*) $g_s(K)$ of a knot $K$, defined as follows. An oriented, smoothly embedded surface $(F, \partial F) \subset (D^4, \partial D^4 = S^3)$ with $\partial F = K$ is called a *slice surface* of $K$.

DEFINITION 2.6.1. The integer

$$g_s(K) = \min\{g(F) \mid (F, \partial F) \subset (D^4, S^3) \text{ is a slice surface for } K\}$$

is the ***slice genus*** (or four-ball genus) of the knot $K$. A knot $K$ is a ***slice knot*** if $g_s(K) = 0$, that is, if it admits a slice disk.

The invariant $g_s$ provides a connection between knot theory and 4-dimensional topology; see also Section 8.6. The slice genus is related to the Seifert genus and the unknotting number by the inequalities:

$$g_s(K) \leq g(K), \qquad g_s(K) \leq u(K). \tag{2.9}$$

The first is immediate: just push the interior of a Seifert surface into the interior of $D^4$. For the second, note that a $d$-step unknotting of $K$ (followed by capping off the unknot at the end) can be viewed as an immersed disk in $D^4$ with $d$ double points. Resolving the double points gives a smoothly embedded genus $d$ surface which meets $\partial D^4 = S^3$ at $K$. In more detail, this resolution is done by removing two small disks at each double point of the immersed disk, and replacing them with an embedded annulus. Clearly, for each double point, this operation drops the Euler characteristic by two and hence increases the genus by one. One can find knots $K$ for which the differences $g(K) - g_s(K)$ and $u(K) - g_s(K)$ are arbitrarily large. (See for instance Exercise 2.6.2(b) and Example 8.7.1.)

EXERCISE 2.6.2. **(a)** Show that a ribbon knot is slice. In particular, verify that the knots $K(B, k)$ from Lemma 2.5.4 are slice.
**(b)** Show that for any knot $K$, $K\#m(-K)$ is a slice knot. Show that $K\#m(-K)$ is, indeed, ribbon.

REMARK 2.6.3. There is no known example of a slice knot which is not ribbon. Indeed, the ***slice-ribbon conjecture*** of Fox [**57**] asserts that any slice knot is ribbon. The conjecture has been verified for 2-bridge knots [**124**] and for certain Montesinos knots [**116**], but it is open in general.

A further property, the *Fox-Milnor condition*, of the Alexander polynomial can be used to show that certain knots are not slice.

THEOREM 2.6.4 (Fox-Milnor, [**56, 58**]). *If $K$ is a slice knot, then there is a polynomial $f$ with the property that $\Delta_K(t) = f(t) \cdot f(t^{-1})$.* $\square$

EXERCISE 2.6.5. Compute the slice genus of the figure-eight knot $W_2$ (cf. Figure 2.6) and of the right-handed trefoil knot $T_{2,3}$.

Like the unknotting number $u(K)$, the slice genus $g_s(K)$ is poorly understood; in fact it is unknown even for some small-crossing knots. However, there are some classical lower bounds on the slice genus; we review here one coming from the signature (generalizing Corollary 2.3.10):

THEOREM 2.6.6. *For a knot $K \subset S^3$, $\frac{1}{2}|\sigma(K)| \leq g_s(K)$.*

We return to a proof of Theorem 2.6.6 after some further discussion.

The bound in Theorem 2.6.6 is typically not sharp. For example, as we will see, the slice genus of the $(p,q)$ torus knot $T_{p,q}$ is $\frac{1}{2}(p-1)(q-1)$, while the signature can be significantly smaller. (For a recursive formula for $\sigma(T_{p,q})$ see [**156**].) For example, $\frac{1}{2}\sigma(T_{3,7}) = -4$ (cf. Exercise 2.3.7(h)), while $g_s(T_{3,7}) = u(T_{3,7}) = 6$. Similarly, in Chapter 8 (see Remark 8.6.5) we will show that $g_s(W_0^-(T_{-2,3})) = 1$, while (according to Exercise 2.5.3) it has vanishing signature.

The conclusion of Theorem 2.6.4 holds even when the hypothesis that $K$ is slice is replaced by the following weaker condition:

DEFINITION 2.6.7. A knot $K$ is called ***topologically slice*** if there is a continuous embedding $\phi\colon (D^2 \times D^2, (\partial D^2) \times D^2) \to (D^4, \partial D^4 = S^3)$ such that $\phi(\partial D^2 \times \{0\})$ is $K$.

Note that the "normal" $D^2$-direction (required by the above definition) automatically exists for smooth embeddings of $D^2$ in $D^4$. The topologically slice condition on $K$ is strictly weaker than the (smoothly) slice condition: for example the Whitehead double of any knot (with respect to the Seifert framing) is a topologically slice knot, but in many cases (for example, for the negatively clasped Whitehead double of the left-handed trefoil knot) it is not smoothly slice. The fact that these knots are topologically slice follows from a famous result of Freedman [**59**] (see also [**67**]), showing that any knot whose Alexander polynomial $\Delta_K(t) = 1$ is topologically slice. The fact that $W_0^-(T_{-2,3})$ is not smoothly slice will be demonstrated using the $\tau$ invariant in grid homology, cf. Lemma 8.6.4. In particular, the condition that $\Delta_K = 1$ is not sufficient for a knot to admit a smooth slice disk. Recall that both the Kinoshita-Terasaka knot and the Conway knot have $\Delta_K = 1$. The Kinoshita-Terasaka knot is smoothly slice, while the (smooth) slice genus of the Conway knot is unknown. Note that the distinction between smooth and topological does not appear for the Seifert genus, cf. [**2**].

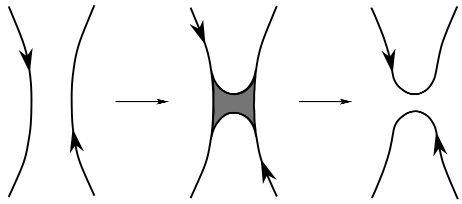

FIGURE 2.21. **A saddle move.** Adding a band to $\vec{L}$ (on the left) we get the link $\vec{L}'$ (on the right), and the two links are related by a saddle move.

EXERCISE 2.6.8. Find a slice disk for the Kinoshita-Terasaka knot.

The rest of this section is devoted to the proof of Theorem 2.6.6. During the course of the proof, we give some preparatory material which will also be used in Chapter 8, where we present an analogous bound coming from grid homology.

We prefer to recast Theorem 2.6.6 in terms of knot cobordisms, defined as follows. Given two oriented links $\vec{L}_0, \vec{L}_1 \subset S^3$, a *cobordism* between them is a smoothly embedded, compact, oriented surface-with-boundary $W \subset S^3 \times [0,1]$ such that $W \cap (S^3 \times \{i\})$ is $\vec{L}_i$ for $i = 0, 1$, and the orientation of $W$ induces the orientation of $\vec{L}_1$ and the negative of the orientation of $\vec{L}_0$ on the two ends.

We will prove the following variant of Theorem 2.6.6. (The proof we describe here is similar to the one given by Murasugi [**154**].)

THEOREM 2.6.9. *Suppose that $W$ is a smooth genus $g$ cobordism between the knots $K_1$ and $K_2$. Then*

$$|\sigma(K_1) - \sigma(K_2)| \leq 2g.$$

Before we provide the details of the proof, we need a definition.

DEFINITION 2.6.10. Given two oriented links $\vec{L}$ and $\vec{L}'$, we say that $\vec{L}$ and $\vec{L}'$ are related by a ***saddle move*** if there is a smoothly embedded, oriented rectangle $R$ with oriented edges $e_1, \dots, e_4$, whose interior is disjoint from $\vec{L}$, with the property that $\vec{L} \cap R = (-e_1) \cup (-e_3)$, and $\vec{L}'$ is obtained by removing $e_1$ and $e_3$ from $\vec{L}$ and attaching $e_2$ and $e_4$ with the given orientations (and smoothing the corners). This relation is clearly symmetric in $\vec{L}$ and $\vec{L}'$, see Figure 2.21. (Notice that the connected sum of two knots is a special case of this operation.) If we have $k$ disjoint rectangles between $\vec{L}$ and $\vec{L}'$ as above, we say that $\vec{L}$ and $\vec{L}'$ are related by $k$ ***simultaneous saddle moves***.

In the course of the verification of the inequality of Theorem 2.6.9, we use the following standard result. (See also Section B.5.) For the statement, we introduce the following notational convention: given a knot $K$ and an integer $n$, let $\mathcal{U}_n(K)$ denote the link obtained by adding $n$ unknotted, unlinked components to $K$.

PROPOSITION 2.6.11 (cf. Section B.5). *Suppose that two knots $K_1$ and $K_2$ can be connected by a smooth, oriented, genus $g$ cobordism $W$. Then, there are knots $K_1'$ and $K_2'$ and integers $b$ and $d$ with the following properties:*

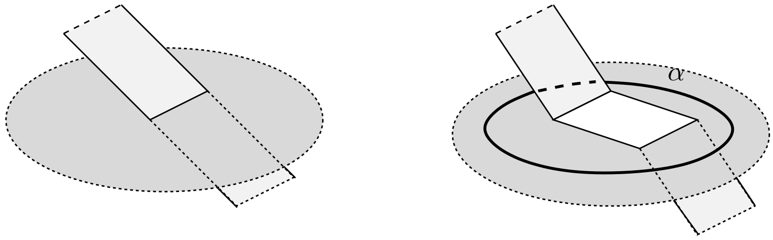


FIGURE 2.22. **Resolution of a ribbon singularity.** By pulling apart the bands slightly, we get a Seifert surface for the knot we got by attaching the bands to $\mathcal{U}_d(K)$. The curve $\alpha$ is indicated in the picture on the right.

*(1)* $\mathcal{U}_b(K_1)$ *can be obtained from* $K_1'$ *by* $b$ *simultaneous saddle moves.*
*(2)* $K_1'$ *and* $K_2'$ *can be connected by a sequence of* $2g$ *saddle moves.*
*(3)* $\mathcal{U}_d(K_2)$ *can be obtained from* $K_2'$ *by* $d$ *simultaneous saddle moves.* □

The proof of this proposition relies on the concept of *normal forms* of cobordisms between knots, as explained in Section B.5.

With Proposition 2.6.11 at our disposal, the proof of Theorem 2.6.9 will easily follow from the two lemmas below:

LEMMA 2.6.12. *If* $\vec{L}$ *and* $\vec{L}'$ *are oriented links that differ by a saddle move, then* $|\sigma(\vec{L}) - \sigma(\vec{L}')| \le 1$.

**Proof.** A Seifert surface for $\vec{L}$ can be obtained from one for $\vec{L}'$ by adding a band to it, cf. the proof of Proposition 2.3.9. Thus, a Seifert matrix for $\vec{L}$ is obtained by adding one row and one column to a Seifert matrix of $\vec{L}'$. This fact immediately implies that the signature can change by at most one (cf. Exercise 2.3.2(a)). □

LEMMA 2.6.13. *Let* $K_1$ *and* $K_2$ *be knots with the property that* $K_2$ *can be obtained from* $\mathcal{U}_d(K_1)$ *by* $d$ *simultaneous saddle moves. Then,* $\sigma(K_1) = \sigma(K_2)$.

**Proof.** Fix a Seifert surface $\Sigma$ for $K_1$ and the spanning disks for the $d$ unknot components in $\mathcal{U}_d(K_1)$. By making the bands sufficiently thin, we can arrange that the intersections of the saddle bands with the spanning disks or $\Sigma$ are ribbon singularities, as shown in Figure 2.20 (or on the left in Figure 2.22). A Seifert surface $\Sigma'$ for $K_2$ can be constructed by pulling the bands slightly apart at the ribbon singularities, as shown on the right in Figure 2.22. Each time we apply this operation, we increase the genus of the surface $\Sigma$ by one, hence we increase the number of rows (and columns) of the Seifert matrix by two. One of the two new homology elements, called $\alpha_p$ at the ribbon singularity $p$, can be visualized on the picture: it encircles the square we opened up. The linking number of $\alpha_p$ with $\alpha_p^+$ vanishes. Furthermore, the linking number of $\alpha_p$ with all homology elements on the Seifert surface $\Sigma$, and with the other $\alpha_q$ also vanish.

The surfaces $\Sigma$ and $\Sigma'$ give Seifert forms $S$ and $S'$. We wish to compare the signatures of the bilinear forms $Q$ and $Q'$ represented by $S + S^T$ and $S' + (S')^T$.

There is a natural embedding $H_1(\Sigma) \hookrightarrow H_1(\Sigma')$, and the restriction of $Q'$ to $H_1(\Sigma)$ is $Q$. Since the determinant of a knot is always non-trivial (cf. Exercise 2.3.7(a)), it follows that $Q$ and $Q'$ are both non-degenerate; so there is a perpendicular splitting (with respect to $Q'$)

$$H_1(\Sigma';\mathbb{R}) \cong H_1(\Sigma;\mathbb{R}) \oplus V.$$

The curves $\alpha_p$ are linearly independent, since surgery along them gives a connected surface. Thus, the $\alpha_p$ span a half-dimensional subspace of $V$, moreover $Q'$ vanishes on their span. Since $Q'$ is non-degenerate on $V$, it follows that the signature of $V$ vanishes; and hence the signature of $Q$ equals the signature of $Q'$. □

**Proof of Theorem 2.6.9.** The theorem is now a direct consequence of Proposition 2.6.11, Lemma 2.6.12 and Lemma 2.6.13. □

It follows that the signature bounds the slice genus:

**Proof of Theorem 2.6.6.** Removing a small ball around some point on a smooth slice surface gives a smooth genus $g$ cobordism from $K$ to the unknot. Applying Theorem 2.6.9 and the fact that the signature of the unknot vanishes, the result follows at once. □

Remark 2.6.14. The above proof of Theorem 2.6.6 rests on the normal form for cobordisms (Proposition 2.6.11), whose hypothesis is that the surface is smoothly embedded. With different methods it can be shown that $\frac{1}{2}|\sigma(K)| \leq g_{top}(K)$, for the *topological slice genus* $g_{top}(K)$, the minimal genus of a locally flat embedded surface in $D^4$ bounding $K$ [**119**, Theorem 8.19]. Consequently, the signature $\sigma(K)$ vanishes for any topologically slice knot, and therefore it cannot be used to distinguish topological and smooth sliceness.

## 2.7. The Goeritz matrix and the signature

We include here a handy formula, due to Gordon and Litherland [**78**], for computing the signature of a link in terms of its diagram. (This material will be needed in Section 10.3, where we compute the grid homology for alternating knots.)

Let $\mathcal{D}$ be a diagram of a link. The diagram admits a chessboard coloring: the components of the complement of the diagram in the plane can be colored black and white in such a manner that domains with the same color do not share sides. Indeed, the diagram $\mathcal{D}$ admits two such colorings; choose the one where the unbounded region is white and call this unbounded region $d_0$. Let the other white regions be denoted by $d_1, \dots, d_n$.

Definition 2.7.1. The black regions can be glued together to form a compact surface, the ***black surface*** $F_b \subset \mathbb{R}^3$ with the given link as its boundary $\partial F_b$: at each crossing glue the domains together with a twisted band to restore the crossing in the diagram.

Exercise 2.7.2. Consider the alternating diagram of the $(2, 2n+1)$ torus knot $T_{2,2n+1}$ given by Figure 2.3. Show that the surface $F_b$ is homeomorphic to the Möbius band, so $F_b$ is not a Seifert surface.

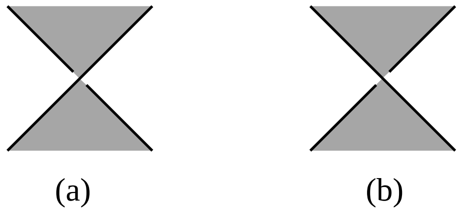


FIGURE 2.23. **The sign $\epsilon = \pm 1$ associated to a crossing in the diagram.** If the crossing is positioned as (a) with respect to the black regions, we associate $+1$ to it, while if the crossing has the shape of (b), then we associate $-1$ to it.

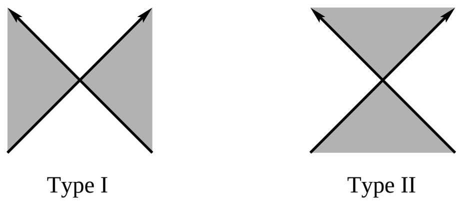


FIGURE 2.24. **Types of crossings in an oriented diagram.**

The chessboard coloring gives rise to a matrix defined as follows. First associate to each crossing $p$ of the diagram $\mathcal{D}$ a sign $\epsilon(p) \in \{\pm 1\}$ shown in Figure 2.23. (Conventions on $\epsilon$ are not uniform in the literature; we are using the one from [**18**].)

DEFINITION 2.7.3. Define the ***unreduced Goeritz matrix*** $G' = (g_{i,j})_{i,j=0}^{n}$ as follows. For $i \neq j$, let

$$g_{i,j} = -\sum_p \epsilon(p),$$

where the sum is taken over all crossings $p$ shared by the white domains $d_i$ and $d_j$; for $i = j$, let

$$g_{i,i} = -\sum_{k \neq i} g_{i,k}.$$

The ***reduced Goeritz matrix*** $G = G(\mathcal{D})$ is obtained from $G'$ by considering the $n$ rows and columns corresponding to $i, j > 0$.

Recall that the link (and hence its projection $\mathcal{D}$) is equipped with an orientation. Classify a crossing $p$ of $\mathcal{D}$ as type I or type II according to whether at $p$ the positive quadrant is white or black; see Figure 2.24. The type of a crossing is insensitive to which of the two strands passes over the other one; but it takes the orientation of the link into account. Define $\mu(\mathcal{D})$ as $\sum \epsilon(p)$, where the summation is for all crossings in $\mathcal{D}$ of type II. The Goeritz matrix (together with the correction term $\mu(\mathcal{D})$ above) can be used to give an explicit formula for computing the signature of a link $\vec{L}$ from a diagram $\mathcal{D}$. This formula is often more convenient than the original definition using the Seifert form of a Seifert surface. (The proof given below follows [**190**].)

THEOREM 2.7.4 (Gordon-Litherland formula, [**78**]). *Suppose that $\mathcal{D}$ is a diagram of a link $\vec{L}$ with reduced Goeritz matrix $G = G(\mathcal{D})$. Let $\sigma(G)$ denote the signature of the symmetric matrix $G$. Then, $\sigma(\vec{L})$ is equal to $\sigma(G) - \mu(\mathcal{D})$.*

In the course of the proof of this theorem we will need the following definition and lemma (the proof of which will be given in Appendix B).

DEFINITION 2.7.5. The diagram $\mathcal{D}$ of a link $\vec{L}$ is ***special*** if it is connected, and the associated black surface $F_b$ (from Definition 2.7.1) is a Seifert surface for $\vec{L}$.

LEMMA 2.7.6 (see Proposition B.3.3). *Any oriented link admits a special diagram.* □

Using the above result, the proof of Theorem 2.7.4 will be done in two steps. First we assume that $\mathcal{D}$ is a special diagram, and check the validity of the formula for the signature in this case. In the second step we show that $\sigma(G) - \mu(\mathcal{D})$ is a link invariant; i.e., it is independent of the chosen projection.

LEMMA 2.7.7. *Suppose that $\mathcal{D}$ is a special diagram of the oriented link $\vec{L}$. Then the signature of the reduced Goeritz matrix $G(\mathcal{D})$ is equal to $\sigma(L)$, and $\mu(\mathcal{D}) = 0$.*

**Proof.** The contour of any bounded white domain provides a circle, hence a one-dimensional homology class in $F_b$. We claim that in this way we construct a basis for $H_1(F_b;\mathbb{R})$. To show linear independence, for each crossing $c$ consider the relative first homology class $p_c$ in $H_1(F_b, \partial F_b;\mathbb{R})$ represented by the arc in $F_b$ that is the pre-image of the crossing. For a crossing adjacent to the unbounded domain the corresponding arc is intersected by a single contour, and working our way towards the inner domains, an inductive argument establishes linear independence.

Let $B$ denote the number of black regions, $W$ the number of white regions, and $C$ the number of crossings. Thinking of the connected projection as giving a cell decomposition of $S^2$, we see that $W + B - C = 2$. By definition we have $\chi(F_b) = B - C$. It follows that the first homology of $F_b$ has dimension $W - 1$; thus the contours give a basis for $H_1(F_b;\mathbb{R})$.

A local computation shows that the reduced Goeritz matrix is equal to $S + S^T$, where $S$ is the Seifert matrix of $F_b$ for the above basis. The definition immediately provides the identity $\sigma(G(\mathcal{D})) = \sigma(\vec{L})$.

If $F_b$ is a Seifert surface for $\vec{L}$, the diagram $\mathcal{D}$ has no type II crossing, hence for a special diagram $\mathcal{D}$ the correction term $\mu(\mathcal{D})$ is equal to zero. □

LEMMA 2.7.8. *Fix an oriented link $\vec{L}$ and consider a diagram $\mathcal{D}$ of it. The difference $\sigma(G) - \mu(\mathcal{D})$ is independent of the chosen diagram $\mathcal{D}$, and is an invariant of $\vec{L}$.*

**Proof.** By the Reidemeister Theorem 2.1.4, the claim follows once we show that $\sigma(G) - \mu(\mathcal{D})$ remains unchanged if we perform a Reidemeister move.

The first Reidemeister move creates one new domain, which in the chessboard coloring is either black or white. If it is black, the new crossing is of type I and the Goeritz matrix remains unchanged, hence the quantity $\sigma(G) - \mu(\mathcal{D})$ remains unchanged, as well. If the new domain is white, then the new crossing $p$ is of type II, hence $\mu$ changes by $\epsilon(p)$. The Goeritz matrix also changes, as follows. Let $d_{new}$ denote the new white domain, and $d_{next}$ the domain sharing a crossing with $d_{new}$. The new Goeritz matrix, written in the basis provided by the domains with the exception of taking $d_{next} + d_{new}$ instead of $d_{next}$, is the direct sum of the Goeritz matrix we had before the move, and the $1 \times 1$ matrix $(\epsilon(p))$. The invariance follows again.

For the second Reidemeister move, we have two cases again, depending on whether the bigon enclosed by the two arcs is black or white in the chessboard coloring. If it is black, then the matrix $G$ does not change, and the two new intersections have the same type, with opposite $\epsilon$-values, hence $\mu$ does not change either. If the new domain is white, then $\mu$ does not change under the move by the same reasoning as before. Now, however, the matrix changes, but (as a simple computation shows) its signature remains the same, verifying the independence.

The invariance under the Reidemeister move $R_3$ needs a somewhat longer case-analysis, corresponding to the various orientations of the three strands involved. Interpret the move as pushing a strand over a crossing $p$, and suppose that a black region disappears and a new white region is created. Inspecting each case, one sees that $\mu$ changes to $\mu - \epsilon(p)$, while $G$ aquires a new row and column, and after an appropriate change of basis this row and column contains only zeros except one term -$\epsilon(p)$ in the diagonal; hence the invariance follows as before. □

After these preparations we are ready to provide the proof of the Gordon-Litherland formula:

**Proof of Theorem 2.7.4.** Consider the given diagram $\mathcal{D}$ and a special diagram $\mathcal{D}'$ for the fixed oriented link $\vec{L}$. By Lemma 2.7.8

$$\sigma(G(\mathcal{D})) - \mu(\mathcal{D}) = \sigma(G(\mathcal{D}')) - \mu(\mathcal{D}'),$$

while for the special diagram $\mathcal{D}'$ (by Lemma 2.7.7) we have $\sigma(G(\mathcal{D}')) = \sigma(\vec{L})$ and $\mu(\mathcal{D}') = 0$, verifying the identity of the theorem. □

EXERCISE 2.7.9. Compute the signature $\sigma(T_{3,3n+1})$ as a function of $n$.

If $\Sigma$ is a Seifert surface for $\vec{L}$, then $-\Sigma$ is a Seifert surface for $-\vec{L}$. Thus, if $S$ is the Seifert matrix for $\vec{L}$, then $S^T$ is the Seifert matrix for $-\vec{L}$. The signature, determinant and the Alexander polynomial of an oriented link therefore remains unchanged if we reverse the orientations of all its components.

If we reverse the orientation of only some components of a link, however, the situation is different. As Exercise 2.4.5(b) shows, the Alexander polynomial changes in general. As it will be explained in Chapter 10, the determinant of the link will stay unchanged under such reversal of orientations.

The signature of a link depends on the orientation of the link, and it changes in a predictable way if we reverse the orientations of some of its components. Later we will need the exact description of this change, which was first established by Murasugi [**155**]. Here we follow the elegant derivation of [**78**], using the Gordon-Litherland formula of Theorem 2.7.4.

COROLLARY 2.7.10. *Let $\vec{L}_1$ and $\vec{L}_2$ be two disjoint, oriented links. Then,*

$$\sigma(\vec{L}_1 \cup \vec{L}_2) = \sigma((-\vec{L}_1) \cup \vec{L}_2) - 2\ell k(\vec{L}_1, \vec{L}_2).$$

**Proof.** Let $\vec{L} = \vec{L}_1 \cup \vec{L}_2$. Fix a diagram $\mathcal{D}$ for the oriented link $\vec{L}_1 \cup \vec{L}_2$, and let $\mathcal{D}'$ be the induced diagram for $(-\vec{L}_1) \cup \vec{L}_2$, obtained by changing the orientations on $L_1$. Since reversing the orientation on some of the components of $\mathcal{D}$ leaves the Goeritz matrix unchanged, the Gordon-Litherland formula gives

$$\sigma(\vec{L}_1 \cup \vec{L}_2) - \sigma((-\vec{L}_1) \cup \vec{L}_2) = \mu(\mathcal{D}') - \mu(\mathcal{D}).$$

The identification

$$\mu(\mathcal{D}') - \mu(\mathcal{D}) = -2\ell k(\vec{L}_1, \vec{L}_2)$$

is now a straightforward matter: at those crossings where both strands belong either to $\vec{L}_1$ or to $\vec{L}_2$ the same quantity appears in $\mu(\mathcal{D}')$ and in $\mu(\mathcal{D})$. At crossings of strands from $\vec{L}_1$ and $\vec{L}_2$ the orientation reversal changes the type, but leaves the quantity $\epsilon(p)$ unchanged. Summing up these contributions (as required in the sum given by $\mu(\mathcal{D}') - \mu(\mathcal{D})$) we get $-2\ell k(\vec{L}_1, \vec{L}_2)$ (cf. Definition 2.1.12), concluding the proof. □

The Gordon-Litherland formula has an interesting consequence for alternating links. To describe this corollary, we introduce the following notion. The *compatible coloring* for an alternating link arranges for each crossing to have the coloring shown in Figure 2.23(b). It is easy to see that a connected alternating diagram always has a unique compatible coloring.

Suppose now that $\mathcal{D}$ is a connected alternating diagram of a link $L$. Let $\mathrm{Neg}(\mathcal{D})$ (and similarly, $\mathrm{Pos}(\mathcal{D})$) denote the number of negative (resp. positive) crossings in $\mathcal{D}$, and let $\mathrm{White}(\mathcal{D})$ (and $\mathrm{Black}(\mathcal{D})$) denote the number of white (resp. black) regions, for the compatible coloring.

COROLLARY 2.7.11. *Let $\vec{L}$ be a link which admits a connected, alternating diagram $\mathcal{D}$. Equip $\mathcal{D}$ with a compatible coloring. Then,*

$$\sigma(\vec{L}) = \mathrm{Neg}(\mathcal{D}) - \mathrm{White}(\mathcal{D}) + 1 \quad \text{and} \quad \sigma(\vec{L}) = \mathrm{Black}(\mathcal{D}) - \mathrm{Pos}(\mathcal{D}) - 1. \tag{2.10}$$

**Proof.** Thinking of the knot projection as giving a cell decomposition of $S^2$, it follows that

$$\mathrm{White}(\mathcal{D}) + \mathrm{Black}(\mathcal{D}) = \mathrm{Pos}(\mathcal{D}) + \mathrm{Neg}(\mathcal{D}) + 2;$$

so it suffices to prove only one of the two formulas in Equation (2.10).

Suppose first that for the compatible coloring of $\mathcal{D}$ we have that the unbounded domain is white. From our coloring conventions on the alternating projection it is clear that $\epsilon(p) = -1$ for all crossings, and furthermore positive crossings are of type I and negative crossings are of type II. Therefore, $\mu(\mathcal{D}) = -\mathrm{Neg}(\mathcal{D})$.

Next we claim that the Goeritz matrix of a compatibly colored, connected, alternating link diagram is negative definite. We see this as follows. By the alternating property it follows that $\epsilon(p) = -1$ for all crossings. Let $m$ denote the number of crossings in the diagram. Consider the negative definite lattice $\mathbb{Z}^m$, equipped with a basis $\{e_p\}_{p=1}^m$ so that $\langle e_p, e_q \rangle = -\delta_{pq}$ (with $\delta_{pq}$ being the Kronecker delta). Think of the basis vectors $e_p$ as being in one-to-one correspondence with the crossings in the projection. Consider next the vector space whose basis vectors correspond to the bounded white regions $\{d_i\}_{i=1}^n$ in the diagram. At each crossing, label one of the white quadrants with $+1$ and the other with $-1$. For $i = 1, \dots, n$ and $p = 1, \dots, m$, let $c_{i,p}$ be zero if the $p^{th}$ crossing does not appear on the boundary of $d_i$ or if it appears twice on the boundary of $d_i$; otherwise, let $c_{i,p}$ be $\pm 1$, depending on the sign of the quadrant at the $p^{th}$ crossing in $d_i$. Consider the linear map sending $d_i$ to $\sum_p c_{i,p} \cdot e_p$. Since $\mathcal{D}$ is connected, this map is injective. (This follows from the inductive argument used in the proof of Lemma 2.7.7.) It is now straightforward to check that this linear map realizes an embedding of the lattice specified by the Goeritz matrix $G(\mathcal{D})$ into the standard, negative definite lattice. It follows at once that the Goeritz matrix is negative definite, as claimed.

The above argument shows that $\sigma(G(\mathcal{D}))$ is equal to $-(\mathrm{White}(\mathcal{D}) - 1)$, and so the Gordon-Litherland formula immediately implies the corollary.

Assume now that the compatible coloring on $\mathcal{D}$ provides a black unbounded domain. Reverse all crossings of $\mathcal{D}$ to get the *mirror diagram* $m(\mathcal{D})$, which represents the mirror link $m(\vec{L})$. Since the reversal also reverses the colors of the domains in the compatible coloring, the unbounded domain of the compatible coloring on $m(\mathcal{D})$ is white. For this diagram the previous argument then shows

$$\sigma(m(\vec{L})) = \mathrm{Neg}(m(\mathcal{D})) - \mathrm{White}(m(\mathcal{D})) + 1.$$

Since $\mathrm{Neg}(m(\mathcal{D})) = \mathrm{Pos}(\mathcal{D})$, $\mathrm{White}(m(\mathcal{D})) = \mathrm{Black}(\mathcal{D})$ and $\sigma(m(\vec{L})) = -\sigma(\vec{L})$, we get

$$\sigma(\vec{L}) = \mathrm{Black}(\mathcal{D}) - \mathrm{Pos}(\mathcal{D}) - 1.$$

□

CHAPTER 3

# Grid diagrams

In this chapter we introduce the concept of a *grid diagram*, giving a convenient combinatorial way to represent knots and links in $S^3$. Grid diagrams will play an essential role in the rest of the book. These diagrams, as a tool for studying knots and links, made their first appearance in the work of Brunn in the late $19^{th}$ century [**17**]. Other variants have been used since then, for example, in *bridge positions* [**127**], or in *arc presentations* of Cromwell and Dynnikov [**27, 37**]. Dynnikov used grid diagrams in his algorithm for recognizing the unknot [**37**]; see also [**12**]. Our presentation rests on Cromwell's theorem which describes the moves connecting different grid presentations of a given link type.

In Section 3.1 we introduce planar grid diagrams and their grid moves. Planar grid diagrams can be naturally transferred to the torus, to obtain *toroidal grid diagrams*, used in the definition of grid homology. Toroidal grid diagrams are discussed in Section 3.2. In Section 3.3 we show how grid diagrams can be used to compute the Alexander polynomial, while in Section 3.4 we introduce a method which provides Seifert surfaces for knots and links in grid position. Finally, in Section 3.5 we describe a presentation of the fundamental group of a link complement that is naturally associated to a grid diagram.

## 3.1. Planar grid diagrams

The present section will concern the following object:

DEFINITION 3.1.1. A ***planar grid diagram*** $\mathbb{G}$ is an $n \times n$ grid on the plane; that is, a square with $n$ rows and $n$ columns of small squares. Furthermore, $n$ of these small squares are marked with an $X$ and $n$ of them are marked with an $O$; and these markings are distributed subject to the following rules:

- (G-1) Each row has a single square marked with an $X$ and a single square marked with an $O$.
- (G-2) Each column has a single square marked with an $X$ and a single square marked with an $O$.
- (G-3) No square is marked with both an $X$ and an $O$.

The number $n$ is called the ***grid number*** of $\mathbb{G}$.

We denote the set of squares marked with an $X$ by $\mathbb{X}$ and the set of squares marked with an $O$ by $\mathbb{O}$. Sometimes, we will find it convenient to label the $O$-markings $\{O_i\}_{i=1}^n$. A grid diagram can be described by two permutations $\sigma_{\mathbb{O}}$ and $\sigma_{\mathbb{X}}$. If there is an $O$-marking in the intersection of the $i^{th}$ column and the $j^{th}$ row, then

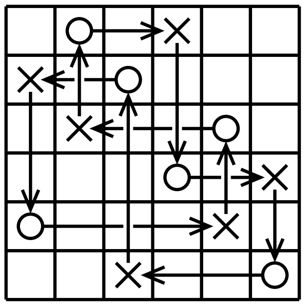

FIGURE 3.1. **The knot associated to the pictured grid diagram, with orientation and crossing conventions.** The diagram can be described by the two permutations $\sigma_{\mathbb{O}}$ and $\sigma_{\mathbb{X}}$, specifying the locations of the $O$'s and $X$'s. Above, the two permutations are $\sigma_{\mathbb{O}} = (2,6,5,3,4,1)$ and $\sigma_{\mathbb{X}} = (5,4,1,6,2,3)$.

the permutation $\sigma_{\mathbb{O}}$ maps $i$ to $j$. We will indicate this permutation as an $n$-tuple, $(\sigma_{\mathbb{O}}(1), \dots, \sigma_{\mathbb{O}}(n))$. (By convention, we regard the left-most column and the bottom-most row as first.) The permutation $\sigma_{\mathbb{X}}$ is defined analogously, using the $X$-markings in place of the $O$-markings.

In this section, we will use the terms "planar grid diagram" and simply "grid diagram" interchangeably. Care must be taken once we introduce the notion of a "toroidal grid diagram", later in the chapter.

**3.1.1. Specifying links via planar grid diagrams.** A grid diagram $\mathbb{G}$ specifies an oriented link $\vec{L}$ via the following procedure. Draw oriented segments connecting the $X$-marked squares to the $O$-marked squares in each column; then draw oriented segments connecting the $O$-marked squares to the $X$-marked squares in each row, with the convention that the vertical segments always cross above the horizontal ones. See Figure 3.1 for an example. In this case, we say that $\mathbb{G}$ is a *grid diagram for* $\vec{L}$.

REMARK 3.1.2. The permutation $\sigma_{\mathbb{X}} \cdot \sigma_{\mathbb{O}}^{-1}$ can be decomposed as a product of $\ell$ disjoint cycles for some $\ell$. This number is equal to the number of components of the link specified by the grid diagram.

LEMMA 3.1.3. *Every oriented link in $S^3$ can be represented by a grid diagram.*

**Proof.** Approximate the link $\vec{L}$ by a PL-embedding with the property that the projection admits only horizontal and vertical segments. At a crossing for which the horizontal segment is an over-crossing, apply the modification indicated in Figure 3.2. Finally, move the link into general position, so that different horizontal (or vertical) segments are not collinear. Mark the turns by $X$'s and $O$'s, chosen so that vertical segments point from $X$ to $O$, while horizontal segments point from $O$ to $X$. The result is a grid diagram representing $\vec{L}$. $\square$

EXAMPLES 3.1.4. **(a)** Given $p, q > 1$, define a $(p+q)\times(p+q)$ grid $\mathbb{G}(p,q)$ by $\sigma_{\mathbb{O}} = (p+q, p+q-1, \dots, 2, 1)$ and $\sigma_{\mathbb{X}} = (p, p-1, \dots, 1, p+q, p+q-1, \dots, p+2, p+1)$. For

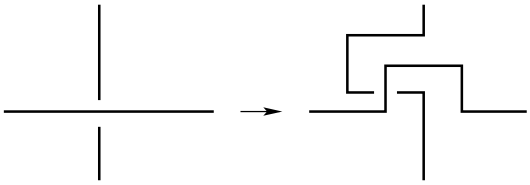

FIGURE 3.2. **The local modification for correcting crossings.**

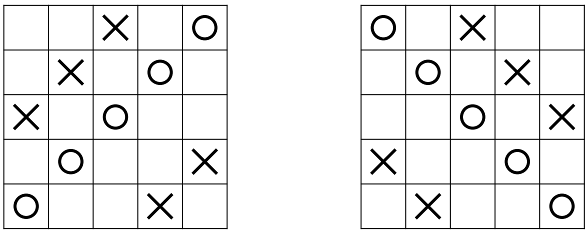

FIGURE 3.3. **Grid diagrams for the trefoils.** The left-handed trefoil $T_{-2,3}$ is on the left; the right-handed trefoil $T_{2,3}$ is on the right.

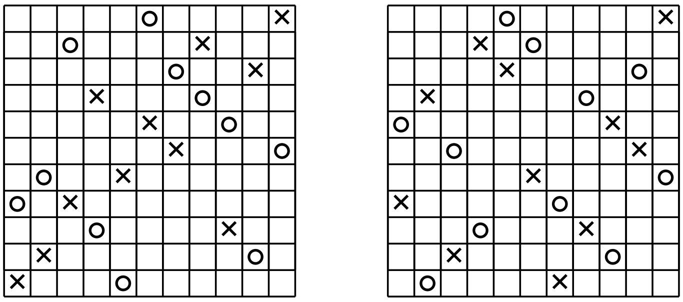

FIGURE 3.4. **Grid diagrams for the Conway knot (left) and the Kinoshita-Terasaka knot (right).**

$\mathbb{G}(2,3)$ see the right picture in Figure 3.3. When $(p,q)=1$, $\mathbb{G}(p,q)$ represents the torus knot $T_{p,q}$, cf. Exercise 3.1.5(a). More generally, $\mathbb{G}(p,q)$ represents the torus link $T_{p,q}$. **(b)** Figure 3.4 provides grid presentations of the Kinoshita-Terasaka and Conway knots. **(c)** The diagram of Figure 3.5 is a grid diagram for the Borromean rings.

EXERCISE 3.1.5. **(a)** Show that when $(p,q)=1$, $\mathbb{G}(p,q)$ represents the $(p,q)$ torus knot $T_{p,q}$.
**(b)** Find a grid presentation of the twist knot $W_n$ from Example 2.1.5. (*Hint*: For the special case $n=3$ consult Figure 3.6. Notice that both diagrams present the same knot, which is $5_2$ in the knot tables.)
**(c)** Consider the permutations $\sigma_{\mathbb{X}}=(p+1,p+2,\ldots,p+q,1,\ldots,p)$ and $\sigma_{\mathbb{O}}=(1,2,\ldots,p+q)$. Show that the resulting $(p+q)\times(p+q)$ grid diagram represents $T_{-p,q}$, the mirror of the torus knot $T_{p,q}$.

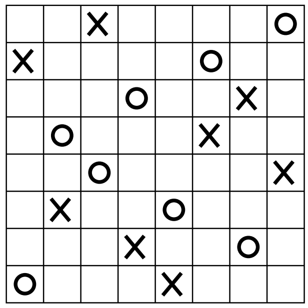

FIGURE 3.5. **Grid diagram for the Borromean rings.**

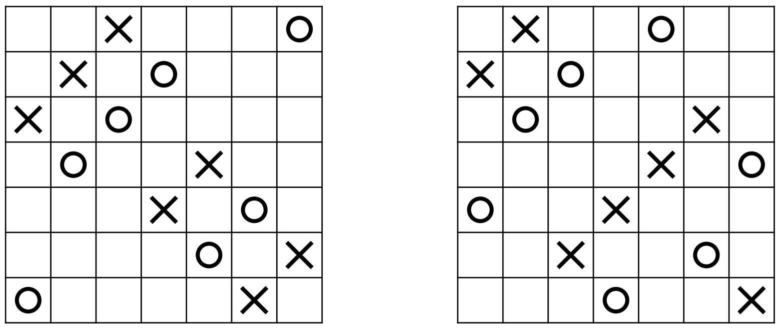

FIGURE 3.6. **Two grid diagrams of the $5_2$ knot, isotopic to the twist knot $W_3$.**

**(d)** Show that by reversing the roles of $\mathbb{X}$ and $\mathbb{O}$, the resulting diagram represents the same link with the opposite orientation.
**(e)** Similarly, by reflecting a given grid $\mathbb{G}$ across the diagonal, the resulting grid $\mathbb{G}'$ represents the same link as $\mathbb{G}$, but with the opposite orientation.
**(f)** Suppose that the grid $\mathbb{G}$ represents the knot $K$. Reflect $\mathbb{G}$ through the horizontal symmetry axis of the grid square and show that the resulting grid diagram $\mathbb{G}^*$ represents $m(K)$, the mirror image of $K$.
**(g)** Find diagrams for the Hopf links $H_\pm$.

**3.1.2. Grid moves.** Following Cromwell [**27**] (compare also Dynnikov [**37**]), we define two moves on planar grid diagrams.

DEFINITION 3.1.6. Each column in a grid diagram determines a closed interval of real numbers that connects the height of its $O$-marking with the height of its $X$-marking. Consider a pair of consecutive columns in a grid diagram $\mathbb{G}$. Suppose that the two intervals associated to the consecutive columns are either disjoint, or one is contained in the interior of the other. Interchanging these two columns gives rise to a new grid diagram $\mathbb{G}'$. We say that the two grid diagrams $\mathbb{G}$ and $\mathbb{G}'$ differ by a ***column commutation***. A ***row commutation*** is defined analogously, using rows in place of columns. A column or a row commutation is called a ***commutation move***, cf. Figure 3.7.

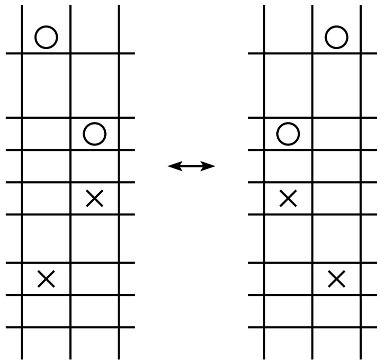

FIGURE 3.7. **The commutation move of two consecutive columns in a grid diagram.** Rotation by $90^\circ$ gives an example of a row commutation.

The second move on grid diagrams will change the grid number.

DEFINITION 3.1.7. Suppose that $\mathbb{G}$ is an $n \times n$ grid diagram. A grid diagram $\mathbb{G}'$ is called a ***stabilization*** of $\mathbb{G}$ if it is an $(n+1) \times (n+1)$ grid diagram obtained by splitting a row and column in $\mathbb{G}$ in two, as follows. Choose some marked square in $\mathbb{G}$, and erase the marking in that square, in the other marked square in its row, and in the other marked square in its column. Now, split the row and column in two (i.e. add a new horizontal and a new vertical line). There are four ways to insert markings in the two new columns and rows in the $(n+1) \times (n+1)$ grid to obtain a grid diagram; see Figure 3.8 in the case where the initial square in $\mathbb{G}$ was marked with an $X$. Let $\mathbb{G}'$ be any of these four new grid diagrams. The inverse of a stabilization is called a ***destabilization***.

We will find it useful to classify the various types of stabilizations in a grid diagram. To this end, observe that for any stabilization, the original marked square gets subdivided into four squares, arranged in a $2 \times 2$ block. Exactly three of these new squares will be marked. The type of a stabilization is encoded by a letter $X$ or an $O$, according to the marking on the original square chosen for stabilization (or equivalently, which letter appears twice in the newly-introduced $2 \times 2$ block), and by the position of the square in the $2 \times 2$ block which remains empty, which we indicate by a direction: *northwest* $NW$, *southwest* $SW$, *southeast* $SE$, or *northeast* $NE$. It is easy to see that a stabilization changes the projection either by a planar isotopy or by a Reidemeister move $R_1$. For example, in the diagrams of Figure 3.8 the stabilizations *X:NW*, *X:NE*, *X:SE* give isotopies while *X:SW* corresponds to the Reidemeister move $R_1$.

DEFINITION 3.1.8. We call commutations, stabilizations, and destabilizations ***grid moves*** collectively.

Grid diagrams are an effective tool for constructing knot invariants, thanks to the following theorem of Cromwell [**27**], see also [**37**] and Section B.4:

THEOREM 3.1.9 (Cromwell [**27**]). *Two planar grid diagrams represent equivalent links if and only if there is a finite sequence of grid moves that transform one into the other.* $\square$

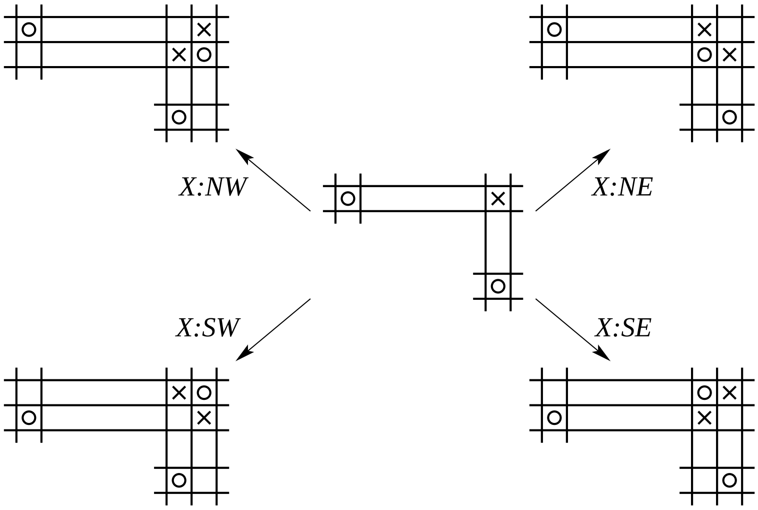


FIGURE 3.8. **The stabilization at an $X$-marking.** There are four different stabilizations which can occur at a given $X$-marking: *X:NW*, *X:NE*, *X:SE*, and *X:SW*. The further four types of stabilizations (i.e. at $O$-markings) can be derived from these diagrams by interchanging all $X$- and $O$-markings.

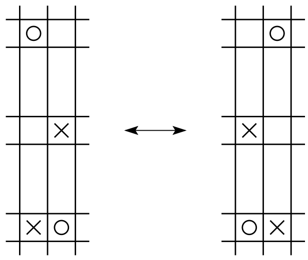

FIGURE 3.9. **A switch of two special columns.** Rotate both diagrams by $90°$ to get an example of a switch of two special rows.

**3.1.3. Other moves between grid diagrams.** Interchanging two consecutive rows or columns can be a commutation move; there are two other possibilities:

DEFINITION 3.1.10. Consider two consecutive columns in a grid diagram. These columns are called ***special*** if the $X$-marking in one of the columns occurs in the same row as the $O$-marking in the other column. If $\mathbb{G}'$ is obtained from $\mathbb{G}$ by interchanging a pair of special columns, then we say that $\mathbb{G}$ and $\mathbb{G}'$ are related by a ***switch***. Similarly, if two consecutive rows have an $X$- and an $O$-marking in the same column, interchanging them is also called a switch. See Figure 3.9.

Clearly, grid diagrams that differ by a switch determine the same link type.

EXERCISE 3.1.11. Show that a switch can be expressed as a sequence of commutations, stabilizations, and destabilizations.

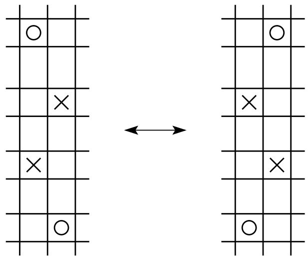

FIGURE 3.10. **A cross-commutation move.**

DEFINITION 3.1.12. Fix two consecutive columns (or rows) in a grid diagram $\mathbb{G}$, and let $\mathbb{G}'$ be obtained by interchanging those two columns (or rows). Suppose that the interiors of their corresponding intervals intersect non-trivially, but neither is contained in the other; then we say that the grid diagrams $\mathbb{G}$ and $\mathbb{G}'$ are related by a ***cross-commutation***.

The proof of the following proposition is straightforward:

PROPOSITION 3.1.13. *If $\mathbb{G}$ and $\mathbb{G}'$ are two grid diagrams that are related by a cross-commutation, then their associated oriented links $\vec{L}$ and $\vec{L}'$ are related by a crossing change.* $\square$

Grid diagrams can be used to show that any knot can be untied by a finite sequence of crossing changes (compare Exercise 2.3.8). Pick an $X$-marking and move the row containing the $O$-marking sharing the column with the chosen $X$-marking until these two markings occupy neighbouring squares. These moves are either commutations, switches (as such, leaving the link type unchanged), or cross-commutations, causing crossing changes. Then commute the column of the chosen $X$-marking until it reaches the $O$-marking in its row (compare Figure 3.12) and destabilize. This procedure reduces the grid number of the diagram. Repeatedly applying the procedure we turn the initial grid diagram into a $2 \times 2$ grid diagram representing the unknot, while changing the diagram by planar isotopies, Reidemeister moves and crossing changes only.

## 3.2. Toroidal grid diagrams

We find it convenient to transfer our planar grid diagrams to the torus $\mathbb{T}$ obtained by identifying the top boundary segment with the bottom one, and the left boundary segment with the right one. In the torus, the horizontal and vertical segments (which separate the rows and columns of squares) become horizontal and vertical circles. The torus inherits its orientation from the plane. We call the resulting object a *toroidal grid diagram*.

Conversely, a toroidal grid diagram can be cut up to give a planar grid diagram in $n^2$ different ways. We call these *planar realizations* of the given toroidal grid diagram. It is straightforward to see that two different planar realizations of the same grid diagram represent isotopic links. The relationship between these different planar realizations can be formalized with the help of the following:

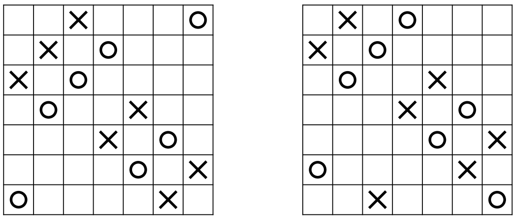

FIGURE 3.11. **Cyclic permutation.** By moving the top row of the left grid to the bottom, we get the grid on the right. In a cyclic permutation we can move several consecutive rows from top to bottom (or from bottom to top), and there is a corresponding move for columns as well.

DEFINITION 3.2.1. Let $\mathbb{G}$ be a planar grid diagram, and let $\mathbb{G}'$ be a new planar diagram obtained by cyclically permuting the rows or the columns of $\mathbb{G}$. (Notice that this move has no effect on the induced toroidal grid diagram.) In this case, we say that $\mathbb{G}'$ is obtained from $\mathbb{G}$ by a ***cyclic permutation***. See Figure 3.11 for an example.

Clearly, two different planar realizations of a toroidal grid diagram can be connected by a sequence of cyclic permutations.

The toroidal grid diagram inherits a little extra structure from the planar diagram. Thinking of the coordinate axes on the plane as oriented, there are induced orientations on the horizontal and vertical circles: explicitly, the grid torus is expressed as a product of two circles $\mathbb{T} = S^1 \times S^1$, where $S^1 \times \{p\}$ is a horizontal circle and $\{p\} \times S^1$ is a vertical circle; and both the horizontal and vertical circles are oriented. At each point in the torus, there are four preferred directions, which we think of as *North*, *South*, *East*, and *West*. (More formally, "North" refers to the oriented tangent vector of the circles $\{p\} \times S^1$; "South" to the opposite direction; "East" refers to the positive tangent vector of the circles $S^1 \times \{p\}$; and "West" to its opposite.) Correspondingly, each of the squares in the toroidal grid has a northern edge, an eastern edge, a southern edge, and a western edge.

Commutation and stabilization moves have natural adaptations to the toroidal case. For example, two toroidal grid diagrams differ by a commutation move if they have planar realizations which differ by a commutation move. Stabilization moves on toroidal grids are defined analogously. The classification of the types of stabilizations carries over to the toroidal case.

The grid chain complex (introduced in the next chapter) is associated to a toroidal grid diagram for a knot $K$. The resulting homology, however, depends on only $K$. The proof of this statement will hinge on Theorem 3.1.9: we will check that grid homology is invariant under grid moves. In the course of the proof it will be helpful to express certain grid moves in terms of others.

LEMMA 3.2.2. *A stabilization of type O:NE (respectively O:SE, O:NW, or O:SW) can be realized by a stabilization of type X:SW (respectively X:NW, X:SE, or X:NE), followed by a sequence of commutation moves on the torus.*

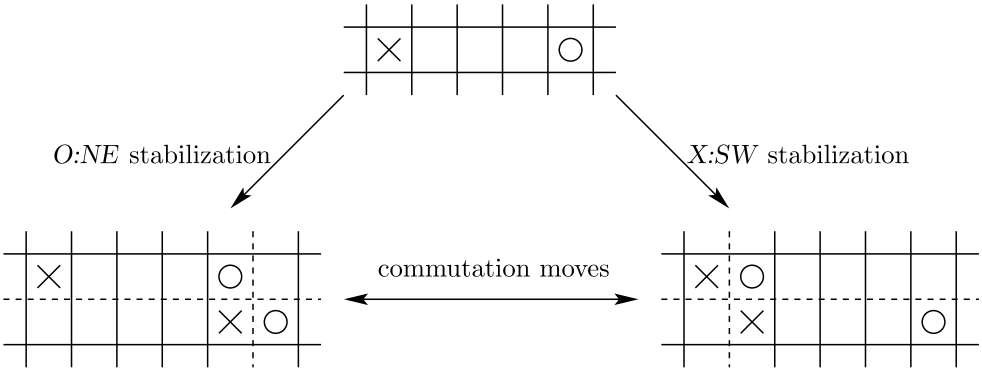


FIGURE 3.12. **A stabilization of type *O:NE* is equivalent to an *X:SW* stabilization and a sequence of commutations.**

**Proof.** Let $\mathbb{G}$ be a grid diagram and $\mathbb{G}_1$ be the stabilization of $\mathbb{G}$ at an $O$-marking. Commute the new length one vertical segment repeatedly until it meets another $X$–marking, and let $\mathbb{G}_2$ denote the resulting grid diagram. A type $X$ destabilization on $\mathbb{G}_2$ gives $\mathbb{G}$ back. See Figure 3.12 for an illustration. □

COROLLARY 3.2.3. *Any stabilization can be expressed as a stabilization of type X:SW followed by sequence of switches and commutations.*

**Proof.** First use Lemma 3.2.2 to express stabilizations of type $O$ in terms of stabilizations of type $X$ (and commutations). Next note that stabilizations *X:SE*, *X:SW*, *X:NE*, *X:NW* differ from each other by one or two switches. □

In a similar spirit, we have the following lemma, which will be used in Chapter 12:

LEMMA 3.2.4. *A cyclic permutation is equivalent to a sequence of commutations in the plane, stabilizations, and destabilizations of types X:NW, X:SE, O:NW, and O:SE.*

**Proof.** Consider the case of moving a horizontal segment from the top to the bottom, and suppose moreover that the left end of that segment is marked $X_1$, and the right end is marked $O_2$. Let $O_1$ (respectively $X_2$) be the other marking in the column containing $X_1$ (respectively $O_2$). Apply a stabilization of type *X:NW* at $X_2$, and commute the resulting horizontal segment of length 1 to the bottom of the diagram. We now have a vertical segment stretching the height of the diagram; apply commutation moves until it is just to the right of the column containing $X_1$. Now the horizontal segment starting at $X_1$ is of length 1, and so can be commuted down until it is just above $O_1$, where we can apply a destabilization of type *O:SE* to get the desired cyclic permutation. See Figure 3.13 for a picture of the sequence of moves we just performed. The other cases are handled similarly. □

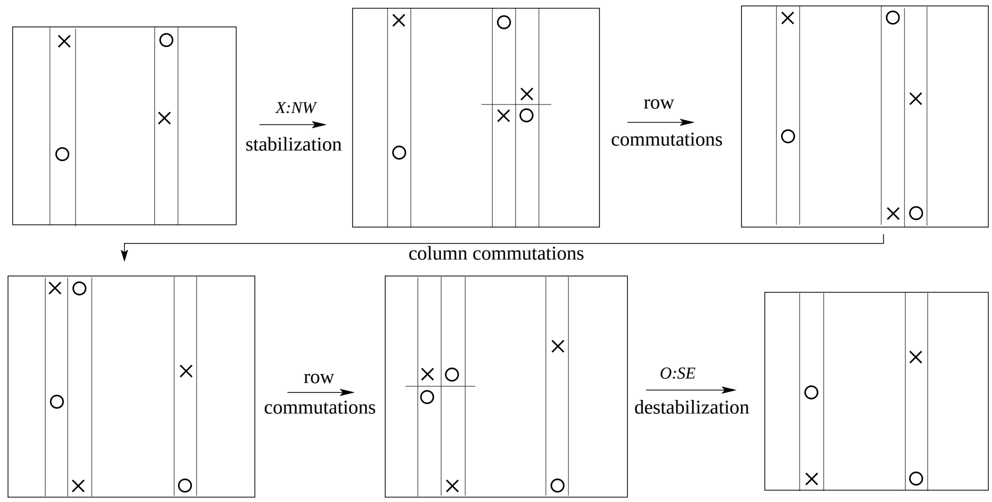


FIGURE 3.13. **The steps of the proof of Lemma 3.2.4.**

## 3.3. Grids and the Alexander polynomial

In this section grids will refer to planar grids, unless explicitly stated otherwise. Let $\mathbb{G}$ be an $n \times n$ planar grid diagram for a link placed in the $[0, n] \times [0, n]$ square on the plane. (The horizontal segments of the grid now have integral $y$-coordinates, while the vertical ones have integral $x$-coordinates. The $O$- and $X$-markings have half-integer coordinates.) Remember that the grid can be specified by the two permutations $\sigma_{\mathbb{O}}$ and $\sigma_{\mathbb{X}}$ describing the locations of the two sets of markings.

Recall the following construction from elementary topology:

DEFINITION 3.3.1. Let $\gamma$ be a closed, piecewise linear, oriented (not necessarily embedded and possibly disconnected) curve $\gamma$ in the plane and a point $p \in \mathbb{R}^2 - \gamma$. The ***winding number*** $w_\gamma(p)$ of $\gamma$ around the point $p$ is defined as follows. Draw a ray $\rho$ from $p$ to $\infty$, and let $w_\gamma(p)$ be the algebraic intersection of $\rho$ with $\gamma$. The winding number is independent of the choice of the ray $\rho$.

With this terminology in place, we associate a matrix to the grid $\mathbb{G}$ as follows.

DEFINITION 3.3.2. Fix a grid diagram $\mathbb{G}$ representing the link $\vec{L}$. Form the $n \times n$ matrix whose $(i, j)^{th}$ entry (the element in the $i^{th}$ row and $j^{th}$ column) is obtained by raising the formal variable $t$ to the power given by $(-1)$-times the winding number of the link diagram given by $\mathbb{G}$ around the $(j-1, n-i)^{th}$ lattice point with $1 \leq i, j \leq n$. Call this matrix the ***grid matrix***, and denote it by $\mathbf{M}(\mathbb{G})$.

Notice that the left-most column and the bottom-most row of $\mathbf{M}(\mathbb{G})$ consist of 1's only. To explain our above convention, note that the $(1, 1)$ entry of a matrix is in the upper left corner, while in our convention for grids the bottom-most row is the first. As an example for the grid diagram in Figure 3.1 (compare Figure 3.14), the grid matrix is

$$\begin{pmatrix} 1 & 1 & t & t & 1 & 1 \\ 1 & t^{-1} & 1 & t & 1 & 1 \\ 1 & t^{-1} & t^{-1} & 1 & t^{-1} & 1 \\ 1 & t^{-1} & t^{-1} & 1 & 1 & t \\ 1 & 1 & 1 & t & t & t \\ 1 & 1 & 1 & 1 & 1 & 1 \end{pmatrix}.$$

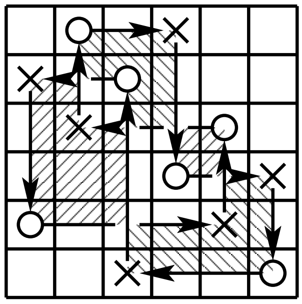

FIGURE 3.14. For the grid diagram illustrated in Figure 3.1, we shade regions according to the winding number of the knot: diagonal hatchings from lower left to upper right indicate regions with winding number $+1$, the other hatchings indicate winding number $-1$, and no hatchings indicate winding number $0$.

EXERCISE 3.3.3. Consider the $2\times 2$ and $3\times 3$ grids diagrams for the unknot, given by Figure 3.15. Compute the determinants of the associated matrices.

Consider the function $\det(\mathbf{M}(\mathbb{G}))$ associated to the diagram. According to Exercise 3.3.3, one immediately realizes that this determinant is not a link invariant: it does depend on the choice of the grid diagram representing the given link. However, as we will see, after a suitable normalization of this quantity, we obtain the Alexander polynomial of the link represented by the grid. To describe the normalization, we consider the following quantity $a(\mathbb{G})$ associated to the grid. For an $O$ and an $X$ consider the four corners of the square in the grid occupied by the marking and sum up the winding numbers in these corners. By summing these contributions for all $O$'s and $X$'s and dividing the result by 8, we get a number $a(\mathbb{G})$ associated to the $n\times n$ grid. Finally, let $\epsilon(\mathbb{G})\in\{\pm 1\}$ be the sign of the permutation that connects $\sigma_{\mathbb{O}}$ and $(n, n-1, ..., 1)$.

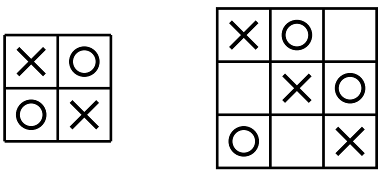

FIGURE 3.15. **Two grids representing the unknot.** It is easy to see that the associated determinants $\det(\mathbf{M}(\mathbb{G}))$ are different.

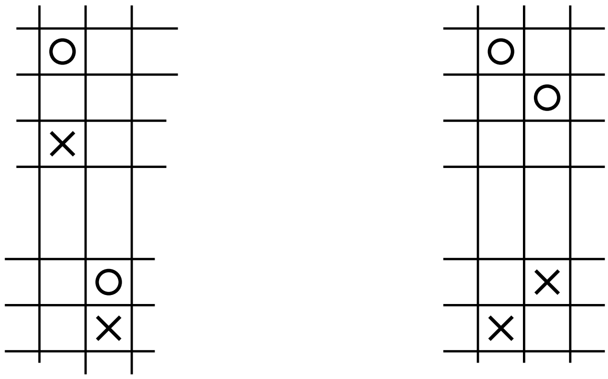

FIGURE 3.16. **The two cases in Lemma 3.3.7.** On the left the $y$-projections of the $O-X$ intervals are disjoint, while on the right the projections are nested. The diagrams represent two consecutive columns of the grid (say the $i^{th}$ and $(i+1)^{st}$), and therefore the vertical lines correspond to the $i^{th}$, $(i+1)^{st}$ and $(i+2)^{nd}$ columns of the grid matrix.

DEFINITION 3.3.4. Suppose that $\mathbb{G}$ is an $n \times n$ grid. Define the function $D_{\mathbb{G}}(t)$ to be the product

$$\epsilon(\mathbb{G}) \cdot \det(\mathbf{M}(\mathbb{G})) \cdot (t^{-\frac{1}{2}} - t^{\frac{1}{2}})^{1-n} t^{a(\mathbb{G})}.$$

EXERCISE 3.3.5. Compute $D_{\mathbb{G}}(t)$ for the two grids in Figure 3.15.

The next theorem connects the function $D_{\mathbb{G}}(t)$ to the Alexander polynomial.

THEOREM 3.3.6. *Let $\mathbb{G}$ be a grid diagram that represents $\vec{L}$. Then, the function $D_{\mathbb{G}}(t)$ is a link invariant and it coincides with the symmetrized Alexander polynomial $\Delta_{\vec{L}}(t)$ of the link $\vec{L}$ (as it is defined in Equation* (2.3)*).*

To prove Theorem 3.3.6, we establish some invariance properties of $D_{\mathbb{G}}(t)$.

LEMMA 3.3.7. *The function $D_{\mathbb{G}}(t)$ is invariant under commutation moves.*

**Proof.** Suppose that the grid $\mathbb{G}'$ is derived from $\mathbb{G}$ by commuting the $i^{th}$ and $(i+1)^{st}$ columns. Then the matrices $\mathbf{M}(\mathbb{G})$ and $\mathbf{M}(\mathbb{G}')$ differ in the $(i+1)^{st}$ column only.

We distinguish two cases, depending on whether the two intervals we are about to commute project disjointly to the $y$-axis, or one projection contains the other one (the two possibilities are shown by the left and right diagrams of Figure 3.16). In the first case, subtract the $i^{th}$ column from the $(i+1)^{st}$ in $\mathbf{M}(\mathbb{G})$ and the $(i+2)^{nd}$ from the $(i+1)^{st}$ in $\mathbf{M}(\mathbb{G}')$. The resulting matrices will differ only in the sign of the $(i+1)^{st}$ column, hence their determinants are opposites of each other. Since neither the size of the grid nor the quantity $a(\mathbb{G})$ changes, while $\epsilon(\mathbb{G}) = -\epsilon(\mathbb{G}')$, the invariance of $D_{\mathbb{G}}(t)$ under such commutation follows at once.

In the second case, we distinguish further subcases, depending on the relative positions of the $O$- and $X$-markings in the two columns. In the right diagram of

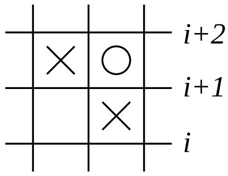


FIGURE 3.17. **The convention used in the proof of Lemma 3.3.8.**

Figure 3.16 we show the case when in both columns the $O$-marking is over the $X$-marking; the further three cases can be given by switching one or both pairs within their columns. In the following we will give the details of the argument only for the configuration shown by Figure 3.16; the verifications for the other cases proceed along similar lines.

As before, we subtract one column from the other one in each matrix. The choice of the columns in this case is important. In the case shown by Figure 3.16 we subtract the $(i+2)^{nd}$ column from the $(i+1)^{st}$; in general we subtract the column on the side of the shorter $O$-$X$-interval (that is, on the side where the two markings in the column are closer to each other). After performing the subtraction in both matrices $\mathbf{M}(\mathbb{G})$ and $\mathbf{M}(\mathbb{G}')$, we realize that the $(i+1)^{st}$ columns of the two matrices differ not only by a sign, but also by a multiple of $t$. A simple calculation shows that this difference is compensated by the difference in the terms originating from $a(\mathbb{G})$ and $a(\mathbb{G}')$, while the sign difference is absorbed by the change of $\epsilon$. This results that $D_{\mathbb{G}}(t)$ remains unchanged under commuting columns. A similar argument verifies the result when we commute rows, completing the argument. $\square$

LEMMA 3.3.8. *The function $D_{\mathbb{G}}(t)$ is invariant under stabilization moves.*

**Proof.** Consider the case where the stabilization is of type *X:SW*. In the matrix of the stabilized diagram, if we subtract the $(i+2)^{nd}$ row of Figure 3.17 from the $(i+1)^{st}$ row (passing between the two $X$'s in the stabilization), then we get a matrix which has a single non-zero term in this row. The determinant of the minor corresponding to this single element is, up to sign, the determinant of the matrix we had before the stabilization. The sign change is compensated by the introduction of $\epsilon(\mathbb{G})$, while the $t$-power in front of the determinant of the minor is absorbed by the change of the quantity $a(\mathbb{G})$ and the change of the size of the diagram, showing that $D_{\mathbb{G}}(t)$ remains unchanged. Other stabilizations work similarly. $\square$

Combining the above lemmas with Cromwell's Theorem 3.1.9, the function $D_{\mathbb{G}}(t)$ is a link invariant. Therefore, if $\mathbb{G}$ represents the link type $\vec{L}$ then $D_{\mathbb{G}}(t)$ will be denoted by $D_{\vec{L}}(t)$.

The proof of Theorem 3.3.6 will use the fact that $D_{\vec{L}}$ satisfies the skein relation. We start with a definition adapting the notion of an oriented skein triple to the grid context.

DEFINITION 3.3.9. Let $(\vec{L}_+, \vec{L}_-, \vec{L}_0)$ be an oriented skein triple, as in Definition 2.4.9. A ***grid realization of the oriented skein triple*** consists of four

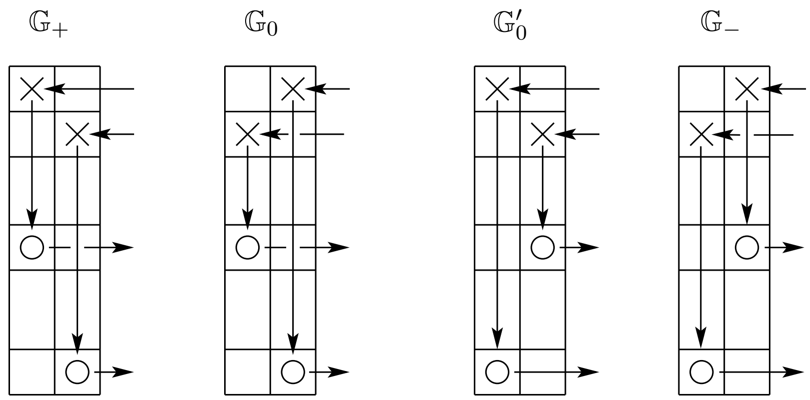


FIGURE 3.18. **The four grid diagrams which show up in the skein relation.**

grid diagrams $\mathbb{G}_+$, $\mathbb{G}_-$, $\mathbb{G}_0$, and $\mathbb{G}_0'$, representing the links $\vec{L}_+$, $\vec{L}_-$, $\vec{L}_0$, and $\vec{L}_0$ respectively. These diagrams are further related as follows: $\mathbb{G}_+$ and $\mathbb{G}_-$ differ by a cross-commutation, $\mathbb{G}_0$ and $\mathbb{G}_0'$ differ by a commutation, and $\mathbb{G}_+$ and $\mathbb{G}_0$ differ in the placement of their $X$-markings. See Figure 3.18 for a picture.

LEMMA 3.3.10. *Any oriented skein triple has a grid realization.*

**Proof.** Consider the diagrams $(\mathcal{D}_+, \mathcal{D}_-, \mathcal{D}_0)$ given by the skein triple. Approximate the diagrams by horizontal and vertical segments as explained in the proof of Lemma 3.1.3, with the additional property that in the small disk where the diagrams differ, the approximation is as given by $\mathbb{G}_+, \mathbb{G}_-$ and $\mathbb{G}_0'$ of Figure 3.18, while outside of the disk the three approximations are identical. Applying the commutation move on the first two columns of the grid $\mathbb{G}_0'$ we get $\mathbb{G}_0$, concluding the argument. $\square$

PROPOSITION 3.3.11. *The invariant $D_{\vec{L}}(t)$ satisfies the skein relation, that is, for an oriented skein triple $(\vec{L}_+, \vec{L}_-, \vec{L}_0)$ we have*

$$D_{\vec{L}_+}(t) - D_{\vec{L}_-}(t) = (t^{\frac{1}{2}} - t^{-\frac{1}{2}}) D_{\vec{L}_0}(t).$$

**Proof.** Let $(\vec{L}_+, \vec{L}_-, \vec{L}_0)$ be an oriented skein triple, and let $(\mathbb{G}_+, \mathbb{G}_-, \mathbb{G}_0, \mathbb{G}_0')$ be its grid realization, provided by Lemma 3.3.10. These grid diagrams agree in the placements of their $\mathbb{X}$- and $\mathbb{O}$-markings in all but two consecutive columns, which we think of as left-most. In these two columns of $\mathbb{G}_+$ we either move the two $X$-markings (transforming $\mathbb{G}_+$ to $\mathbb{G}_0$), or the two $O$-markings (giving $\mathbb{G}_0'$ from $\mathbb{G}_+$), or both (realizing a cross-commutation, transforming $\mathbb{G}_+$ to $\mathbb{G}_-$). In Figure 3.18 we depict the left-most two columns of these grids.

Now, the four associated grid matrices differ only in their second columns; and in fact, we have the relation

$$\det(\mathbf{M}(\mathbb{G}_+)) + \det(\mathbf{M}(\mathbb{G}_-)) = \det(\mathbf{M}(\mathbb{G}_0)) + \det(\mathbf{M}(\mathbb{G}_0')). \tag{3.1}$$

It is straigthforward to verify that

$$a(\mathbb{G}_-) = a(\mathbb{G}_+) = a(\mathbb{G}_0) + \frac{1}{2} = a(\mathbb{G}'_0) - \frac{1}{2},$$
$$\epsilon(\mathbb{G}_+) = -\epsilon(\mathbb{G}_-) = \epsilon(\mathbb{G}_0) = -\epsilon(\mathbb{G}'_0).$$

Combining these with Equation (3.1) gives the skein relation for $D_{\vec{L}}(t)$. □

**Proof of Theorem 3.3.6.** The Alexander polynomial for an oriented link satisfies the skein relation (Theorem 2.4.10). In fact, it is not hard to see that the Alexander polynomial is characterized by this relation, and its normalization for the unknot. Since $D_{\vec{L}}(t)$ satisfies this skein relation (Proposition 3.3.11), and $D_{\mathcal{O}}(t) = 1$ (as can be seen by checking in a $2 \times 2$ grid diagram), the result follows. □

The determinant of the grid matrix can be thought of as a weighted count of permutations, where the weight is obtained as a monomial in $t$, with exponent given by a winding number. In Chapter 4, grid homology will be defined as the homology of a bigraded chain complex whose generators correspond to these permutations, equipped with two gradings.

## 3.4. Grid diagrams and Seifert surfaces

It turns out that planar grid diagrams can also be applied to study Seifert surfaces of knots and links. Suppose that the $n \times n$ grid diagram $\mathbb{G}$ represents the knot $K \subset S^3$. Consider the *winding matrix* $\mathbf{W}(\mathbb{G})$ associated to $\mathbb{G}$ in the following way: the $(i,j)^{th}$ entry is the winding number of the projection of $K$ given by the grid $\mathbb{G}$ around the $(j-1, n-i)^{th}$ lattice point with $1 \leq i, j \leq n$. In the following we describe a method which produces a Seifert surface for $K$ based on $\mathbf{W}(\mathbb{G})$.

Let $R_i$ (and similarly $C_j$) denote the $n \times n$ matrix with 1's in the $i^{th}$ row ($j^{th}$ column), and 0 everywhere else. Obviously, by adding sufficiently many $R_i$'s or $C_j$'s, or both, any integral matrix can be turned into one which has only non-negative entries.

Definition 3.4.1. Define the ***complexity*** $c(A)$ of a non-negative matrix $A$ to be the sum of all its entries: $c(A) = \sum_{i,j} a_{i,j}$. An integral matrix $A \in M_n(\mathbb{Z})$ with non-negative entries is called ***minimal*** if its complexity is minimal among those non-negative integral matrices which can be given by repeatedly adding/subtracting $C_i$'s and $R_j$'s to $A$.

The following lemma gives a criterion for minimality:

Lemma 3.4.2. *The matrix $A = (a_{i,j}) \in M_n(\mathbb{Z})$ with non-negative entries is minimal if and only if there is a permutation $\sigma \in \mathfrak{S}_n$ such that $a_{i,\sigma(i)} = 0$ for all $i \in \{1, \ldots, n\}$.*

**Proof.** Suppose that there is a permutation $\sigma$ with the property that $a_{i,\sigma(i)} = 0$ for all $i$. Consider integers $m_i$ and $n_i$ for $i = 1, \ldots, n$ so that

$$A' = A + \sum_i n_i R_i + \sum_i m_i C_i$$

is a matrix with non-negative entries. Since $a_{i,\sigma(i)} = 0$, we conclude that $n_i + m_{\sigma(i)} \geq 0$ for all $i = 1, \ldots, n$. Clearly,

$$c(A') = c(A) + \sum_{i=1}^{n} n(n_i + m_{\sigma(i)}) \geq c(A),$$

so the complexity of $A$ is minimal, as claimed.

For the converse direction, let $\mathcal{C}$ denote the set of columns, while $\mathcal{R}$ the set of rows of the given non-negative matrix $A$. Connect $c_j \in \mathcal{C}$ with $r_i \in \mathcal{R}$ if and only if the $(i,j)^{th}$ entry $a_{i,j}$ of $A$ is equal to zero. Let $G$ denote the resulting bipartite graph on $2n$ vertices. According to Hall's Theorem [**82**] (a standard result in graph theory) either there is a perfect matching in $G$, providing the desired permutation, or there is a subset $C \subset \mathcal{C}$ such that the cardinality of the set $R$ formed by those elements in $\mathcal{R}$ which are connected to $C$ is smaller than $|C|$. Now if we add the $R_j$'s with $j \in R$ to $A$, the columns corresponding to elements of $C$ become positive, hence can be subtracted while keeping the matrix non-negative. Since $|C| > |R|$, we reduced the complexity of $A$, hence it was non-minimal. □

Returning to the matrix $\mathbf{W}(\mathbb{G})$, add and subtract appropriate $R_i$'s and $C_j$'s until it becomes a minimal, non-negative integral matrix. Let us denote the result by $H$. (Notice that this matrix is not uniquely associated to $\mathbf{W}(\mathbb{G})$ — it depends on the way we turned our starting matrix into a minimal, non-negative one.)

Lemma 3.4.3. *Adjacent entries of $H$ differ by at most one; i.e.*

$$|h_{i,j} - h_{i,j+1}| \leq 1, \qquad |h_{i+1,j} - h_{i,j}| \leq 1, \tag{3.2}$$

*where $i$ and $j$ are taken modulo $n$; e.g. we are viewing the last column as adjacent to the first one. More generally, for each $2 \times 2$ block of entries in the matrix $H$ (viewed on the torus), there is a non-negative integer $a$ so that the block has one of the following five possible shapes, up to rotation by multiples of $90°$. In cases where the center of the $2 \times 2$ block is unmarked, the possibilities are:* $\begin{array}{c|c} a & a \\ \hline a & a \end{array}$, $\begin{array}{c|c} a & a+1 \\ \hline a & a+1 \end{array}$ *and* $\begin{array}{c|c} a & a+1 \\ \hline a+1 & a+2 \end{array}$. *In cases where the center is marked with an $O$ or an $X$, the possibilities are* $\begin{array}{c|c} a & a \\ \hline a & a+1 \end{array}$ *and* $\begin{array}{c|c} a & a+1 \\ \hline a+1 & a+1 \end{array}$.

**Proof.** Consider a $2 \times 2$ block in $\mathbf{W}(\mathbb{G})$, with entries $\begin{array}{c|c} a_{i,j} & a_{i,j+1} \\ \hline a_{i+1,j} & a_{i+1,j+1} \end{array}$. By thinking about winding numbers, it is clear that $a_{i,j} + a_{i+1,j+1} - a_{i,j+1} - a_{i+1,j} = 0$ unless the corner point corresponds to an $O$- or $X$-marking, in which case $a_{i,j} + a_{i+1,j+1} - a_{i,j+1} - a_{i+1,j} = \pm 1$. Since the expression $a_{i,j} + a_{i+1,j+1} - a_{i,j+1} - a_{i+1,j}$ is unchanged after the addition of $C_i$ or $R_j$, we conclude that for each $i$ and $j$,

$$|h_{i,j} - h_{i,j+1} - h_{i+1,j} + h_{i+1,j+1}| \leq 1; \tag{3.3}$$

and for each fixed $j$ there are at most two $i$ for which equality holds. Moreover, for fixed $j$, we can find $k$ and $\ell$ so that $h_{k,j} = h_{\ell,j+1} = 0$. Since the entries of $H$ are all non-negative, it follows that $|h_{i,j} - h_{i,j+1}| \leq 1$ for all $i$. The same reasoning gives the other bound.

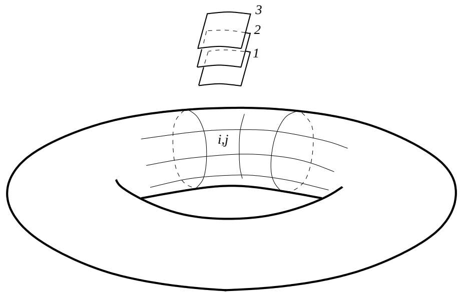


FIGURE 3.19. **Squares over the grid.** In this picture, $h_{i,j} = 3$.

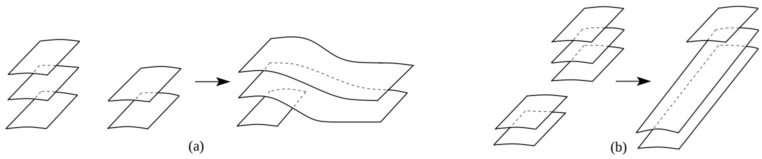


FIGURE 3.20. **Gluing squares to construct the embedding of $F_H$.** Neighbouring stacks of squares are glued together either from the top (as in (a)) or from the bottom (as in (b)).

Combining the bounds from Equations (3.2) and (3.3), we arrive at the five possibilities for the $2 \times 2$ blocks listed above. $\square$

Next we associate a surface $F_H \subset S^3$ to $H$. Consider first a disjoint union of squares $s^k_{i,j}$ with $i,j \in \{1,\ldots,n\}$ and $k \in \{1,\ldots h_{i,j}\}$. Glue the right edge of $s^k_{i,j}$ to the left edge of $s^k_{i,j+1}$ for $k \leq \min(h_{i,j}, h_{i,j+1})$, and the bottom edge of $s^{h_{i,j}-k}_{i,j}$ to the top edge of $s^{h_{i+1,j}-k}_{i+1,k}$ for $0 \leq k \leq \min(h_{i,j}, h_{i+1,j}) - 1$. The result $F_H$ is an oriented two-manifold with boundary, equipped with an orientation-preserving map to the torus. It is connected, since $H$ vanishes somewhere.

We can find an embedding of $F_H$ into $S^3$, as follows. View the grid torus as standardly embedded in $S^3$, and view $\{s^k_{i,j}\}^{h_{i,j}}_{k=1}$ as a collection of disjoint squares, stacked above the $(i,j)^{th}$ square in the grid torus, so that $s^{k+1}_{i,j}$ is above $s^k_{i,j}$ in the pile; see Figure 3.19. Instead of the edge identifications described earlier, we glue the various squares together by attaching strips; see Figure 3.20. The result is an embedding of the surface $F_H$ constructed above into $S^3$.

PROPOSITION 3.4.4. *Suppose that the knot $K \subset S^3$ is represented by the grid diagram $\mathbb{G}$. Assume that the minimal, non-negative matrix $H$ is given by adding and subtracting $R_i$'s and $C_j$'s to the matrix $\mathbf{W}(\mathbb{G})$ associated to $\mathbb{G}$. Then, the above embedding of the 2-complex $F_H$ is a Seifert surface of $K$.*

**Proof.** We have seen that $F_H$ is a 2-dimensional connected, oriented manifold embedded in $S^3$. By analyzing the local behavior from Lemma 3.4.3, it follows that the boundary of $F_H$ is isotopic to $K$. See Figure 3.21 for an example. $\square$

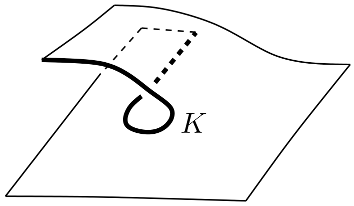


FIGURE 3.21. **A portion of $F_H$.** We have illustrated here the portion of $F_H$ over a $2\times 2$ block, one with multiplicity 2 and the others with multiplicity 1. The the knot $K$ is drawn thicker.

EXERCISE 3.4.5. Draw the local picture of the embedding of $F_H$ over a $2\times 2$ block for the five possibilities listed in Lemma 3.4.3, with $a=2$.

We will compute the Euler characteristic of $F_H$ via a formula for any surface-with-boundary obtained by gluing squares, in the following sense:

DEFINITION 3.4.6. A ***nearly flattened surface*** is a topological space $F$ which is obtained as a disjoint union of oriented squares, which are identified along certain pairs of edges via orientation-reversing maps; and only edges of different squares are identified. The resulting space $F$ is naturally a CW complex, with 0-cells corresponding to the corners in the squares (modulo identifications), 1-cells corresponding to edges of the squares (possibly identified in pairs), and 2-cells corresponding to squares. A ***flattened surface*** is a nearly flattened surface with the property that every 0-cell which is not contained on the boundary is a corner for exactly four rectangles.

A flattened surface is homeomorphic to a compact two-manifold with boundary.

LEMMA 3.4.7. *Let $F$ be a flattened surface. At each corner $p\in F$ (i.e. each point of $F$ coming from some corner of some rectangle), let $n_p$ denote the number of squares which meet at $p$. Let $C_{\partial F}$ denote the set of corner points in $\partial F$. Then, the Euler characteristic of $F$ is computed as*

$$\chi(F)=\sum_{p\in C_{\partial F}}\left(\frac{1}{2}-\frac{n_p}{4}\right). \tag{3.4}$$

**Proof.** Take a sum over all the squares in $F$ with the following weights: each square is counted with weight 1, each edge on each square with weight $-\frac{1}{2}$, and each corner (on each square) is counted with weight $\frac{1}{4}$. Adding up these weights, each 2-cell is counted with weight 1 (which is the contribution of each 2-cell to $\chi(F)$), each interior edge with total weight $-1$ (the contribution of the corresponding 1-cell to $\chi(F)$), and each boundary edge with contribution $-\frac{1}{2}$ (which is $\frac{1}{2}$ greater than the contribution to $\chi(F)$), and each corner point with weight $\frac{n_p}{4}$. Since the total contribution of each square vanishes, we conclude that

$$\chi(F)=\sum_{p\in C_{\partial F}}\left(1-\frac{n_p}{4}\right)-\frac{1}{2}\#\{e\subset\partial F\}.$$

Since the Euler characteristic of the boundary vanishes, and it is computed by $\#\{p \in C_{\partial F}\} - \#\{e \subset \partial F\}$, we can subtract half this Euler characteristic to deduce the claimed formula. □

DEFINITION 3.4.8. Given a square $Q$ in the grid marked with an $X$ or an $O$, let $\theta(Q, H)$ denote the average of the four $h_{i,j}$ adjoining $Q$. Given a matrix $H$, let $\theta(H) = \sum_{X \in \mathbb{X}} \theta(X, H) + \sum_{O \in \mathbb{O}} \theta(O, H)$.

PROPOSITION 3.4.9. *Fix a grid diagram $\mathbb{G}$ for a knot $K$ with grid number $n$, and let $H$ be any minimal matrix with non-negative entries associated to $\mathbf{W}(\mathbb{G})$. The Euler characteristic of $F_H$ is given by $n - \theta(H)$; so the genus of $F_H$ is given by*

$$g(F_H) = \frac{1}{2}\theta(H) - \frac{n-1}{2}. \tag{3.5}$$

**Proof.** Clearly, $F_H$ is a nearly flattened surface. We can check that it is a flattened surface by analyzing the local picture above each $2 \times 2$ block in $H$. When all four local multiplicities equal to $a$, the center point lifts to $a$ different 0-cells, none of which is contained in the boundary, and each of which appears as the corner of exactly four rectangles. When three of the local multiplicities equal one another, the center point lifts to a single corner point contained on the boundary of the surface. When two of the local multiplicites are $a$ and the other two are $a+1$, the center point lifts to $a$ different interior 0-cells, and a single 0-cell on the boundary, which is contained in two edges. Finally, when there are three different local multiplicities $a$, $a+1$, and $a+2$, the center point lifts to $a$ interior 0-cells, and two 0-cells appearing on the boundary, and each is contained in two 1-cells.

Consider Equation (3.4), which, according to Lemma 3.4.7, computes the Euler characteristic of $F_H$. The boundary points for $F_H$ for which $n_p \neq 2$ (i.e. for which the contribution to the right-hand-side of Equation (3.4) does not vanish) are exactly those $2n$ points which are marked with an $O$ or an $X$; i.e. those which lie over the center point of the $2 \times 2$ blocks where exactly three of the local multiplicites are equal to one another. For these points, $n_p$ is the sum of the local multiplicities at the four adjacent entries. Lemma 3.4.7 gives the stated result. □

By considering various grid presentations of the fixed knot $K$, and various ways to turn $\mathbf{W}(\mathbb{G})$ into a minimal, non-negative matrix, the above algorithm provides a large collection of Seifert surfaces.

COROLLARY 3.4.10. *For a fixed grid diagram $\mathbb{G}$ the Euler characteristic of $F_H$ is independent of the choice of the minimal, non-negative matrix $H$ (obtained by adding and subtracting rows to $\mathbf{W}(\mathbb{G})$) used in its construction.*

**Proof.** Observe that $\theta(M)$ grows by 2 whenever we add a row or a column to the matrix $M$, and also the complexity increases by $n$. It follows at once from Lemma 3.4.2 that for two minimal complexity, non-negative matrices $H$ and $H'$ derived from $\mathbf{W}(\mathbb{G})$, $\theta(H) = \theta(H')$. By Proposition 3.4.9 the Euler characteristic of $F_H$ can be computed from $\theta(H)$ and the grid number $n$, implying the claim. □

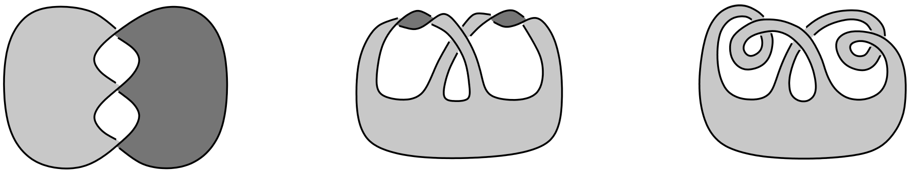

FIGURE 3.22. **Isotopy of a Seifert surface.** A Seifert surface of the right-handed trefoil knot (shown on the left) is isotoped to a disk with 1-handles attached to it (in the middle). In the final figure, further isotopies are applied so that the projection is an orientation preserving immersion.

The above corollary shows that each grid diagram $\mathbb{G}$ representing a knot $K$ determines an integer $g(\mathbb{G})$, the *associated genus* of $\mathbb{G}$, which is the genus of any Seifert surface of $K$ constructed from $\mathbb{G}$ by the above procedure.

PROPOSITION 3.4.11. *If $K$ is a knot with Seifert genus $g$, then there is a grid diagram $\mathbb{G}$ for $K$ whose associated genus is $g$.*

**Proof.** Any Seifert surface $F$ for $K$ can be thought of as obtained from a disk by adding handles. After isotopy, we can think of these handles as very thin bands. After further isotopies, we can assume that the Seifert surface immerses orientation preservingly onto the plane, see Figure 3.22, for example. Approximate the cores of the one-handles so that their projections consist of horizontal and vertical segments only. Performing a further local move as in Figure 3.2, we can arrange that for all crossings, the vertical segments are overcrossings. Approximate the result to get a grid diagram $\mathbb{G}$, and a surface $F_0$, isotopic to the original $F$, which projects onto $\mathbb{G}$. The projection of the Seifert surface produces a matrix $H_0$ all of whose coefficients are $0$, $1$, and $2$; the coefficients of $2$ correspond to the intersections of the projections of the bands. We claim that the genus of the Seifert surface $F$ is greater than or equal to the genus associated to the grid. Indeed, the genus of $F_0$ is computed by the same formula as in Equation (3.5):

$$g(F_0) = \frac{1}{2}\theta(H_0) - \frac{n-1}{2}.$$

Lemma 3.4.2 gives a minimal complexity non-negative matrix $H$ with

$$H + \sum_i m_i C_i + \sum_j n_j R_j = H_0,$$

and $\sum_i m_i + n_i \geq 0$. Since $\theta(H) + 2(\sum m_i + n_i) = \theta(H_0)$, it follows that $\theta(H) \leq \theta(H_0)$, and (by Proposition 3.4.9), $g(F_H) \leq g(F_0)$. Applying this reasoning to a surface $F$ with minimal genus (among Seifert surfaces for $K$), we conclude that $g(F_H) = g(F_0)$. $\square$

EXERCISE 3.4.12. Find a Seifert surface for the trefoil knot $T_{2,3}$ with the method above, using the grid diagram of Figure 3.3. Do the same for the figure-eight knot, using the grid of Figure 3.1.

EXAMPLES 3.4.13. We demonstrate the above construction by two other examples. Let us first consider the Conway knot (of Figure 2.7), represented by the grid diagram of Figure 3.4. The winding matrix $\mathbf{W}(\mathbb{G})$ is now equal to

$$\begin{pmatrix} 0 & 0 & 0 & 0 & 0 & 0 & -1 & -1 & -1 & -1 & -1 \\ 0 & 0 & 0 & -1 & -1 & -1 & -2 & -2 & -1 & -1 & -1 \\ 0 & 0 & 0 & -1 & -1 & -1 & -2 & -3 & -2 & -2 & -1 \\ 0 & 0 & 0 & -1 & 0 & 0 & -1 & -2 & -2 & -2 & -1 \\ 0 & 0 & 0 & -1 & 0 & 0 & 0 & -1 & -1 & -2 & -1 \\ 0 & 0 & 0 & -1 & 0 & 0 & 0 & 0 & 0 & -1 & 0 \\ 0 & 0 & -1 & -2 & -1 & 0 & 0 & 0 & 0 & -1 & 0 \\ 0 & -1 & -2 & -2 & -1 & 0 & 0 & 0 & 0 & -1 & 0 \\ 0 & -1 & -2 & -2 & -2 & -1 & -1 & -1 & -1 & -1 & 0 \\ 0 & -1 & -1 & -1 & -1 & 0 & 0 & 0 & 0 & 0 & 0 \\ 0 & 0 & 0 & 0 & 0 & 0 & 0 & 0 & 0 & 0 & 0 \end{pmatrix}.$$

Adding $C_i$'s to the columns with multiplicities $(0,1,2,2,2,1,2,3,2,2,1)$ we get a non-negative matrix, and then adding $C_1$ and subtracting $R_6$ and $R_{11}$ we get a minimal non-negative matrix. Using this matrix the construction provides a Seifert surface of genus three for the Conway knot.

In a similar manner, we consider the Kinoshita-Terasaka knot of Figure 2.7, and represent it by the grid diagram we get from the grid of Figure 3.4 after commuting the first two columns. Then, after taking the winding matrix, and adding $C_i$'s to the columns with multiplicities $(0,0,0,1,0,1,1,1,2,1,1)$, then adding $C_1$ and subtracting $R_8$ and $R_{10}$ we get the non-negative minimal matrix

$$\begin{pmatrix} 1 & 0 & 0 & 1 & 0 & 0 & 0 & 0 & 1 & 0 & 0 \\ 1 & 0 & 0 & 1 & 1 & 1 & 0 & 0 & 1 & 0 & 0 \\ 1 & 0 & 0 & 1 & 1 & 2 & 1 & 1 & 2 & 1 & 0 \\ 1 & 1 & 1 & 2 & 2 & 3 & 2 & 2 & 2 & 1 & 0 \\ 1 & 1 & 0 & 1 & 1 & 2 & 1 & 1 & 1 & 1 & 0 \\ 1 & 1 & 0 & 0 & 0 & 1 & 0 & 0 & 0 & 0 & 0 \\ 1 & 1 & 0 & 0 & 0 & 1 & 1 & 1 & 1 & 1 & 1 \\ 0 & 0 & 0 & 0 & 0 & 1 & 1 & 0 & 0 & 0 & 0 \\ 1 & 1 & 1 & 1 & 0 & 1 & 1 & 0 & 1 & 1 & 1 \\ 0 & 0 & 0 & 1 & 0 & 1 & 1 & 0 & 1 & 0 & 0 \\ 1 & 0 & 0 & 1 & 0 & 1 & 1 & 1 & 2 & 1 & 1 \end{pmatrix}.$$

A simple calculation shows that the corresponding Seifert surface has genus two.

## 3.5. Grid diagrams and the fundamental group

A planar grid diagram determines a simple presentation of the link group $\pi_1(S^3 \setminus L)$ of the underlying link as follows.

The generators $\{x_1, \ldots, x_n\}$ correspond to the vertical segments in the grid diagram (connecting the $O$- and the $X$-markings). The relations $\{r_1, \ldots, r_{n-1}\}$ correspond to the horizontal lines separating the rows. The relation $r_j$ is the product of the generators corresponding to those vertical segments which meet the $j^{th}$ horizontal line, in the order they are encountered, from left to right. See Figure 3.23.

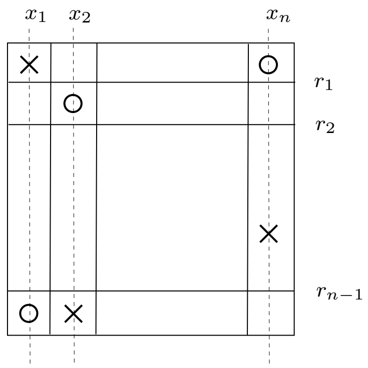


FIGURE 3.23. **The presentation of the fundamental group of the knot complement from a grid diagram.**

LEMMA 3.5.1. *The presentation*

$$\langle x_1, \dots, x_n \mid r_1, \dots, r_{n-1} \rangle \tag{3.6}$$

*described above is a presentation of the link group* $\pi_1(S^3 \setminus L)$ *of* $L$.

**Proof.** The result follows from the Seifert-Van Kampen theorem for a suitable decomposition of the link complement into two open subsets. (See for instance [**137**].) To visualize this decomposition, consider the planar grid $\mathbb{G}$ and assume that the link is isotoped into the following position. In the usual coordinates $(x, y, z)$ of $\mathbb{R}^3$ (with the understanding that the planar grid lies in the plane $\{z = 0\}$) we assume that the horizontal segments of the grid presenting $L$ are in the plane $\{z = 0\}$, while the vertical segments are in the plane $\{z = 1\}$. Over the markings $\mathbb{X}$ and $\mathbb{O}$, these segments are joined by segments parallel to the $z$-axis. The resulting polygon in $\mathbb{R}^3$ is a PL representative of $L$.

Take $X_1 = \{(x, y, z) \in \mathbb{R}^3 \setminus L \mid z > 0\}$ and $X_2 = \{(x, y, z) \in \mathbb{R}^3 \setminus L \mid z < 1\}$, decomposing the knot complement into two path-connected open subsets, in such a way that $X_1 \cap X_2$ is also path-connected. Fix the basepoint $x_0$ on the plane $\{z = \frac{1}{2}\}$. By choosing convenient generators of the free groups $\pi_1(X_1, x_0)$ and $\pi_1(X_2, x_0)$, the Seifert-Van Kampen theorem provides the desired presentation of the link group $\pi_1(\mathbb{R}^3 \setminus L, x_0) = \pi_1(S^3 \setminus L, x_0)$. $\square$

EXAMPLE 3.5.2. Consider the planar grid diagram of Figure 3.3, representing the right-handed trefoil knot $T_{2,3}$. The knot group $G$ has the presentation

$$\langle x_1, x_2, x_3, x_4, x_5 \mid x_1x_3, \quad x_1x_2x_3x_4, \quad x_1x_2x_4x_5, \quad x_2x_5 \rangle.$$

Since $x_3 = x_1^{-1}$, $x_5 = x_2^{-1}$, and $x_4 = x_1x_2^{-1}x_1^{-1}$, $G$ has the simpler presentation $\langle x_1, x_2 \mid x_1x_2x_1 = x_2x_1x_2 \rangle$. Taking $u = x_1x_2$ and $v = x_2x_1x_2$, the above presentation is equivalent to $\langle u, v \mid u^3 = v^2 \rangle$.

EXERCISE 3.5.3. Using the grid diagram of Figure 3.5, find a presentation of the link group of the Borromean rings.

CHAPTER 4

# Grid homology

The aim of the present chapter is to define the chain complexes for computing grid homology, following [**135, 136**]. We define three versions: $\widetilde{GC}(\mathbb{G})$, $\widehat{GC}(\mathbb{G})$, and $GC^-(\mathbb{G})$. The first of these is the simplest, and the first two are both specializations of the last one, which in turn is a specialization of a more complicated algebraic object $\mathcal{GC}^-(\mathbb{G})$ that we will meet in Chapter 13. In this chapter, and in fact, all the way until Chapter 8, we will consider primarily the case of knots.

This chapter is organized as follows. Section 4.1 introduces *grid states*, the generators of the grid chain complexes. Differentials count rectangles in the torus, and in Section 4.2 we describe how rectangles can connect grid states. In Section 4.3, we define two functions, the Maslov function and the Alexander function on grid states; these functions will induce the bigradings on the grid complexes. In Section 4.4 we define the grid complex $\widetilde{GC}$, the variant with the minimal amount of algebraic structure. In Section 4.5, we give a quick overview of some of the basic constructions from homological algebra (chain complexes, chain homotopies, quotient complexes) which will be of immediate use. (For more, see Appendix A.) In Section 4.6, we define further versions of the grid complex $GC^-$ and $\widehat{GC}$. In Section 4.7, we interpret the Alexander function in terms of the winding number, leading to an expression of the Euler characteristic of $\widetilde{GH}$ and $\widehat{GH}$ in terms of the Alexander polynomial. Section 4.8 gives some concrete calculations of grid homology. In Section 4.9, we conclude with some remarks relating the combinatorial constructions with analogous holomorphic constructions.

## 4.1. Grid states

Consider a toroidal grid diagram for a knot $K$ with grid number $n$, as described in Section 3.1. Think of each square in the grid as bounded by two horizontal and two vertical arcs. The horizontal arcs can be assembled to form $n$ horizontal circles in the torus, denoted $\boldsymbol{\alpha} = \{\alpha_i\}_{i=1}^n$, and the vertical ones can be assembled to form $n$ vertical circles, denoted $\boldsymbol{\beta} = \{\beta_i\}_{i=1}^n$.

Definition 4.1.1. A ***grid state*** for a grid diagram $\mathbb{G}$ with grid number $n$ is a one-to-one correspondence between the horizontal and vertical circles. More geometrically, a grid state is an $n$-tuple of points $\mathbf{x} = \{x_1, \dots, x_n\}$ in the torus, with the property that each horizontal circle contains exactly one of the elements of $\mathbf{x}$ and each vertical circle contains exactly one of the elements of $\mathbf{x}$. The set of grid states for $\mathbb{G}$ is denoted $\mathbf{S}(\mathbb{G})$.

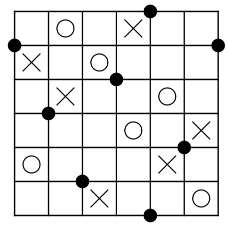

FIGURE 4.1. **A grid state in $\mathbf{S}(\mathbb{G})$.** Labelling the circles from left to right and bottom to top in this picture, the grid state corresponds to the permutation $(1,2,3,4,5,6) \mapsto (6,4,2,5,1,3)$.

A grid state $\mathbf{x}$ can be thought of as a graph of a permutation; i.e. if $\mathbf{x} = \{x_1,\ldots,x_n\}$, then $\sigma = \sigma_{\mathbf{x}}$ is specified by the property that $x_i = \alpha_{\sigma(i)} \cap \beta_i$. The correspondence between grid states and permutations is, of course, not canonical: it depends on a numbering of the horizontal and vertical circles.

When illustrating the diagrams and the states, we use planar grids; that is, cut the toroidal grid along a vertical and a horizontal circle. The square obtained by cutting up the torus is a *fundamental domain* for the torus, and the induced planar grid diagram is the planar realization of the grid diagram. Figure 4.1 provides an illustration of a typical grid state in a grid diagram for the figure-eight knot. To emphasize the side identifications used in going from the planar to the toroidal grid, we repeat components of the grid state on the left and the right edge, and the top and the bottom edge.

## 4.2. Rectangles connecting grid states

The chain complexes associated to a grid diagram are generated by grid states, and their differentials count rectangles connecting states. The various versions of the grid complex differ in how they count count rectangles. We formalize the concept of connecting rectangles, as follows.

Fix two grid states $\mathbf{x},\mathbf{y} \in \mathbf{S}(\mathbb{G})$, and an embedded rectangle $r$ in the torus whose boundary lies in the union of the horizontal and vertical circles, satisfying the following relationship. The sets $\mathbf{x}$ and $\mathbf{y}$ overlap in $n-2$ points in the torus, and the four points left out are the four corners of $r$. There is a further condition stated in terms of the orientation $r$ inherits from the torus. The oriented boundary of $r$ consists of four oriented segments, two of which are vertical and two of which are horizontal. The rectangle $r$ *goes from* $\mathbf{x}$ *to* $\mathbf{y}$ if the horizontal segments in $\partial r$ point from the components of $\mathbf{x}$ to the components of $\mathbf{y}$, while the vertical segments point from the components of $\mathbf{y}$ to the components of $\mathbf{x}$.

More formally, if $r$ is a rectangle, let $\partial_\alpha r$ denote the portion of the boundary of $r$ in the horizontal circles $\alpha_1 \cup \ldots \cup \alpha_n$, and let $\partial_\beta r$ denote the portion of the boundary of $r$ in the vertical ones. The boundary inherits an orientation from $r$. The rectangle $r$ goes from $\mathbf{x}$ to $\mathbf{y}$ if

$$\partial(\partial_\alpha r) = \mathbf{y} - \mathbf{x} \qquad \text{and} \qquad \partial(\partial_\beta r) = \mathbf{x} - \mathbf{y},$$

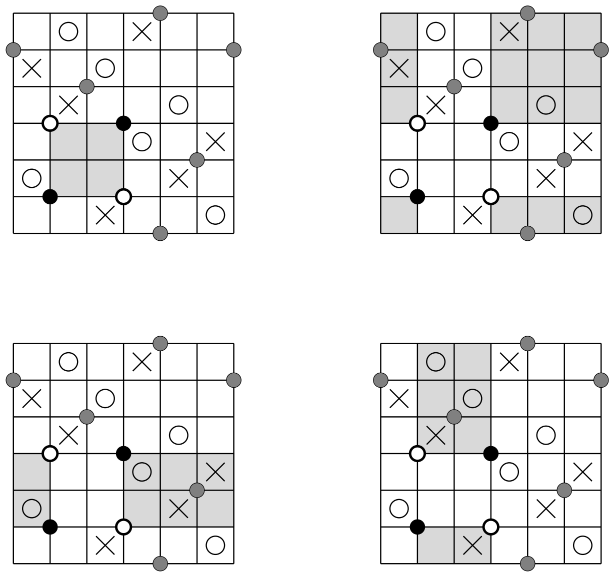

FIGURE 4.2. **Two grid states and the four rectangles connecting them.** Black ones appear in only one, call it $\mathbf{x}$; white dots appear in only the other one, call it $\mathbf{y}$; and gray dots appear in both. The two rectangles on the top row go from $\mathbf{x}$ to $\mathbf{y}$, and other two go from $\mathbf{y}$ to $\mathbf{x}$. The top left rectangle is empty, and the other three are not.

where $\mathbf{x} - \mathbf{y}$ is thought of as a formal sum of points; e.g. at points in $p \in \mathbf{x} \cap \mathbf{y}$, the difference cancels.

If there is a rectangle from $\mathbf{x}$ to $\mathbf{y}$, then all but two points in $\mathbf{x}$ must also be in $\mathbf{y}$. Thinking of grid states as corresponding to permutations, this is equivalent to the condition that the permutation $\xi$ associated to $\mathbf{x}$ and the permutation $\eta$ associated to $\mathbf{y}$ are related by the property that $\xi \cdot \eta^{-1}$ is a transposition.

For $\mathbf{x}, \mathbf{y} \in \mathbf{S}(\mathbb{G})$, let $\mathrm{Rect}(\mathbf{x}, \mathbf{y})$ denote the set of rectangles from $\mathbf{x}$ to $\mathbf{y}$. The set $\mathrm{Rect}(\mathbf{x}, \mathbf{y})$ is either empty, or it consists of exactly two rectangles, in which case $\mathrm{Rect}(\mathbf{y}, \mathbf{x})$ also consists of two rectangles. See Figure 4.2 for an illustration.

When we speak of a "rectangle", we will think of it as the geometric subset of the torus, together with the initial and the terminal grid states $\mathbf{x}$ and $\mathbf{y}$. Thus, if $\mathbf{x} \neq \mathbf{x}'$, a rectangle from $\mathbf{x}$ to $\mathbf{y}$ is always thought of as different from a rectangle from $\mathbf{x}'$ to $\mathbf{y}'$, even if their underlying polygons in the torus are the same. The underlying polygon is called the *support* of the rectangle.

Label the four corners of any rectangle as *northeast*, *southeast*, *northwest*, and *southwest*. This can be done, for example, by lifting $r$ to the universal cover, which inherits a preferred pair of coordinates: the horizontal direction which is oriented eastward, and the vertical direction, which is oriented northward, following the conventions of Section 3.2. Sometimes we refer to the northwest corner as the upper left one, and the southeast corner as the lower right one.

If $r$ is a rectangle from $\mathbf{x}$ to $\mathbf{y}$, then $r$ contains elements of $\mathbf{x}$ and $\mathbf{y}$ on its boundary. The northeast and southwest corners of $r$ are elements of $\mathbf{x}$, called *initial corners*, and the southeast and northwest corners of $r$ are elements of $\mathbf{y}$, called *terminal corners*. The rectangle $r$ might in addition contain elements of $\mathbf{x}$ in its interior $\mathrm{Int}(r)$. Note that $\mathbf{x} \cap \mathrm{Int}(r) = \mathbf{y} \cap \mathrm{Int}(r)$.

The following rectangles will play a special role in our subsequent constructions:

DEFINITION 4.2.1. A rectangle $r \in \mathrm{Rect}(\mathbf{x}, \mathbf{y})$ is called an ***empty rectangle*** if

$$\mathbf{x} \cap \mathrm{Int}(r) = \mathbf{y} \cap \mathrm{Int}(r) = \emptyset.$$

The set of empty rectangles from $\mathbf{x}$ to $\mathbf{y}$ is denoted $\mathrm{Rect}^{\circ}(\mathbf{x}, \mathbf{y})$.

## 4.3. The bigrading on grid states

The grid complexes are equipped with two gradings called the *Maslov grading* and the *Alexander grading*, both induced by integral-valued functions on grid states for a toroidal grid diagram. The aim of this section is to construct these functions. Key properties of both functions are stated in the next two propositions, whose proofs will occupy the rest of the section. We start with the Maslov function.

PROPOSITION 4.3.1. *For any toroidal grid diagram $\mathbb{G}$, there is a function*

$$M_{\mathbb{O}} \colon \mathbf{S}(\mathbb{G}) \to \mathbb{Z},$$

*called the **Maslov function on grid states**, which is uniquely characterized by the following two properties:*

*(M-1) Let $\mathbf{x}^{NWO}$ be the grid state whose components are the upper left corners of the squares marked with $O$. Then,*

$$M_{\mathbb{O}}(\mathbf{x}^{NWO}) = 0. \tag{4.1}$$

*(M-2) If $\mathbf{x}$ and $\mathbf{y}$ are two grid states that can be connected by some rectangle $r \in \mathrm{Rect}(\mathbf{x}, \mathbf{y})$, then*

$$M_{\mathbb{O}}(\mathbf{x}) - M_{\mathbb{O}}(\mathbf{y}) = 1 - 2\#(r \cap \mathbb{O}) + 2\#(\mathbf{x} \cap \mathrm{Int}(r)). \tag{4.2}$$

Note that $M_{\mathbb{O}}$ is independent of the placement of the $X$-markings. There is another function, $M_{\mathbb{X}}$ defined as in Proposition 4.3.1, only using the $X$-markings in place of the $O$-markings. Unless explicitly stated otherwise, the Maslov function on states refers to $M_{\mathbb{O}}$; and we will usually drop $\mathbb{O}$ from its notation.

DEFINITION 4.3.2. The ***Alexander function on grid states*** is defined in terms of the Maslov functions by the formula

$$A(\mathbf{x}) = \frac{1}{2}(M_{\mathbb{O}}(\mathbf{x}) - M_{\mathbb{X}}(\mathbf{x})) - \left(\frac{n-1}{2}\right). \tag{4.3}$$

Key properties of the Alexander function are captured in the following:

PROPOSITION 4.3.3. *Let $\mathbb{G}$ be a toroidal grid diagram for a knot. The function $A$ is characterized, up to an overall additive constant, by the following property. For any rectangle $r \in \mathrm{Rect}(\mathbf{x}, \mathbf{y})$ connecting two grid states $\mathbf{x}$ and $\mathbf{y}$,*

$$A(\mathbf{x}) - A(\mathbf{y}) = \#(r \cap \mathbb{X}) - \#(r \cap \mathbb{O}). \tag{4.4}$$

*Furthermore, $A$ is integral valued.*

We prove Proposition 4.3.1 first. This is done by constructing a candidate function for $M_{\mathbb{O}}$, and verifying that it has the properties specified in Proposition 4.3.1. The candidate function is defined in terms of a planar realization of the toroidal grid, using the following construction.

DEFINITION 4.3.4. Consider the partial ordering on points in the plane $\mathbb{R}^2$ specified by $(p_1, p_2) < (q_1, q_2)$ if $p_1 < q_1$ and $p_2 < q_2$. If $P$ and $Q$ are sets of finitely many points in the plane, let $\mathcal{I}(P, Q)$ denote the number of pairs $p \in P$ and $q \in Q$ with $p < q$. We symmetrize this function, defining

$$\mathcal{J}(P, Q) = \frac{\mathcal{I}(P, Q) + \mathcal{I}(Q, P)}{2}.$$

Consider a fundamental domain $[0, n) \times [0, n)$ for the torus in the plane, with its left and bottom edges included. A grid state $\mathbf{x} \in \mathbf{S}(\mathbb{G})$ can be viewed as a collection of points with integer coordinates in this fundamental domain. Similarly, $\mathbb{O} = \{O_i\}_{i=1}^n$ can be viewed as a collection of points in the plane with half-integer coordinates in the fundamental domain.

During the course of our proof, we will find that $M_{\mathbb{O}}$ is given by the formula

$$M_{\mathbb{O}}(\mathbf{x}) = \mathcal{J}(\mathbf{x}, \mathbf{x}) - 2\mathcal{J}(\mathbf{x}, \mathbb{O}) + \mathcal{J}(\mathbb{O}, \mathbb{O}) + 1, \tag{4.5}$$

which we write more succinctly as

$$M_{\mathbb{O}}(\mathbf{x}) = \mathcal{J}(\mathbf{x} - \mathbb{O}, \mathbf{x} - \mathbb{O}) + 1,$$

thinking of $\mathcal{J}$ as extended bilinearly over formal sums and formal differences of subsets of the plane. Correspondingly, $M_{\mathbb{X}}$ is given by

$$M_{\mathbb{X}}(\mathbf{x}) = \mathcal{J}(\mathbf{x} - \mathbb{X}, \mathbf{x} - \mathbb{X}) + 1.$$

LEMMA 4.3.5. *Fix a planar realization of a toroidal grid diagram. The function $M(\mathbf{x}) = \mathcal{J}(\mathbf{x} - \mathbb{O}, \mathbf{x} - \mathbb{O}) + 1$ satisfies Properties (M-1) and (M-2).*

**Proof.** Let $NW(O_i)$ denote the northwest corner of the square marked with $O_i$, and then project it to the fundamental domain. Clearly,

$$\begin{aligned} M(\mathbf{x}^{NWO}) =& \#\{(i,j) \big| NW(O_i) < NW(O_j)\} - \#\{(i,j) \big| NW(O_i) < O_j\} \\ & - \#\{(i,j) \big| O_i < NW(O_j)\} + \#\{(i,j) \big| O_i < O_j\} + 1. \end{aligned} \tag{4.6}$$

To verify Equation (4.1), we count the number of times each pair $(i, j)$ appears in the four sets on the right of Equation (4.6). We break this analysis into the following cases:

- If $i \neq j$ and neither $O_i$ nor $O_j$ is in the top row, then the following four inequalities are equivalent: $O_i < O_j$, $NW(O_i) < O_j$, $O_i < NW(O_j)$, and $NW(O_i) < NW(O_j)$.
- If $O_j$ is in the top row and $i \neq j$, then $O_i < O_j$ is equivalent to $NW(O_i) < O_j$; while neither of $O_i < NW(O_j)$ nor $NW(O_i) < NW(O_j)$ can hold (since $NW(O_j)$ is in the bottom segment).
- If $O_i$ is in the top row and $i \neq j$, neither $O_i < O_j$ nor $O_i < NW(O_j)$ can hold, while $NW(O_i) < O_j$ is equivalent to $NW(O_i) < NW(O_j)$.

- When $i = j$, there is exactly one $O_i$-marking for which $NW(O_i) < O_i$, when the $O_i$ is in the top row. Note also that the three other inequalities $O_i < O_i$, $O_i < NW(O_i)$ and $NW(O_i) < NW(O_i)$ are never satisfied.

The total to the right-hand-side of Equation (4.6) from the first three cases are all 0, while the last case contributes $-1$. It follows that $M(\mathbf{x}^{NWO}) = 0$; i.e. $M$ satisfies Property (M-1), as stated.

We verify that $M$ satisfies Property (M-2), starting with the case where the rectangle $r$ is contained in the fundamental domain for the torus used to define $M$. Label the southwest, northeast, northwest, and southeast corners of $r$ by $x_1$, $x_2$, $y_1$, and $y_2$ respectively. Clearly,

$$\mathbf{x} = \{x_1, x_2\} \cup \mathbf{p} \text{ and } \mathbf{y} = \{y_1, y_2\} \cup \mathbf{p},$$

where $\mathbf{p} = \mathbf{x} \cap \mathbf{y}$. It is easy to see that

$$\begin{aligned}\mathcal{J}(\mathbf{x},\mathbf{x}) - \mathcal{J}(\mathbf{y},\mathbf{y}) = 1 &+ \#\{x \in \mathbf{p} \big| x > x_1\} + \#\{x \in \mathbf{p} \big| x > x_2\} \\ &+ \#\{x \in \mathbf{p} \big| x < x_1\} + \#\{x \in \mathbf{p} \big| x < x_2\} - \#\{x \in \mathbf{p} \big| x > y_1\} \\ &- \#\{x \in \mathbf{p} \big| x > y_2\} - \#\{x \in \mathbf{p} \big| x < y_1\} - \#\{x \in \mathbf{p} \big| x < y_2\} \\ &= 1 + 2\{x \in \mathbf{p} \big| x_1 < x < x_2\} = 1 + 2\#(\mathbf{x} \cap \operatorname{Int}(r)).\end{aligned}$$

Above, the contribution of 1 comes from the pair $x_1 < x_2$. Similarly,

$$\begin{aligned}2\mathcal{J}(\mathbf{x},\mathbb{O}) - 2\mathcal{J}(\mathbf{y},\mathbb{O}) &= \#\{O_i \in \mathbb{O} \big| O_i > x_1\} + \#\{O_i \in \mathbb{O} \big| O_i > x_2\} \\ &+ \#\{O_i \in \mathbb{O} \big| O_i < x_1\} + \#\{O_i \in \mathbb{O} \big| O_i < x_2\} - \#\{O_i \in \mathbb{O} \big| O_i > y_1\} \\ &- \#\{O_i \in \mathbb{O} \big| O_i > y_2\} - \#\{O_i \in \mathbb{O} \big| O_i < y_1\} - \#\{O_i \in \mathbb{O} \big| O_i < y_2\} \\ &= 2\#\{O_i \in \mathbb{O} \big| x_1 < O_i < x_2\} = 2\#(\mathbb{O} \cap r).\end{aligned}$$

The above two equations imply that Equation (4.2) holds when $r$ is contained in the fundamental domain used to define Equation (4.5).

Next suppose that $r$ satisfies Equation (4.2). Suppose that $r' \in \operatorname{Rect}(\mathbf{y},\mathbf{x})$ is the rectangle with the property that $r$ and $r'$ meet along both horizontal edges, so that, in particular, both have the same width $v$. Then, since every column contains an $O$, and every vertical circle contains a component of $\mathbf{x}$, it follows that

$$\begin{gathered}\#(r' \cap \mathbb{O}) + \#(r \cap \mathbb{O}) = v \\ \#(\mathbf{x} \cap \operatorname{Int}(r')) + \#(\mathbf{x} \cap \operatorname{Int}(r)) = v - 1.\end{gathered}$$

These two equations, together with Equation (4.2) (for $r$), show that

$$M(\mathbf{y}) - M(\mathbf{x}) = 1 - 2\#(r' \cap \mathbb{O}) + 2\#(\mathbf{x} \cap \operatorname{Int}(r')),$$

which is the analogue of Equation (4.2) for $r'$.

In exactly the same manner, Equation (4.2) for $r$ implies the same property for the rectangle that shares two vertical edges with $r$.

It follows that if Equation (4.2) holds for any rectangle $r \in \operatorname{Rect}(\mathbf{x},\mathbf{y})$, then the same holds for any other rectangle in $\operatorname{Rect}(\mathbf{x},\mathbf{y}) \cup \operatorname{Rect}(\mathbf{y},\mathbf{x})$. It is easy to see that at least one of the four rectangles in $\operatorname{Rect}(\mathbf{x},\mathbf{y}) \cup \operatorname{Rect}(\mathbf{y},\mathbf{x})$ is contained in the fundamental domain, for which we have already verified Equation (4.2); and hence the function defined in Equation (4.5) satisfies Property (M-2). □

**Proof of Proposition 4.3.1.** Lemma 4.3.5 verifies the existence of a function that satisfies Properties (M-1) and (M-2). To see that the function is uniquely characterized by these properties, observe that for any two grid states $\mathbf{x}$ and $\mathbf{y}$, there is a sequence of grid states $\mathbf{x} = \mathbf{x}_1, \mathbf{x}_2, \dots, \mathbf{x}_k = \mathbf{y}$ and rectangles $r_i \in \mathrm{Rect}(\mathbf{x}_i, \mathbf{x}_{i+1})$. This follows from the fact that the symmetric group is generated by transpositions. Thus the function $M(\mathbf{x})$ is uniquely determined up to an overall additive constant by Equation (4.2). Equation (4.1) specifies this constant. $\square$

Note that Equation (4.5) specifies $M_{\mathbb{O}}$ using a fundamental domain; but the properties from Proposition 4.3.1 that uniquely characterize $M_{\mathbb{O}}$ make no reference to this choice. It follows that $M_{\mathbb{O}}$ is independent of the fundamental domain.

Next, we verify Equation (4.4), characterizing the Alexander function $A$.

**Proof of Proposition 4.3.3.** By Equation (4.2), if $r \in \mathrm{Rect}(\mathbf{x}, \mathbf{y})$ is any rectangle connecting the two grid states $\mathbf{x}$ and $\mathbf{y}$, then

$$M_{\mathbb{O}}(\mathbf{x}) - M_{\mathbb{O}}(\mathbf{y}) = 1 - 2\#(r \cap \mathbb{O}) + 2\#(\mathbf{x} \cap \mathrm{Int}(r))$$
$$M_{\mathbb{X}}(\mathbf{x}) - M_{\mathbb{X}}(\mathbf{y}) = 1 - 2\#(r \cap \mathbb{X}) + 2\#(\mathbf{x} \cap \mathrm{Int}(r))$$

Taking the difference of these two equations, and applying Equation (4.3), we conclude that Equation (4.4) holds. The function $A$ is characterized up to an additive constant by Equation (4.4), since we can connect any two grid states by a sequence of rectangles.

The fact that $M$ takes values in $\mathbb{Z}$ implies only that $A$ takes values in $\frac{1}{2}\mathbb{Z}$. In view of Equation (4.4), to see that the Alexander function is integral, it suffices to show that there is one grid state $\mathbf{x}$ for which $A(\mathbf{x})$ is integral. Taking $\mathbf{x} = \mathbf{x}^{NWO}$, and using Equation (4.1), it suffices to show that

$$M_{\mathbb{X}}(\mathbf{x}^{NWO}) \equiv n - 1 \pmod 2. \tag{4.7}$$

To this end, we find a sequence of grid states $\mathbf{x}_i \in \mathbf{S}(\mathbb{G})$ for $i = 1, \dots, n$, with the following properties:

- $\mathbf{x}_1 = \mathbf{x}^{NWX}$ is the grid state whose components are the northwest corners of the squares marked with $X$,
- $\mathbf{x}_n = \mathbf{x}^{NWO}$,
- there is a (not necessarily empty) rectangle connecting $\mathbf{x}_i$ to $\mathbf{x}_{i+1}$.

This sequence of can be found, since the permutation that connects $\mathbf{x}^{NWO}$ to $\mathbf{x}^{NWX}$ is a cycle of length $n$ (since the grid represents a knot), and such a cycle can be written as a product of $n-1$ transpositions. By Equation (4.1), $M_{\mathbb{X}}(\mathbf{x}_1) = 0$; so Equation (4.7) now follows from the mod 2 reduction of Equation (4.2). $\square$

EXERCISE 4.3.6. Consider the grid diagram $\mathbb{G}$ of Figure 4.3. Show that $\mathbb{G}$ represents $W_0^-(T_{-2,3})$, the 0-framed, negative Whitehead double of the left-handed trefoil knot. Determine the Maslov and Alexander gradings of the grid state $\mathbf{x}$ indicated in the diagram. This example will play a crucial role in Section 8.6.

The following result will be useful later:

PROPOSITION 4.3.7. *Let $\mathbf{x}^{SWO}$ be the grid state whose components are the lower left (SW) corners of the squares marked with $O$. Then, $M(\mathbf{x}^{SWO}) = 1 - n$ for any $n \times n$ grid.*

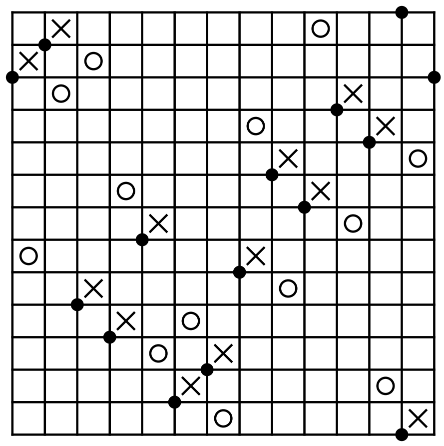

FIGURE 4.3. **Grid diagram for the 0-framed, negative Whitehead double of the left-handed trefoil knot.** The grid state $\mathbf{x}$ depicted in the diagram has Maslov grading 2.

**Proof.** Using the formula $M(\mathbf{x}^{SWO}) = \mathcal{J}(\mathbf{x}^{SWO} - \mathbb{O}, \mathbf{x}^{SWO} - \mathbb{O}) + 1$, we see that almost all terms cancel in pairs, except for the $n$ pairs $O_i$ and their corresponding $SW(O_i)$. The result follows. $\square$

EXERCISE 4.3.8. Let $\mathbb{G}$ be any grid diagram, and let $\mathbf{x}^{SEO}$ and $\mathbf{x}^{NEO}$, respectively, be the grid state whose components are the lower resp. the upper right corners of the squares marked with $O$. Compute $M(\mathbf{x}^{SEO})$ and $M(\mathbf{x}^{NEO})$.

## 4.4. The simplest version of grid homology

In the various grid complexes studied in the present book, the boundary maps count certain empty rectangles. The various constructions differ in how the empty rectangles are counted, in terms of how they interact with the $\mathbb{X}$- and $\mathbb{O}$-markings. (Compare also Section 5.5, where a different construction is outlined.) The simplest version of the grid complex is the following:

DEFINITION 4.4.1. The ***fully blocked grid chain complex*** associated to the grid diagram $\mathbb{G}$ is the chain complex $\widetilde{GC}(\mathbb{G})$, whose underlying vector space over $\mathbb{F} = \mathbb{Z}/2\mathbb{Z}$ has a basis corresponding to the set of grid states $\mathbf{S}(\mathbb{G})$, and whose differential is specified by

$$\tilde{\partial}_{\mathbb{O},\mathbb{X}}(\mathbf{x}) = \sum_{\mathbf{y}\in\mathbf{S}(\mathbb{G})} \#\{r \in \mathrm{Rect}^\circ(\mathbf{x},\mathbf{y}) \big| r\cap\mathbb{O} = r\cap\mathbb{X} = \emptyset\}\cdot\mathbf{y}. \tag{4.8}$$

Here $\#\{\cdot\}$ denotes the number of elements in the set modulo 2. (The subscript on $\tilde{\partial}_{\mathbb{O},\mathbb{X}}$ indicates the fact that the map counts rectangles that are disjoint from $\mathbb{O}$ and $\mathbb{X}$.)

The reader is invited to show that $\tilde{\partial}^2_{\mathbb{O},\mathbb{X}} = 0$. This is verified by interpreting the terms in $\tilde{\partial}^2_{\mathbb{O},\mathbb{X}}$ as counts of regions in the grid diagram that are compositions of two rectangles, and then showing that such regions have exactly two different decompositions into two rectangles, giving rise to pairwise cancelling terms in $\tilde{\partial}^2_{\mathbb{O},\mathbb{X}}$. A more general fact will be proved in Lemma 4.6.7 below.

The Maslov and Alexander functions on $\mathbf{S}(\mathbb{G})$ induce two gradings on $\widetilde{GC}(\mathbb{G})$: we define $\widetilde{GC}_d(\mathbb{G}, s)$ to be the $\mathbb{F}$-vector space generated by grid states $\mathbf{x}$ with $M(\mathbf{x}) = d$ and $A(\mathbf{x}) = s$. It follows quickly from Equations (4.2) and (4.4) that the restriction of $\tilde{\partial}_{\mathbb{O},\mathbb{X}}$ to $\widetilde{GC}_d(\mathbb{G}, s)$ maps into $\widetilde{GC}_{d-1}(\mathbb{G}, s)$. Thus, the bigrading descends to a bigrading on the homology groups of $\widetilde{GC}(\mathbb{G})$. Explicitly, letting

$$\widetilde{GH}_d(\mathbb{G}, s) = \frac{\operatorname{Ker}(\tilde{\partial}_{\mathbb{O},\mathbb{X}}) \cap \widetilde{GC}_d(\mathbb{G}, s)}{\operatorname{Im}(\tilde{\partial}_{\mathbb{O},\mathbb{X}}) \cap \widetilde{GC}_d(\mathbb{G}, s)},$$

then

$$\widetilde{GH}(\mathbb{G}) = \bigoplus_{d,s\in\mathbb{Z}} \widetilde{GH}_d(\mathbb{G}, s).$$

A *bigraded vector space* $X$ is a vector space equipped with a splitting indexed by a pair of integers: $X = \bigoplus_{d,s\in\mathbb{Z}} X_{d,s}$. In this language, the Maslov and Alexander functions give $\widetilde{GH}(\mathbb{G})$ the structure of a bigraded vector space.

DEFINITION 4.4.2. The ***fully blocked grid homology*** of $\mathbb{G}$, denoted $\widetilde{GH}(\mathbb{G})$, is the homology of the chain complex $(\widetilde{GC}(\mathbb{G}), \tilde{\partial}_{\mathbb{O},\mathbb{X}})$, thought of as a bigraded vector space.

EXERCISE 4.4.3. Let $\mathcal{O}$ denote the unknot. Compute $\widetilde{GH}(\mathbb{G})$ for a $2 \times 2$ grid for $\mathcal{O}$. Compute $\widetilde{GH}(\mathbb{G})$ for a $3 \times 3$ grid for $\mathcal{O}$.

The above exercise demonstrates the fact that the total dimension of the homology $\widetilde{GH}(\mathbb{G})$ depends on the grid presentation of the knot. In fact, the following will be proved in Section 5.3:

THEOREM 4.4.4. *If $\mathbb{G}$ is a grid diagram with grid number $n$ representing a knot $K$, then the renormalized dimension $\dim_{\mathbb{F}}(\widetilde{GH}(\mathbb{G}))/2^{n-1}$ is an integer-valued knot invariant; in particular, it is independent of the chosen grid presentation of $K$.*

## 4.5. Background on chain complexes

Theorem 4.4.4 might seem mysterious at this point. Indeed, even the fact that the dimension of $\widetilde{GH}(\mathbb{G})$ is divisible by $2^{n-1}$ is surprising. To verify this latter fact, it is helpful to enrich our coefficient ring to a polynomial algebra and to define a version of the grid complex over this algebra.

In the present section, we recall the necessary tools from homological algebra needed to study this enrichment. This material is essentially standard, with a small modifications needed to accommodate the natural gradings arising in grid homology. More details, and proofs of some of these results, are provided in Appendix A.

Fix a commutative ring $\mathbb{K}$ with unit, which in our applications will be either $\mathbb{Z}$, the finite field $\mathbb{Z}/p\mathbb{Z}$ for some prime $p$, or $\mathbb{Q}$. In fact, through most of this text, we will take $\mathbb{K} = \mathbb{Z}/2\mathbb{Z} = \mathbb{F}$. Consider the polynomial ring $\mathcal{R} = \mathbb{K}[V_1, \ldots, V_n]$ in $n$ formal variables $V_1, \ldots, V_n$. (We also allow $n = 0$, so that $\mathcal{R} = \mathbb{K}$.)

DEFINITION 4.5.1. A ***bigraded*** $\mathcal{R}$***-module*** $M$ is an $\mathcal{R}$-module, together with a splitting $M = \bigoplus_{d,s\in\mathbb{Z}} M_{d,s}$ as a $\mathbb{K}$-module, so that for each $i = 1,\ldots,n$, the restriction of $V_i$ to $M_{d,s}$ maps into $M_{d-2,s-1}$. A ***bigraded*** $\mathcal{R}$***-module homomorphism*** is a homomorphism $f\colon M \to M'$ between two bigraded $\mathcal{R}$-modules that sends $M_{d,s}$ to $M'_{d,s}$ for all $d,s\in\mathbb{Z}$. More generally, an $\mathcal{R}$-module homomorphism from $f\colon M\to M'$ is said to be ***homogeneous of degree*** $(m,t)$ if it sends $M_{d,s}$ to $M'_{d+m,s+t}$ for all $d,s\in\mathbb{Z}$.

A ***bigraded chain complex over*** $\mathcal{R} = \mathbb{K}[V_1,\ldots,V_n]$ is a bigraded $\mathcal{R}$-module $C$, equipped with an $\mathcal{R}$-module homomorphism $\partial\colon C\to C$ with $\partial\circ\partial = 0$ that maps $C_{d,s}$ into $C_{d-1,s}$; in particular, $\partial$ is a homomorphism of $\mathcal{R}$-modules that is homogeneous of degree $(-1,0)$.

The case where $n=1$ will be of particular relevance to us. In this case, we write the algebra $\mathcal{R}$ simply as $\mathbb{K}[U]$. When $n=0$ and $\mathbb{K}=\mathbb{F}$, the bigraded modules are bigraded vector spaces, the structures we encountered in Section 4.4.

DEFINITION 4.5.2. Let $(C,\partial)$ and $(C',\partial')$ be two bigraded chain complexes over $\mathcal{R} = \mathbb{K}[V_1,\ldots,V_n]$. A ***chain map*** $f\colon (C,\partial)\to(C',\partial')$ is a homomorphism of $\mathcal{R}$-modules, satisfying the property that $\partial'\circ f = f\circ\partial$. The chain map $f$ is called a ***bigraded chain map*** if it is also a bigraded homomorphism. More generally, a chain map is called ***homogeneous of degree*** $(m,t)$ if the underlying homomorphism is bigraded of degree $(m,t)$. An ***isomorphism*** of bigraded chain complexes is a bigraded chain map $f\colon (C,\partial)\to(C',\partial')$ for which there is another bigraded chain map $g\colon (C',\partial')\to(C,\partial)$ with $f\circ g = \mathrm{Id}_{C'}$ and $g\circ f = \mathrm{Id}_C$. If there is an isomorphism from $(C,\partial)$ to $(C',\partial')$, we say that they are ***isomorphic bigraded chain complexes***, and write $(C,\partial)\cong(C',\partial')$.

A bigraded chain map $f\colon C\to C'$ between two bigraded chain complexes over $\mathcal{R}$ induces a well-defined bigraded map on homology, denoted $H(f)\colon H(C)\to H(C')$.

If $(C,\partial)$ and $(C',\partial')$ are bigraded chain complexes over $\mathcal{R}$, and $f\colon (C,\partial)\to(C',\partial')$ is a chain map, we can form the quotient complex $(C',\partial')/\mathrm{Im}(f)$, which is also a chain complex over $\mathcal{R}$. When $f$ is homogenous of degree $(m,t)$, the quotient complex is also a bigraded chain complex of $\mathcal{R}$-modules.

For example, if $(C,\partial)$ is a bigraded chain complex over $\mathcal{R} = \mathbb{K}[V_1,\ldots,V_n]$ with $n\geq 1$, then multiplication by $V_i$ $i\in\{1,\ldots,n\}$ is a chain map $V_i\colon (C,\partial)\to(C,\partial)$. In this case, the quotient complex is denoted $\frac{C}{V_i}$; or more suggestively $\frac{C}{V_i=0}$. This construction can be iterated; e.g. we can take the quotient of the chain complex by the map $V_j\colon \frac{C}{V_i}\to\frac{C}{V_i}$; the corresponding quotient will be denoted $\frac{C}{V_i=V_j=0}$.

A short exact sequence of chain complexes induces a long exact sequence on homology, according to the following:

LEMMA 4.5.3. *Let $(C,\partial)$, $(C',\partial')$, and $(C'',\partial'')$ be three bigraded chain complexes over $\mathcal{R} = \mathbb{K}[V_1,\ldots,V_n]$. Suppose that $f\colon C\to C'$ is a chain map which is homogeneous of degree $(m,t)$, and $g\colon C'\to C''$ is a bigraded chain map, both of which fit into a short exact squence*

$$0 \longrightarrow C \xrightarrow{f} C' \xrightarrow{g} C'' \longrightarrow 0.$$

*Then, there is a homomorphism of $\mathcal{R}$-modules $\delta\colon H(C'') \to H(C)$ that is homogeneous of degree $(-m-1,-t)$, which fits into a long exact sequence*

$$\cdots \longrightarrow H_{d-m,s-t}(C) \xrightarrow{H(f)} H_{d,s}(C') \xrightarrow{H(g)} H_{d,s}(C'') \xrightarrow{\delta} H_{d-m-1,s-t}(C) \longrightarrow \cdots$$

The proof of the above standard result is recalled in Appendix A; see Lemma A.2.1.

Definition 4.5.4. Suppose that $f,g\colon (C,\partial) \to (C',\partial')$ are two bigraded chain maps between two bigraded chain complexes over $\mathcal{R}$. The maps $f$ and $g$ are said to be ***chain homotopic*** if there is an $\mathcal{R}$-module homomorphism $h\colon C \to C'$ that is homogeneous of degree $(1,0)$, and that satisfies the formula

$$f - g = \partial' \circ h + h \circ \partial. \tag{4.9}$$

In this case, $h$ is called a ***chain homotopy from*** $g$ ***to*** $f$. More generally, if $f,g\colon (C,\partial) \to (C',\partial')$ are two chain maps that are homogeneous of degree $(m,t)$, they are called ***chain homotopic*** if there is a map $h\colon C \to C'$ that is an $\mathcal{R}$-module homomorphism homogeneous of degree $(m+1,t)$ and satisfies Equation (4.9)

It is easy to verify that chain homotopic maps induce the same map on homology.

Definition 4.5.5. A chain map $f\colon C \to C'$ is a ***chain homotopy equivalence*** if there is a chain map $\phi\colon C' \to C$, called a ***chain homotopy inverse to*** $f$, with the property that $f\circ\phi$ and $\phi\circ f$ are both chain homotopic to the respective identity maps. If there is a chain homotopy equivalence from $C$ to $C'$, then $C$ and $C'$ are said to be ***chain homotopy equivalent*** complexes.

Proposition 4.5.6. *Let $C$ and $C'$ be two bigraded chain complexes of $\mathcal{R} = \mathbb{K}[V_1,\dots,V_n]$-modules. A chain map $f\colon C \to C'$, homogeneous of degree $(m,t)$, naturally induces a chain map $\overline{f}\colon \frac{C}{V_i} \to \frac{C}{V_i}$ that is also homogeneous of degree $(m,t)$. Moreover, if $g$ is another chain map that is homogeneous of degree $(m,t)$, a chain homotopy $h$ from $f$ to $g$ induces a chain homotopy $\overline{h}$ from $\overline{f}$ to $\overline{g}$.*

**Proof.** Any $\mathcal{R}$-module homomorphism $\phi\colon C \to C'$ induces a $\mathcal{R}$-module homomorphism $\overline{\phi}\colon \frac{C}{V_i} \to \frac{C'}{V_i}$. In this notation, the differential $\partial$ on $C$ induces the differential $\overline{\partial}$ on $\frac{C}{V_i}$. Also, the chain maps $f$, $g$, and the chain homotopy $h$ induce maps $\overline{f}$, $\overline{g}$, and $\overline{h}\colon \frac{C}{V_i} \to \frac{C'}{V_i}$. The relation $\overline{\partial}' \circ \overline{h} + \overline{h} \circ \overline{\partial} = \overline{f} - \overline{g}$ is a consequence of the relation $\partial' \circ h + h \circ \partial = f - g$. $\square$

## 4.6. The grid chain complex $GC^-$

We now enrich the grid complex to a bigraded chain complex over the ring $\mathcal{R} = \mathbb{F}[V_1,\dots,V_n]$. Various specializations of this complex give rise to different versions of grid homology.

To define the enrichment, it is useful to enumerate the set $\mathbb{O} = \{O_i\}_{i=1}^n$. This puts the $O$-markings in one-to-one correspondence with the generators $V_i$ of the polynomial algebra $\mathcal{R}$. Informally, the unblocked grid complex is the $\mathcal{R}$-module generated by grid states, equipped with a differential $\partial_{\mathbb{X}}^-$ counting empty rectangles that may cross the $O$- but not the $X$-markings. The *multiplicity* $O_i(r)$ of the rectangle $r$ at the marking $O_i$ is defined to be either 1 or 0, depending on whether or not $r$ contains $O_i$. This multiplicity is recorded as the exponent of the formal variable $V_i$. More explicitly:

DEFINITION 4.6.1. The ***(unblocked) grid complex*** $GC^-(\mathbb{G})$ is the free module over $\mathcal{R}$ generated by $\mathbf{S}(\mathbb{G})$, equipped with the $\mathcal{R}$-module endomorphism whose value on any $\mathbf{x} \in \mathbf{S}(\mathbb{G})$ is given by

$$\partial^-_{\mathbb{X}}\mathbf{x} = \sum_{\mathbf{y}\in\mathbf{S}(\mathbb{G})} \sum_{\{r\in\mathrm{Rect}^\circ(\mathbf{x},\mathbf{y}) \,\big|\, r\cap\mathbb{X}=\emptyset\}} V_1^{O_1(r)}\cdots V_n^{O_n(r)}\cdot\mathbf{y}. \tag{4.10}$$

The elements $V_1^{k_1}\cdots V_n^{k_n}\cdot\mathbf{x}$ where $\mathbf{x}\in\mathbf{S}(\mathbb{G})$ and $k_1,\dots,k_n$ are arbitrary, non-negative integers form a basis for the $\mathbb{F}$-vector space $GC^-(\mathbb{G})$. Extend the Maslov and Alexander functions (Proposition 4.3.1 and Definition 4.3.2) to this basis by

$$M(V_1^{k_1}\dots V_n^{k_n}\cdot\mathbf{x}) = M(\mathbf{x}) - 2k_1 - \cdots - 2k_n, \tag{4.11}$$

$$A(V_1^{k_1}\dots V_n^{k_n}\cdot\mathbf{x}) = A(\mathbf{x}) - k_1 - \cdots - k_n. \tag{4.12}$$

These extensions equip $GC^-(\mathbb{G})$ with a bigrading: let $GC^-_d(\mathbb{G},s)$ denote the vector subspace spanned by basis vectors $V_1^{k_1}\cdots V_n^{k_n}\cdot\mathbf{x}$ with $M(V_1^{k_1}\cdots V_n^{k_n}\cdot\mathbf{x}) = d$, and $A(V_1^{k_1}\cdots V_n^{k_n}\cdot\mathbf{x}) = s$. If $x\in GC^-(\mathbb{G})$ lies in some $GC^-_d(\mathbb{G},s)$ for some $d$ and $s$, we say that $x$ is *homogeneous with bigrading* $(d,s)$ or simply *homogeneous.* (Note that the element 0 is homogeneous with any bigrading.)

REMARK 4.6.2. In Chapter 13, we will study another variant of the grid complex, $\mathcal{GC}^-(\mathbb{G})$, which has the same underlying $\mathcal{R}$-module as $GC^-(\mathbb{G})$, a grading induced by $M$, and a differential specified by

$$\partial^-\mathbf{x} = \sum_{\mathbf{y}\in\mathbf{S}(\mathbb{G})} \sum_{r\in\mathrm{Rect}^\circ(\mathbf{x},\mathbf{y})} V_1^{O_1(r)}\cdots V_n^{O_n(r)}\cdot\mathbf{y}. \tag{4.13}$$

This complex has a filtration which is a knot invariant, and its total homology is isomorphic to $\mathbb{F}[U]$. The normalization of $M$ specified by Equation (4.1) was chosen so that the generator of this homology module has grading equal to zero.

THEOREM 4.6.3. *The object* $(GC^-(\mathbb{G}),\partial^-_{\mathbb{X}})$ *is a bigraded chain complex over the ring* $\mathbb{F}[V_1,\dots,V_n]$*, in the sense of Definition 4.5.1.*

We break the proof of Theorem 4.6.3 into pieces, starting with the verification that $\partial^-_{\mathbb{X}}\circ\partial^-_{\mathbb{X}} = 0$. To this end, it is convenient to generalize the notion of rectangles.

Recall that the circles $\alpha_1,\dots,\alpha_g,\beta_1,\dots,\beta_g$ divide the torus into oriented squares $S_1,\dots,S_{n^2}$. A formal linear combination of the closures of these squares, $\mathcal{D} = \sum a_i\cdot\overline{S_i}$ with $a_i\in\mathbb{Z}$, has a boundary, which is a formal linear combination of intervals contained inside $\alpha_1\cup\cdots\cup\alpha_n\cup\beta_1\cup\cdots\cup\beta_n$. Let $\partial_\alpha\mathcal{D}$ be the portion of the boundary contained in $\alpha_1\cup\cdots\cup\alpha_n$ and $\partial_\beta\mathcal{D}$ be the portion in $\beta_1\cup\cdots\cup\beta_n$.

DEFINITION 4.6.4. Fix $\mathbf{x},\mathbf{y}\in\mathbf{S}(\mathbb{G})$. A ***domain*** $\psi$ from $\mathbf{x}$ to $\mathbf{y}$ is a formal linear combination of the closures of the squares in $\mathbb{G}\setminus(\boldsymbol{\alpha}\cup\boldsymbol{\beta})$, with the property that $\partial(\partial_\alpha\psi) = \mathbf{y}-\mathbf{x}$ and hence $\partial(\partial_\beta\psi) = \mathbf{x}-\mathbf{y}$. In these equations, the two sides represent a formal linear combinations of points; e.g. if $\mathbf{x} = \{x_1,\dots,x_n\}$ and $\mathbf{y} = \{y_1,\dots,y_n\}$, then $\mathbf{x}-\mathbf{y} = \sum_{i=1}^n(x_i-y_i)$. Denote the set of domains from

$\mathbf{x}$ to $\mathbf{y}$ by $\pi(\mathbf{x},\mathbf{y})$. A domain $\psi$ is called ***positive*** if each square in the torus (with its orientation inherited from the torus) appears in the expression for $\psi$ with non-negative multiplicity.

REMARK 4.6.5. The grid diagram $\mathbb{G}$ equips the torus with a $CW$-decomposition, whose 0-cells are the $n^2$ intersection points of the horizontal and the vertical circles; its 1-cells are the $2n^2$ intervals on the horizontal and vertical circles between consecutive intersections of these circles, and its 2-cells are the $n^2$ small squares of the grid diagram. A formal sum $\psi$ of rectangles is a 2-chain in this $CW$-complex structure. The group of 1-chains splits as the sum of the span of the horizontal intervals and vertical intervals. The 1-chain $\partial_\alpha\psi$ is the part of $\partial\psi$ in the span of the horizontal intervals, so the relation $\partial(\partial_\alpha\psi)=\mathbf{y}-\mathbf{x}$ is an equation of 0-chains.

Domains can be composed: if $\phi\in\pi(\mathbf{x},\mathbf{y})$ and $\psi\in\pi(\mathbf{y},\mathbf{z})$, then by adding the two underlying 2-chains we get a new domain, written $\phi*\psi\in\pi(\mathbf{x},\mathbf{z})$.

EXERCISE 4.6.6. **(a)** Show that any two $\mathbf{x},\mathbf{y}\in\mathbf{S}(\mathbb{G})$ can be connected by a domain $\psi\in\pi(\mathbf{x},\mathbf{y})$.
**(b)** Show that any two $\mathbf{x},\mathbf{y}\in\mathbf{S}(\mathbb{G})$ can be connected by a domain $\psi\in\pi(\mathbf{x},\mathbf{y})$ with $\mathbb{X}\cap\psi=\emptyset$.
**(c)** If $\mathbb{G}$ represents a knot, show that any domain $\psi\in\pi(\mathbf{x},\mathbf{y})$ with $\mathbb{X}\cap\psi=\emptyset$ is uniquely determined by its multiplicities at the $\mathbb{O}$. What if $\mathbb{G}$ represents a link?

The next lemma will be used to establish Theorem 4.6.3. Its proof will serve as a prototype for many of the proofs from Chapter 5.

LEMMA 4.6.7. *The operator* $\partial^-_{\mathbb{X}}\colon GC^-(\mathbb{G})\to GC^-(\mathbb{G})$ *satisfies* $\partial^-_{\mathbb{X}}\circ\partial^-_{\mathbb{X}}=0$.

**Proof.** For grid states $\mathbf{x}$ and $\mathbf{z}$ fix $\psi\in\pi(\mathbf{x},\mathbf{z})$ and (for the purposes of this proof) let $N(\psi)$ denote the number of ways we can decompose $\psi$ as a composite of two empty rectangles $r_1*r_2$. Observe that if $\psi=r_1*r_2$ for some $r_1\in\mathrm{Rect}(\mathbf{x},\mathbf{y})$ and $r_2\in\mathrm{Rect}(\mathbf{y},\mathbf{z})$, the following statements hold:

- $\psi\cap\mathbb{X}$ is empty if and only if $r_i\cap\mathbb{X}$ is empty for both $i=1,2$.
- The local multiplicities of $\psi$, $r_1$, and $r_2$ at any $O_i\in\mathbb{O}$ are related by
$$O_i(\psi)=O_i(r_1)+O_i(r_2).$$

It follows that for any $\mathbf{x}\in\mathbf{S}(\mathbb{G})$,
$$\partial^-_{\mathbb{X}}\circ\partial^-_{\mathbb{X}}(\mathbf{x})=\sum_{\mathbf{z}\in\mathbf{S}(\mathbb{G})}\ \sum_{\left\{\psi\in\pi(\mathbf{x},\mathbf{z})\mid\psi\cap\mathbb{X}=\emptyset\right\}}N(\psi)\cdot V_1^{O_1(\psi)}\cdots V_n^{O_n(\psi)}\cdot\mathbf{z}.$$

Consider a pair of empty rectangles $r_1\in\mathrm{Rect}^\circ(\mathbf{x},\mathbf{y})$ and $r_2\in\mathrm{Rect}^\circ(\mathbf{y},\mathbf{z})$, so that $r_1*r_2=\psi$ is a domain with $N(\psi)>0$. There are three basic cases (see also Figure 4.4 for an illustration):

(R-1) $\mathbf{x}\setminus(\mathbf{x}\cap\mathbf{z})$ consists of 4 elements. In this case, the corners of $r_1$ and $r_2$ are all distinct. There is a unique $\mathbf{y}'\in\mathbf{S}(\mathbb{G})$ and rectangles $r_1'\in\mathrm{Rect}^\circ(\mathbf{x},\mathbf{y}')$ and $r_2'\in\mathrm{Rect}^\circ(\mathbf{y}',\mathbf{z})$ so that $r_1$ and $r_2'$ have the same support and $r_2$ and $r_1'$ have the same support. See the top row of Figure 4.4 (and also Figure 4.5). Then, $r_1*r_2=r_1'*r_2'$ and in fact $N(\psi)=2$.

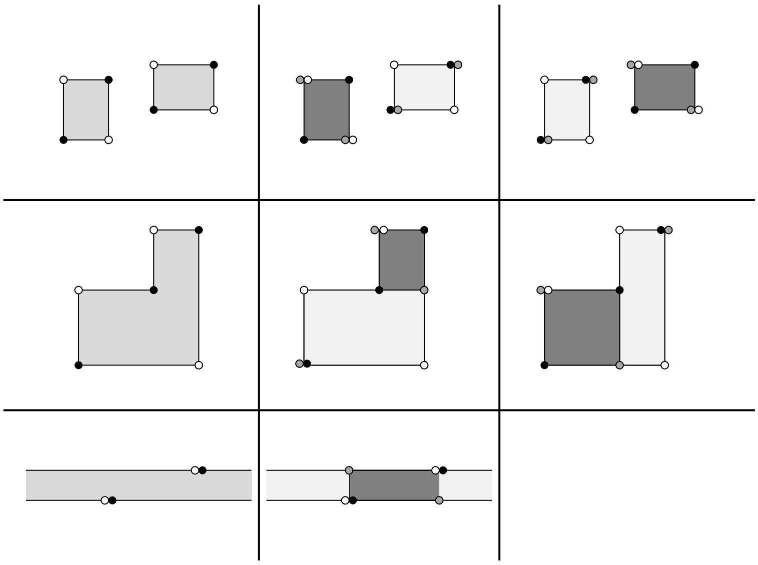

FIGURE 4.4. **Cases in the proof of Lemma 4.6.7.** The left column illustrates the three basic types of domains $\psi$ with $N(\psi) > 0$ (Cases (R-1), (R-2), and (R-3), respectively). The initial grid state is indicated by black dots; the terminal one by the white dots. The second and third columns show the decompositions of the domain in the first column. The first rectangle in the decomposition is darker than the second. The intermediate grid state is indicated by gray dots. In the first row we consider the case of two disjoint rectangles; these rectangles can also overlap as in Figure 4.5.

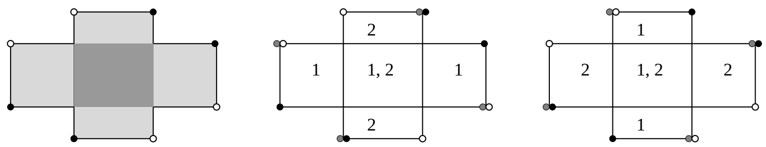


FIGURE 4.5. **Overlapping domains counted in $\partial^-_{\mathbb{X}} \circ \partial^-_{\mathbb{X}} = 0$.** Part of the domain on the left has local multiplicity two (indicated by the darker shading). The next two pictures show the two decompositions of this domain as a juxtaposition of two rectangles. The rectangles are labeled by integers 1 and 2, indicating their order in the decomposition.

(R-2) $\mathbf{x} \setminus (\mathbf{x} \cap \mathbf{z})$ consists of 3 elements. In this case, the local multiplicities of $\psi$ are all 0 or 1 and the corresponding region in the torus has six corners, five of which are $90°$, and one of which is $270°$. Cutting at the $270°$ corner in two different directions gives the two decompositions of $\psi$ as a juxtaposition of empty rectangles $\psi = r_1 * r_2 = r'_1 * r'_2$, where $r_1 \in \pi(\mathbf{x}, \mathbf{y})$, $r_2 \in \pi(\mathbf{y}, \mathbf{z})$, $r'_1 \in \pi(\mathbf{x}, \mathbf{y}')$, and $r'_2 \in \pi(\mathbf{y}', \mathbf{z})$ (with $\mathbf{y} \neq \mathbf{y}'$). In particular, $N(\psi) = 2$ in this case, as well. See the middle row of Figure 4.4.

(R-3) $\mathbf{x} = \mathbf{z}$. In this case, $\psi = r_1 * r_2$, where $r_1$ and $r_2$ intersect along two edges and therefore $\psi$ is an annulus. Since $r_1$ and $r_2$ are empty, this annulus has height or width equal to $1$. Such an annulus is called a *thin annulus*; see the bottom row of Figure 4.4. Thin annuli have $N(\psi) = 1$.

Contributions from Cases (R-1) and (R-2) cancel in pairs, since we are working modulo $2$. There are no contributions from Case (R-3), since every thin annulus contains one $X$-marking in it, concluding the proof of the lemma. □

LEMMA 4.6.8. *The differential $\partial_{\mathbb{X}}^-$ is homogeneous of degree $(-1,0)$.*

**Proof.** If $V_1^{k_1}\cdots V_n^{k_n}\cdot\mathbf{y}$ appears in $\partial_{\mathbb{X}}^-\mathbf{x}$, then there is a rectangle $r \in \mathrm{Rect}^\circ(\mathbf{x},\mathbf{y})$ with $r\cap\mathbb{X}=\emptyset$, and $O_i(r) = k_i$ for $i = 1,\dots,n$. By Equations (4.2) and (4.11),

$$M(V_1^{k_1}\cdots V_n^{k_n}\cdot\mathbf{y}) = M(\mathbf{y}) - 2\#(r\cap\mathbb{O}) = M(\mathbf{x}) - 1,$$

so the Maslov grading drops by one under the differential. Similarly, Equations (4.4) and (4.12) give

$$A(V_1^{k_1}\cdots V_n^{k_n}\cdot\mathbf{y}) = A(\mathbf{y}) - \#(r\cap\mathbb{O}) = A(\mathbf{x}) - \#(r\cap\mathbb{X}). \tag{4.14}$$

Since $r\cap\mathbb{X}=\emptyset$, it follows that $A(V_1^{k_1}\cdots V_n^{k_n}\cdot\mathbf{y}) = A(\mathbf{x})$; i.e. $\partial_{\mathbb{X}}^-$ preserves the Alexander grading. □

**Proof of Theorem 4.6.3.** Equations (4.11) and (4.12) ensure that multiplication by $V_i$ is a homogeneous map of degree $(-2,-1)$; i.e. $GC^-(\mathbb{G})$ is a bigraded module over $\mathbb{F}[V_1,\dots,V_n]$. The differential is defined to be an $\mathcal{R}$-module homomorphism; Lemma 4.6.8 ensures that it is homogeneous of degree $(-1,0)$. The theorem now follows from Lemma 4.6.7. □

The complex $GC^-(\mathbb{G})$ generalizes $\widetilde{GC}(\mathbb{G})$, since

$$\frac{GC^-(\mathbb{G})}{V_1 = \ldots = V_n = 0} \cong \widetilde{GC}(\mathbb{G}). \tag{4.15}$$

We study now further properties of $GC^-(\mathbb{G})$.

LEMMA 4.6.9. *For any pair of integers $i,j \in \{1,\dots,n\}$ multiplication by $V_i$ is chain homotopic to multiplication by $V_j$, when thought of as homogeneous maps from $GC^-(\mathbb{G})$ to itself with degree $(-2,-1)$.*

**Proof.** Variables $V_i$ and $V_j$ are called *consecutive* if there is a square marked by $X$ in the same row as $O_i$ and in the same column as $O_j$. Suppose that $V_i$ and $V_j$ are consecutive, and let $X_i$ denote the $X$-marking in the same row as $O_i$ and in the same column as $O_j$. Define a corresponding homotopy operator that counts rectangles that contain $X_i$ in their interior:

$$\mathcal{H}_i(\mathbf{x}) = \mathcal{H}_{X_i}(\mathbf{x}) = \sum_{\mathbf{y}\in\mathbf{S}(\mathbb{G})}\ \sum_{\{r\in\mathrm{Rect}^\circ(\mathbf{x},\mathbf{y})\,\big|\,\mathrm{Int}(r)\cap\mathbb{X}=X_i\}} V_1^{O_1(r)}\cdots V_n^{O_n(r)}\cdot\mathbf{y}. \tag{4.16}$$

It follows immediately from Proposition 4.3.1 and Equation (4.4) that $\mathcal{H}_i$ is homogeneous of degree $(-1,-1)$. The proof of Lemma 4.6.7 shows that [1]

$$\partial_{\mathbb{X}}^- \circ \mathcal{H}_i + \mathcal{H}_i \circ \partial_{\mathbb{X}}^- = V_i - V_j.$$

In this adaptation, count decompositions of domains $\psi$ with $N(\psi) > 0$ and which contain $X_i$ (and no other $X \in \mathbb{X}$) with multiplicity one in their interior. In addition to the types of pairs appearing in Cases (R-1) and (R-2) of Lemma 4.6.7, there are two thin annuli that contribute to $\partial_{\mathbb{X}}^- \circ \mathcal{H}_i + \mathcal{H}_i \circ \partial_{\mathbb{X}}^-$, and those are the two annuli (horizontal and vertical) through $X_i$. The contributions of these two annuli are multiplication by $V_i$ and multiplication by $V_j$.

For general $V_i$ and $V_j$, since $K$ is a knot there is a sequence of variables $V_i = V_{n_1}, \dots, V_{n_m} = V_j$ where $V_{n_k}$ and $V_{n_{k+1}}$ are consecutive. Adding the chain homotopies, we deduce that $V_i$ is homotopic to $V_j$. □

Remark 4.6.10. Lemma 4.6.9 uses the fact that the grid diagram $\mathbb{G}$ represents a knot, rather than a link: in general, the actions of variables corresponding to different link components are not chain homotopic; cf. also Lemma 8.2.3. For more on the case of links, see Section 9.1 and Chapter 11.

Definition 4.6.11. Fix some $i \in \{1, \dots, n\}$. The ***unblocked grid homology of*** $\mathbb{G}$, denoted $GH^-(\mathbb{G})$, is the homology of $(GC^-(\mathbb{G}), \partial_{\mathbb{X}}^-)$, viewed as a bigraded module over $\mathbb{F}[U]$, where the action of $U$ is induced by multiplication by $V_i$.

Lemma 4.6.9 shows that the grid homology groups, thought of as bigraded modules over $\mathbb{F}[U]$, are independent of the choice of $i$. Lemma 4.6.9 also inspires the following further construction:

Definition 4.6.12. Fix some $i = 1, \dots, n$. The quotient complex $GC^-(\mathbb{G})/V_i$ is called the ***simply blocked grid complex***, and it is denoted $\widehat{GC}(\mathbb{G})$. The ***simply blocked grid homology of*** $\mathbb{G}$, $\widehat{GH}(\mathbb{G})$, is the bigraded vector space obtained as the homology of $\widehat{GC}(\mathbb{G}) = (GC^-(\mathbb{G})/V_i, \partial_{\mathbb{X}}^-)$.

Remark 4.6.13. Explicitly, $GC^-(\mathbb{G})/V_n$ is the bigraded $\mathbb{F}$-vector space with basis $V_1^{k_1} \cdots V_{n-1}^{k_{n-1}} \cdot \mathbf{x}$, where $k_1, \dots, k_{n-1}$ are arbitrary non-negative integers and $\mathbf{x} \in \mathbf{S}(\mathbb{G})$; equipped with a differential $\widehat{\partial}_{\mathbb{X},O_n}$ specified by $\widehat{\partial}_{\mathbb{X},O_n} \circ V_j = V_j \circ \widehat{\partial}_{\mathbb{X},O_n}$ for $j = 1, \dots, n-1$, and for any $\mathbf{x} \in \mathbf{S}(\mathbb{G})$,

$$\widehat{\partial}_{\mathbb{X},O_n}(\mathbf{x}) = \sum_{\mathbf{y} \in \mathbf{S}(\mathbb{G})} \sum_{\{r \in \mathrm{Rect}^\circ(\mathbf{x},\mathbf{y}) \big| r \cap \mathbb{X} = \emptyset, O_n(r) = 0\}} V_1^{O_1(r)} \cdots V_{n-1}^{O_{n-1}(r)} \cdot \mathbf{y}.$$

We shall see that $\widehat{GH}$ is a finite dimensional vector space that is independent of the choice of $i$, in Corollaries 4.6.16 and 4.6.17 below. But first, we explain how to extract the vector space $\widehat{GH}(\mathbb{G})$ from $\widetilde{GH}(\mathbb{G})$, in terms of the following notation. Let $X$ and $Y$ be two bigraded vector spaces

$$X = \bigoplus_{d,s \in \mathbb{Z}} X_{d,s} \qquad \text{and} \qquad Y = \bigoplus_{d,s \in \mathbb{Z}} Y_{d,s}.$$

[1] Note that $V_i - V_j = V_i + V_j$ in $\mathcal{R}$. We write $V_i - V_j$, since that expression is what shows up when we work with $\mathbb{Z}$ coefficients, as in Chapter 15.

Their tensor product $X \otimes Y = \bigoplus_{d,s\in\mathbb{Z}} (X\otimes Y)_{d,s}$ is the bigraded vector space, with

$$(X \otimes Y)_{d,s} = \bigoplus_{\substack{d_1+d_2=d\\ s_1+s_2=s}} X_{d_1,s_1} \otimes Y_{d_2,s_2}. \tag{4.17}$$

DEFINITION 4.6.14. Let $X$ be a bigraded vector space, and fix integers $a$ and $b$. The corresponding ***shift of*** $X$, denoted $X[\![a,b]\!]$, is the bigraded vector space that is isomorphic to $X$ as a vector space and given the bigrading $X[\![a,b]\!]_{d,s} = X_{d+a,s+b}$.

Let $W$ be the two-dimensional bigraded vector space with one generator in bigrading $(0,0)$ and another in bigrading $(-1,-1)$, and let $X$ be any other bigraded vector space, then the tensor product $X \otimes W$ is identified with two copies of $X$, one of which is equipped with a shift in degree:

$$X \otimes W \cong X \oplus X[\![1,1]\!]. \tag{4.18}$$

This can be iterated; for example, $X \otimes W^{\otimes 2} \cong X \oplus X[\![1,1]\!] \oplus X[\![1,1]\!] \oplus X[\![2,2]\!]$.

PROPOSITION 4.6.15. *Let $\mathbb{G}$ be a grid diagram representing a knot. Let $W$ be the two-dimensional bigraded vector space, with one generator in bigrading $(0,0)$ and the other in bigrading $(-1,-1)$. Then, there is an isomorphism*

$$\widetilde{GH}(\mathbb{G}) \cong \widehat{GH}(\mathbb{G}) \otimes W^{\otimes(n-1)} \tag{4.19}$$

*of bigraded vector spaces, where $\widehat{GH}(\mathbb{G}) = H(\frac{GC^-(\mathbb{G})}{V_i})$ for any $i = 1,\dots,n$.*

**Proof.** We will prove by induction on $j$ that

$$H\left(\frac{GC^-(\mathbb{G})}{V_1 = \cdots = V_j = 0}\right) \cong H\left(\frac{GC^-(\mathbb{G})}{V_1 = 0}\right) \otimes W^{\otimes(j-1)}. \tag{4.20}$$

We interpret $W^0$ as a one-dimensional vector space in bigrading $(0,0)$, so that the isomorphism $W^{\otimes a} \otimes W \cong W^{\otimes(a+1)}$ holds for all $a \geq 0$. In the basic case where $j = 1$, Equation (4.20) is a tautology.

For the inductive step, for $j > 1$ consider the short exact sequence
(4.21)

$$0 \longrightarrow \frac{GC^-(\mathbb{G})}{V_1=\cdots=V_{j-1}=0} \xrightarrow{V_j} \frac{GC^-(\mathbb{G})}{V_1=\cdots=V_{j-1}=0} \longrightarrow \frac{GC^-(\mathbb{G})}{V_1=\cdots=V_j=0} \longrightarrow 0.$$

Using Proposition 4.5.6, the chain homotopy between $V_j$ and $V_1$ provided by Lemma 4.6.9, induces a chain homotopy between the chain map

$$V_j \colon \frac{GC^-(\mathbb{G})}{V_1 = \cdots = V_{j-1} = 0} \to \frac{GC^-(\mathbb{G})}{V_1 = \cdots = V_{j-1} = 0}$$

and the 0 map, so the long exact sequence on homology associated to the short exact squence from Equation (4.21) (cf. Lemma 4.5.3) becomes a short exact sequence

$$0 \longrightarrow H(\tfrac{GC^-(\mathbb{G})}{V_1=\cdots=V_{j-1}=0}) \longrightarrow H(\tfrac{GC^-(\mathbb{G})}{V_1=\cdots=V_j=0}) \longrightarrow H(\tfrac{GC^-(\mathbb{G})}{V_1=\cdots=V_{j-1}=0}) \longrightarrow 0,$$

where the second arrow preserves bigradings, and the third is homogeneous of degree $(1,1)$. Thus, this short exact sequence of vector spaces translates into the first isomorphism of bigraded vector spaces appearing in the following:

$$H\left(\frac{GC^-(\mathbb{G})}{V_1=\cdots=V_j=0}\right)\cong H\left(\frac{GC^-(\mathbb{G})}{V_1=\cdots=V_{j-1}=0}\right)\otimes W\cong \widehat{GH}(\mathbb{G})\otimes W^{\otimes(j-1)},$$

and the second isomorphism follows from the inductive hypothesis. This completes the inductive step, verifying Equation (4.20) for all $j=1,\dots,n$.

In view of Equation (4.15), when $j=n$, Equation (4.20) gives Equation (4.19) for $i=1$. Numbering our formal variables differently, we conclude that Equation (4.19) holds for arbitrary $i$. □

The chain complex $\widetilde{GC}(\mathbb{G})$ is finite dimensional over $\mathbb{F}$, so its homology $\widetilde{GH}(\mathbb{G})$ is also finite dimensional. Although $\widehat{GC}(\mathbb{G})$ is infinite dimensional over $\mathbb{F}$, Proposition 4.6.15 has the following immediate consequence:

Corollary 4.6.16. *For a grid diagram $\mathbb{G}$ with grid number $n$, the vector space $\widehat{GH}(\mathbb{G})$ is finite dimensional, the dimension of $\widetilde{GH}(\mathbb{G})$ is divisible by $2^{n-1}$, and in fact $2^{n-1}\cdot\dim_{\mathbb{F}}\widehat{GH}(\mathbb{G})=\dim_{\mathbb{F}}\widetilde{GH}(\mathbb{G})$.* □

Corollary 4.6.17. *The simply blocked grid homology $\widehat{GH}(\mathbb{G})=H(GC^-(\mathbb{G})/V_i)$ is independent of the choice of $i=1,\dots,n$.*

**Proof.** From Proposition 4.6.15, it follows that for $i,j$,

$$H\left(\frac{GC^-(\mathbb{G})}{V_i}\right)\otimes W^{(n-1)}\cong H\left(\frac{GC^-(\mathbb{G})}{V_j}\right)\otimes W^{(n-1)} \tag{4.22}$$

as bigraded vector spaces.

Just as a finite dimensional vector space is determined up to isomorphism by its dimension, a finite dimensional bigraded vector space $Y$ is determined up to isomorphism by its *Poincaré polynomial* $P_Y$, the Laurent polynomial in $q$ and $t$:

$$P_Y(q,t)=\sum_{d,s\in\mathbb{Z}}\dim Y_{d,s}\cdot q^d t^s. \tag{4.23}$$

Letting $Y_i=H(\frac{GC^-(\mathbb{G}))}{V_i})$, Equation (4.22) translates into the equation

$$(1+q^{-1}t^{-1})^{n-1}\cdot P_{Y_i}(q,t)=(1+q^{-1}t^{-1})^{n-1}\cdot P_{Y_j}(q,t),$$

so $P_{Y_i}=P_{Y_j}$, and hence $H(\frac{GC^-(\mathbb{G})}{V_i})\cong H(\frac{GC^-(\mathbb{G})}{V_j})$ as bigraded vector spaces. □

Another relation among the grid homology groups is given by the following:

Proposition 4.6.18. *There is a long exact sequence relating $\widehat{GH}(\mathbb{G})$ and $GH^-(\mathbb{G})$:*

$$\cdots\to GH^-_{d+2}(\mathbb{G},s+1)\xrightarrow{U} GH^-_d(\mathbb{G},s)\to\widehat{GH}_d(\mathbb{G},s)\to GH^-_{d+1}(\mathbb{G},s+1)\dots$$

**Proof.** Consider the short exact sequence

$$0\to GC^-(\mathbb{G})\xrightarrow{V_i} GC^-(\mathbb{G})\to\widehat{GC}(\mathbb{G})\to 0$$

of bigraded chain complexes of $\mathbb{F}[V_i]$-modules, where the first map is, of course, homogeneous of degree $(-2,-1)$. The associated long exact sequence in homology (Lemma 4.5.3) gives the statement of the proposition. □

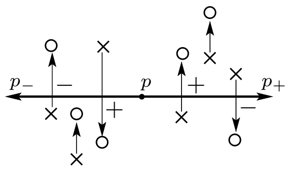


FIGURE 4.6. **Winding numbers**. The diagram illustrates the equality $w_{\mathcal{D}}(p) = \mathcal{I}(p, \mathbb{O} - \mathbb{X})$ (interpreting the winding number as intersection of the knot projection with the ray $p_+$), and at the same time the equality $w_{\mathcal{D}}(p) = \mathcal{I}(\mathbb{O} - \mathbb{X}, p)$ (interpreting the winding number as intersection with the ray $p_-$).

A key feature of the grid homology groups $\widehat{GH}(\mathbb{G})$ and $GH^-(\mathbb{G})$ is that they are knot invariants, in the following sense.

THEOREM 4.6.19. *The homologies $\widehat{GH}(\mathbb{G})$ and $GH^-(\mathbb{G})$ (the former thought of as a bigraded $\mathbb{F}$-vector space, the latter thought of as a bigraded $\mathbb{F}[U]$-module) depend on the grid $\mathbb{G}$ only through its underlying (unoriented) knot $K$.*

The proof of the above theorem will be given in Chapter 5.

## 4.7. The Alexander grading as a winding number

The aim of the present section is to give geometric insight into the bigrading from Section 4.3. Byproducts include a practical formula for computing $A$ and a relationship between grid homology and the Alexander polynomial. The geometric interpretation of the Alexander grading rests on the following formula, which expresses the winding number about a knot projection in terms of planar grid diagrams.

LEMMA 4.7.1. *Let $\mathbb{G}$ be a planar grid diagram of a knot $K$, let $\mathcal{D} = \mathcal{D}(\mathbb{G})$ be the corresponding knot projection in the plane, and let $p$ be any point not on $\mathcal{D}$. Then, the winding number $w_{\mathcal{D}}(p)$ of $\mathcal{D}$ around $p$ is computed by the formula*

$$w_{\mathcal{D}}(p) = \mathcal{J}(p, \mathbb{O} - \mathbb{X}). \tag{4.24}$$

**Proof.** If $p = (x, y)$ is any point not contained in $\mathcal{D}$, then $\mathcal{I}(p, \mathbb{O} - \mathbb{X})$ is the (signed) intersection number of the ray $p_+$ from $p$ to $(+\infty, y)$ with $\mathcal{D}$: the vertical arc connecting some $O$ with $X$ contributes $+1$ if the $O$ lies in this upper right quadrant and the $X$ does not, and it contributes $-1$ if the $X$ lies in this upper right quadrant and the $O$ does not, and it contributes $0$ otherwise; i.e.

$$\#(p_+ \cap \mathcal{D}) = \mathcal{I}(p, \mathbb{O} - \mathbb{X}).$$

Similarly, the intersection number of the ray $p_-$ from $p$ to $(-\infty, y)$ with $\mathcal{D}$ is

$$\#(p_- \cap \mathcal{D}) = \mathcal{I}(\mathbb{O} - \mathbb{X}, p).$$

Clearly, $w_{\mathcal{D}}(p) = \#(p_+ \cap \mathcal{D}) = \#(p_- \cap \mathcal{D})$. Average the above two equations to get Equation (4.24). $\square$

Fix a planar realization of a toroidal grid diagram, and consider the function $A'$ on the grid state $\mathbf{x} \in \mathbf{S}(\mathbb{G})$ defined by

$$A'(\mathbf{x}) = -\sum_{x \in \mathbf{x}} w_{\mathcal{D}}(x). \tag{4.25}$$

As we shall see shortly, $A$ and $A'$ differ by a constant (independent of the grid state). We express this constant in terms of quantities which we have met already in Section 3.3. To this end, recall that each of the $2n$ squares marked with an $X$ or $O$ has 4 corners, giving us a total of $8n$ lattice points on the grid (possibly counted with multiplicity, when the marked squares share a corner), which we denote $p_1, \dots, p_{8n}$. The sum of the winding numbers at these points, divided by 8, was denoted by $a(\mathbb{G})$ in Section 3.3. The precise relationship between $A$ and $A'$ can now be stated as follows:

PROPOSITION 4.7.2. *Choose a planar realization of a toroidal grid diagram $\mathbb{G}$ representing a knot $K$. Let $\mathcal{D}$ be the corresponding diagram of $K$. The Alexander function $A$ can be expressed in terms of the winding numbers $w_{\mathcal{D}}$ by the following formula:*

$$A(\mathbf{x}) = -\sum_{x \in \mathbf{x}} w_{\mathcal{D}}(x) + \frac{1}{8}\sum_{j=1}^{8n} w_{\mathcal{D}}(p_j) - \left(\frac{n-1}{2}\right) = A'(\mathbf{x}) + a(\mathbb{G}) - \frac{n-1}{2}. \tag{4.26}$$

**Proof.** Summing Equation (4.24) over all the components $x \in \mathbf{x}$, gives $A'(\mathbf{x}) = -\mathcal{J}(\mathbf{x}, \mathbb{O} - \mathbb{X})$; so

$$\begin{aligned} A(\mathbf{x}) &= \frac{1}{2}(M_{\mathbb{O}}(\mathbf{x}) - M_{\mathbb{X}}(\mathbf{x})) - \left(\frac{n-1}{2}\right) \\ &= -\mathcal{J}(\mathbf{x}, \mathbb{O} - \mathbb{X}) + \frac{1}{2}(\mathcal{J}(\mathbb{O},\mathbb{O}) - \mathcal{J}(\mathbb{X},\mathbb{X})) - \left(\frac{n-1}{2}\right) \\ &= A'(\mathbf{x}) + \frac{1}{2}\mathcal{J}(\mathbb{O}+\mathbb{X}, \mathbb{O}-\mathbb{X}) - \left(\frac{n-1}{2}\right). \end{aligned}$$

Thus, Equation (4.26) now follows once we show that

$$\frac{1}{2}\mathcal{J}(\mathbb{O}+\mathbb{X}, \mathbb{O}-\mathbb{X}) = \frac{1}{8}\sum_{i=1}^{8n} w_{\mathcal{D}}(p_i). \tag{4.27}$$

To check Equation (4.27), we first verify the following: given any small square (in a planar grid) whose center $z$ is marked with an $O$ or an $X$, if $z_1, \dots, z_4$ denote its four corner points in the plane, then

(4.28)

$$\mathcal{J}(z, \mathbb{O}-\mathbb{X}) = \frac{1}{4}\mathcal{J}(z_1+z_2+z_3+z_4, \mathbb{O}-\mathbb{X}) + \begin{cases} -\frac{1}{4} & \text{if } z \text{ is marked with an } O \\ \frac{1}{4} & \text{if } z \text{ is marked with an } X. \end{cases}$$

Suppose for definiteness that $z$ is marked with an $O$. Then, for any marking $O' \in \mathbb{O}$ with $O \neq O'$,

$$\mathcal{J}(z, O') = \frac{1}{4}\mathcal{J}(z_1+z_2+z_3+z_4, O').$$

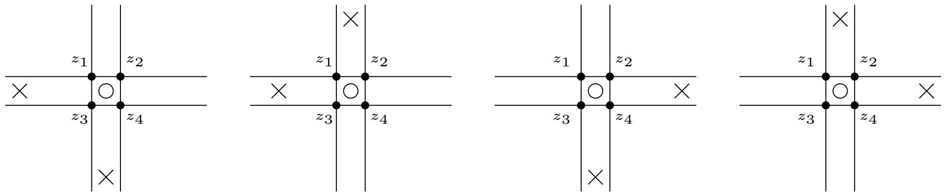

FIGURE 4.7. **Verification of Equation (4.28).** Here are the four cases where the distinguished square $z$ is marked with an $O$. To verify the equation, find the pairs contributing to $\mathcal{J}(z_1+\cdots+z_4, X)$, where $X$ is in the same row or column as $z$, and to $\mathcal{J}(z_1+\cdots+z_4, O)$, where the $O$-marking is at $z$.

Also, for any $X$-marking not in the same row or column as $z$,

$$\mathcal{J}(z,X) = \frac{1}{4}\mathcal{J}(z_1+z_2+z_3+z_4, X).$$

The correction of $-\frac{1}{4}$ comes from the pairing of the $X$-markings in the same row and column as $z$ with the formal sum $z_1+\cdots+z_4$, combined with the pairing of the $O$-marking on $z$ with $z_1+\cdots+z_4$; see Figure 4.7. A similar reasoning gives Equation (4.28) when $z$ is marked with an $X$.

Equation (4.27) follows from summing up Equation (4.28) over all $O$- and $X$-marked squares, and using Lemma 4.7.1. $\square$

LEMMA 4.7.3. *The sign of the permutation that connects* $\mathbf{x}$ *with* $\mathbf{x}^{NWO}$ *is* $(-1)^{M(\mathbf{x})}$.

**Proof.** This is an immediate consequence of Proposition 4.3.1, combined with the mod 2 reductions of Equations (4.1) and (4.2). $\square$

DEFINITION 4.7.4. Let $X = \bigoplus_{d,s} X_d$ be a bigraded vector space. Define the ***graded Euler characteristic of*** $X$ to be the Laurent polynomial in $t$ given by

$$\chi(X) = \sum_{d,s} (-1)^d \dim X_{d,s} \cdot t^s.$$

The Euler characteristic of grid homology is related to the Alexander polynomial, according to the following:

PROPOSITION 4.7.5. *Let* $\mathbb{G}$ *be a grid diagram for a knot* $K$ *with grid index* $n$. *The graded Euler characteristic of the bigraded vector space* $\widetilde{GH}(\mathbb{G})$ *is given by*

$$\chi(\widetilde{GH}(\mathbb{G})) = (1-t^{-1})^{n-1}\cdot \Delta_K(t), \tag{4.29}$$

*where* $\Delta_K(t)$ *is the symmetrized Alexander polynomial of Equation* (2.3).

**Proof.** It is a standard fact that the Euler characteristic of a chain complex agrees with that of its homology (and this fact remains true in the bigraded case). Thus,

$$\chi(\widetilde{GH}(\mathbb{G})) = \chi(\widetilde{GC}(\mathbb{G})) = \sum_{\mathbf{x}\in\mathbf{S}(\mathbb{G})} (-1)^{M(\mathbf{x})} t^{A(\mathbf{x})}.$$

By Proposition 4.7.2 (for the $t$-power) and Lemma 4.7.3 together with Proposition 4.3.7 (for the sign), it follows that this graded Euler characteristic agrees with

$$\sum_{\mathbf{x}}(-1)^{M(\mathbf{x})}t^{A(\mathbf{x})} = (-1)^{n-1}\epsilon(\mathbb{G}) \cdot \det(\mathbf{M}(\mathbb{G})) \cdot t^{a(\mathbb{G})} \cdot t^{\frac{1-n}{2}}.$$

The result now follows from Theorem 3.3.6. □

Proposition 4.7.5 relates the Euler characteristic of $\widetilde{GH}(\mathbb{G})$ and the Alexander polynomial of the underlying knot. This leads quickly to the following relationship between the Alexander polynomial and the graded Euler characteristic of $\widehat{GH}$

$$\chi(\widehat{GH}(K)) = \sum_{d,s}(-1)^d \dim\ \widehat{GH}_d(K,s) \cdot t^s \in \mathbb{Z}[t,t^{-1}]. \tag{4.30}$$

Theorem 4.7.6 ([**173, 192**]). *The graded Euler characteristic of the simply blocked grid homology is equal to the (symmetrized) Alexander polynomial $\Delta_K(t)$:*

$$\chi(\widehat{GH}(K)) = \Delta_K(t).$$

**Proof.** The graded Euler characteristic of the bigraded vector space $W$ from Lemma 4.6.15 is $\chi(W) = 1 - t^{-1}$, so the identity follows immediately from Propositions 4.7.5 and 4.6.15. □

## 4.8. Computations

Assuming Theorem 4.6.19, we can directly compute some of the homology groups defined earlier in this chapter. See also Chapter 10 for more computations.

Proposition 4.8.1. *For the unknot $\mathcal{O}$, $\widehat{GH}(\mathcal{O}) \cong \mathbb{F}$ is supported in bigrading $(0,0)$; and $GH^-(\mathcal{O}) \cong \mathbb{F}[U]$ as $\mathbb{F}[U]$-modules, and its generator has bigrading $(0,0)$.*

**Proof.** In the $2\times 2$ grid diagram $\mathbb{G}$ representing the unknot, there are exactly two generators; call them $\mathbf{p}$ and $\mathbf{q}$, with $A(\mathbf{p}) = 0$, $M(\mathbf{p}) = 0$, $A(\mathbf{q}) = -1$, $M(\mathbf{q}) = -1$. The complex $GC^-(\mathbb{G})$ is generated over $\mathbb{F}[V_1,V_2]$ by these two generators, and its boundary map is specified by

$$\partial^-_{\mathbb{X}}(\mathbf{p}) = 0, \qquad \partial^-_{\mathbb{X}}(\mathbf{q}) = (V_1 + V_2)\cdot\mathbf{p}.$$

The homology of this complex is clearly isomorphic to $\mathbb{F}[U]$, generated by the cycle $\mathbf{p}$; this completes the computation of $GH^-(\mathcal{O})$.

For $\widehat{GH}(\mathcal{O})$, we can set $V_2 = 0$, to obtain the complex over $\mathbb{F}[V_1]$ with generators $\mathbf{p}$ and $\mathbf{q}$, and boundary specified by

$$\partial^-_{\mathbb{X}}(\mathbf{p}) = 0, \qquad \partial^-_{\mathbb{X}}(\mathbf{q}) = V_1\cdot\mathbf{p},$$

whose homology is $\mathbb{F}$, generated by the cycle $\mathbf{p}$. □

With more work, one can show that the grid homology groups of the right-handed trefoil knot $K = T_{2,3}$ are given by:

$$\widehat{GH}_d(K,s) = \begin{cases} \mathbb{F} & \text{if } (d,s) \in \{(0,1),(-1,0),(-2,-1)\} \\ 0 & \text{otherwise.} \end{cases} \tag{4.31}$$

$$GH^-_d(K,s) = \begin{cases} \mathbb{F} & \text{if } (d,s) = (0,1) \text{ or } (d,s) = (-2k,-k) \text{ for } k \geq 1 \\ 0 & \text{otherwise.} \end{cases} \tag{4.32}$$

In the second case, the $\mathbb{F}[U]$-module structure is determined by the property that $U\colon GH^-_{-2k}(K,-k) \to GH^-_{-2k-2}(K,-k-1)$ is an isomorphism for all $k \geq 1$. More succinctly, we write

$$GH^-(K) \cong (\mathbb{F}[U]/U)_{(0,1)} \oplus (\mathbb{F}[U])_{(-2,-1)},$$

where the subscripts on the cyclic $\mathbb{F}[U]$-modules denote the bigradings of their generators.

EXERCISE 4.8.2. Let $K$ denote the right-handed trefoil knot.
**(a)** Use Figure 3.3 to verify Equation (4.31). (*Hint:* Show first that there are no generators for $\widetilde{GC}(\mathbb{G})$ in Alexander grading greater than 1. Next, find generators of $\widetilde{GC}(\mathbb{G})$ in Alexander gradings 0, 1, and $-5$, and apply Proposition 4.6.15.)
**(b)** Verify Equation (4.32). (*Hint:* Proposition 4.6.18 might be helpful.)
**(c)** Let $K$ denote the left-handed trefoil knot. Compute $\widehat{GH}(K)$ and $GH^-(K)$.

REMARK 4.8.3. The result of Exercise 4.8.2 shows that grid homology distinguishes the right-handed trefoil $T_{2,3}$ from its mirror $T_{-2,3}$. See Proposition 7.1.2 for a general description of how homology behaves under reflection.

Restricting attention to a carefully chosen Alexander grading, we can give a more general computation valid for all torus knots.

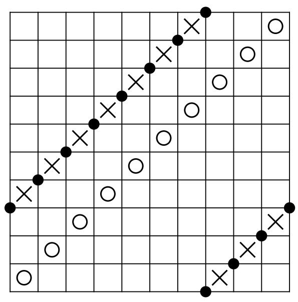

FIGURE 4.8. **Grid diagram for $T_{-3,7}$.** This is the diagram for $T_{-p,q}$ from Exercise 3.1.5(c), when $p = 3$ and $q = 7$. The grid state $\mathbf{x}^+$ is indicated by the heavy dots in the grid.

LEMMA 4.8.4. *Let $p, q > 1$ relatively prime integers. There is a grid diagram $\mathbb{G}$ for $T_{-p,q}$ with the following property. If $\mathbf{x}^+ = \mathbf{x}^{NEX}$ is the grid state which occupies the upper right corner of each square marked with $X$, then this grid state is the unique generator with maximal Alexander grading among all generators, and*

$$A(\mathbf{x}^+) = \frac{(p-1)(q-1)}{2}.$$

**Proof.** Let $\mathbb{G}$ be the $(p+q)\times(p+q)$ grid diagram with $\sigma_{\mathbb{O}}=(1,\dots,p+q)$ and $\sigma_{\mathbb{X}}=(p+1,p+2,\dots,p)$; see Figure 4.8. (Compare also Exercise 3.1.5(c)).

Consider the associated winding matrix $M_{p,q}=\mathbf{W}(\mathbb{G})$. In the $j^{th}$ row, the winding numbers start out zero for a while, they increase by 1's until they reach their maximum, then they stay constant, and then eventually they drop by 1's. More precisely: the left column and bottom row vanish; for $j=1,\dots,q$, in the $j^{th}$ row (from the top), the first $q-j+1$ entries are 0 and all others are positive; while for $j=q+1,\dots,p+q-1$, the last $j-q$ entries and the first entry are 0 and all others are positive.

For example, for the torus knot $T_{-3,7}$ from Figure 4.8, this matrix is

$$M_{3,7}=\begin{pmatrix}0&0&0&0&0&0&0&1&1&1\\0&0&0&0&0&0&1&2&2&1\\0&0&0&0&0&1&2&3&2&1\\0&0&0&0&1&2&3&3&2&1\\0&0&0&1&2&3&3&3&2&1\\0&0&1&2&3&3&3&3&2&1\\0&1&2&3&3&3&3&3&2&1\\0&1&2&2&2&2&2&2&1&0\\0&1&1&1&1&1&1&1&0&0\\0&0&0&0&0&0&0&0&0&0\end{pmatrix}.$$

It follows at once that for $\mathbf{x}^+$ all the winding numbers are zero, and for all other grid states $\mathbf{x}$, the sum of the winding numbers $-A'(\mathbf{x})$ is positive; so by Proposition 4.7.2, $\mathbf{x}^+$ is the unique grid state with maximal Alexander grading.

Elementary computation shows that

$$\mathcal{J}(\mathbf{x}^+,\mathbf{x}^+)=\frac{p(p-1)+q(q-1)}{2}\qquad \mathcal{J}(\mathbb{O},\mathbb{O})=\frac{(p+q)(p+q-1)}{2}$$
$$\mathcal{J}(\mathbf{x}^+,\mathbb{O})=\frac{p^2+q^2}{2}\qquad M_{\mathbb{X}}(\mathbf{x}^+)=1-p-q;$$

so using Definition 4.3.2 we find that

$$A(\mathbf{x}^+)=\frac{1}{2}(M_{\mathbb{O}}(\mathbf{x}^+)-M_{\mathbb{X}}(\mathbf{x}^+))-\frac{p+q-1}{2}=\frac{(p-1)(q-1)}{2}.$$

$\square$

Proposition 4.8.5. *Fix relatively prime, positive integers $p$ and $q$ with $p,q>1$. Some of the grid homology groups $\widehat{GH}(T_{-p,q})$ are given by the following:*

$$\widehat{GH}_d(T_{-p,q},s)=\begin{cases}\mathbb{F} & \text{if } s=\frac{(p-1)(q-1)}{2} \text{ and } d=(p-1)(q-1)\\ 0 & \text{if } s=\frac{(p-1)(q-1)}{2} \text{ and } d\neq(p-1)(q-1)\\ 0 & \text{if } s>\frac{(p-1)(q-1)}{2}.\end{cases}$$

**Proof.** According to Lemma 4.8.4, $\widehat{GC}(T_{-p,q})$ has no generators with Alexander grading greater than $\frac{(p-1)(q-1)}{2}$; and it has a single one with Alexander grading equal to $\frac{(p-1)(q-1)}{2}$. The formulas in the proof of Lemma 4.8.4 also show that $M(\mathbf{x}^+) = (p-1)(q-1)$. $\square$

To give further examples, we find it convenient to encode the grid homology by its Poincaré polynomial $P_K(q,t) = \sum_{d,s} \dim \widehat{GH}_d(K,s)t^s q^d$ (introduced in Equation (1.2)). Using a direct computer computation, Baldwin and Gillam [**5**] computed the grid homology of all knots with at most twelve crossings. In particular, for the eleven crossing Kinoshita-Terasaka knot $KT$ and for its Conway mutant $C$ of Figure 2.7 (compare also [**183**, Section 5.4] and [**180**, Section 3]) they found that:

$$P_{KT}(q,t) = (q^{-3}+q^{-2})t^{-2}+4(q^{-2}+q^{-1})t^{-1}+6q^{-1}+7+4(1+q)t+(q+q^2)t^2, \tag{4.33}$$

$$\begin{aligned} P_C(q,t) = {} & (q^{-4}+q^{-3})t^{-3} + 3(q^{-3}+q^{-2})t^{-2} + 3(q^{-2}+q^{-1})t^{-1} + 2q^{-1} \\ & +3 + 3(1+q)t + 3(q+q^2)t^2 + (q^2+q^3)t^3. \end{aligned} \tag{4.34}$$

(Among non-trivial knots with at most eleven crossings, these are the two knots with Alexander polynomial equal to $1$.)

Although these are not computations one would wish to perform by hand, there are pieces which can be verified directly. For example:

EXERCISE 4.8.6. Consider Figure 4.9, a grid diagram for the Conway knot.
**(a)** Show that the grid states pictured on the figure are the only two grid states in Alexander grading $3$, and that there are no grid states in greater Alexander grading.
**(b)** Show that there are no empty rectangles connecting the two grid states. Use this to verify that the coefficient in front of the $t^3$ term in the Poincaré polynomial of the Conway knot $P_C(q,t)$ is, indeed, $(q^2+q^3)$, as stated in Equation (4.34), and that all higher $t$-powers have vanishing coefficients.

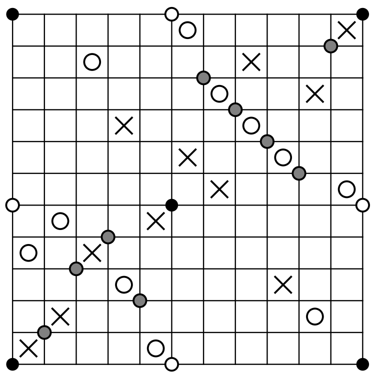

FIGURE 4.9. **Two grid states for the Conway knot.** The white ones appear only in one of the grid states, the black ones appear only in the other, and the gray dots appear in both.

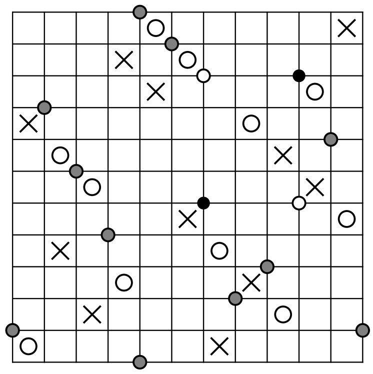

FIGURE 4.10. **Two grid states for the Kinoshita-Terasaka knot.** We have exhibited here two grid states on the same grid, with the same conventions as in Figure 4.9.

EXERCISE 4.8.7. Consider the grid diagram of the Kinoshita-Terasaka knot $KT$ from Figure 4.10. (Notice that the diagram for the Kinoshita-Terasaka knot we gave in Figure 3.4 differs from this diagram by a single commutation.)
**(a)** Show that there are exactly four grid states in Alexander grading $2$, and none with Alexander grading greater than $2$. (*Hint:* Two of the grid states in Alexander grading $2$ are pictured in Figure 4.10. Find the other two.)
**(b)** Show that the homology of the resulting chain complex in Alexander grading $2$ has dimension $2$. Use this to verify that the coefficient in front of $t^2$ in $P_{KT}(q,t)$ is $(q^2+q^1)$, and all coefficients with higher $t$-powers vanish, as stated in Equation (4.33).

REMARK 4.8.8. For a typical grid diagram of the Kinoshita-Terasaka knot with grid number $11$, the number of generators in Alexander grading $2$ is rather large. For the choice we gave here, there are four generators, and this makes the computation of the grid homology in this Alexander grading easy.

## 4.9. Further remarks

The argument from Lemma 4.6.7 is a combinatorial analogue of the proof, in Lagrangian Floer homology, that the Lagrangian Floer complex is, in fact, a chain complex. The proof in that case hinges on Gromov's compactness theorem, together with gluing results for solutions of the relevant non-linear Cauchy-Riemann operator. These results are key ingredients in the development of Lagrangian Floer homology. Likewise, the combinatorial arguments from Lemma 4.6.7, although they are much simpler, also lie at the core of grid homology. Arguments of this type will appear throughout the text. (See for example Lemma 4.6.9 and Lemma 5.1.4.)

CHAPTER 17

# Open problems

In this chapter we collect open problems which are naturally related to grid diagrams and grid homologies. We have divided these problems into two sections: in Section 17.1, we collected problems about grid diagrams and grid homology, and in Section 17.2, we discuss problems in knot Floer homology. Some of the problems in Section 17.1 have already been solved using the holomorphic theory; in that case, we are asking for a proof within the framework of grid homology (i.e. without appealing to the equivalence with the holomorphic theory).

## 17.1. Open problems in grid homology

**Unknot detection.** Knot Floer homology is known to detect the unknot. (See Theorem 1.3.1.) From the equivalence between grid homology and knot Floer homology, it follows that grid homology detects the unknot.

Problem 17.1.1. Use grid diagrams directly to show that grid homology detects the unknot; that is, show that a knot $K \subset S^3$ with $\widehat{GH}(K) = \mathbb{F}$ is the unknot.

**Seifert genus.** In fact, knot Floer homology (and therefore grid homology) detects the Seifert genus of a knot. (See Theorem 1.3.2.) Once again, the proof of this result relies on the holomorphic version of the theory.

Problem 17.1.2. Without appealing to the equivalence with the holomorphic theory, show that grid homology detects the Seifert genus of a knot; that is, for any knot $K \subset S^3$,

$$g(K) = \max\{s \mid \widehat{GH}_*(K, s) \neq 0\}.$$

Note that Dynnikov [**37**] has an algorithm for detecting the unknot using grid diagrams. This result prompts the following question:

Problem 17.1.3. Is there a direct algorithm for detecting knot genus using grid diagrams, in the spirit of Dynnikov's unknot detection algorithm?

An optimistic version of the above is the following question: if $\mathbb{G}$ is a grid diagram for a knot $K$ whose associated genus is minimal among all grid diagrams $\mathbb{G}'$ that differ from $\mathbb{G}$ by sequences of commutation moves, does it follow that either (1) $\mathbb{G}$ can be destabilized after a sequence of commutation moves or (2) the associated genus of $\mathbb{G}$ agrees with the Seifert genus of $K$?

**Fiberedness.** In a similar vein, Theorem 1.3.3 shows that knot Floer homology detects whether or not a knot is fibered. The proof relies on the holomorphic geometric definition of knot Floer homology.

PROBLEM 17.1.4. Without appealing to the equivalence with the holomorphic theory, show that grid homology detects fiberedness of a knot; that is, any knot $K$ of genus $g(K)$ is fibered if and only if $\mathrm{rk}\ \widehat{GH}_*(K, g(K)) = 1$.

A few easier, related problems along these lines are the following.

PROBLEM 17.1.5. Suppose that $K$ is a fibered knot with genus $g(K)$. Is there a grid diagram $\mathbb{G}$ with the property that there is a unique grid state in Alexander grading $s = g(K)$ and no grid states in any larger grading?

For torus knots, a grid diagram with the above property was given in Lemma 4.8.4.

PROBLEM 17.1.6. Show directly that if $\mathbb{G}$ is a grid diagram with a unique grid state $\mathbf{x}$ in some grading $s$ and no grid states in any larger grading, then $K$ is fibered.

A theorem of Stallings [**214**] states that $K$ is fibered if and only if the commutator subgroup of $\pi_1(S^3 \setminus K)$ is finitely generated. Perhaps the presentation of $\pi_1(S^3 \setminus K)$ described in Lemma 3.5.1 is useful in considering these questions.

**Computations.** For knots with sufficiently small grid number, grid homology can be explicitly computed, especially with the help of a computer. Computations of the grid homology groups of infinite families of knots is typically harder. Grid homology groups of certain infinite families of knots were computed in Chapters 9 and 10.

An important infinite family one might wonder about is the case of torus knots. According to Theorem 16.2.6, the knot Floer homology for a positive torus knot can be computed directly from the Alexander polynomial of the knot. That formula can be proved either by working with a suitable genus-1 Heegaard diagram, or by appealing to more abstract principles [**178**].

PROBLEM 17.1.7. Compute the grid homology of the torus knot $T_{p,q}$ purely within the framework of grid homology.

**Naturality.** We have shown that two grid diagrams representing isotopic knots have isomorphic grid homology groups.

PROBLEM 17.1.8. Does an isotopy between two knots induce a well-defined isomorphism between the corresponding unblocked grid homology groups?

There are analogous questions for the simply blocked theory, which involves choosing a particular point $p$ on the knot (corresponding to the special $O_i$ marking in the diagram). In this case, one would expect pointed isotopies to induce maps between the simply blocked invariants.

To put this into context, for $i = 1, 2$, let $(S^3, K_i, p_i)$ be a knot equipped with a basepoint $p_i \in K_i$. In [**98**], it is shown that a diffeomorphism from $S^3$ to itself carrying $K_1$ to $K_2$ and $p_1$ to $p_2$ induces a well-defined isomorphism between the corresponding knot Floer homology groups $\widehat{\mathrm{HFK}}$. Sarkar [**204**] has defined and computed the action of moving the basepoint around the knot.

**Maps associated to knot cobordisms.**

PROBLEM 17.1.9. Does an oriented knot cobordism from $K_1$ to $K_2$ induce a map between the corresponding grid homology groups?

As noted earlier, it is natural to expect that the surfaces appearing above also should have some additional structure.

Candidate maps associated to one-handles appear in Chapters 8 and 9; compare also [**95**].

As a special case, a slice disk should induce an element of knot Floer homology.

Problem 17.1.10. Can knot Floer homology be used to distinguish pairwise non-isotopic slice disks for a given knot?

In a different direction:

Problem 17.1.11. Does an unoriented knot cobordism from $K_1$ to $K_2$ induce a map between the corresponding simply blocked grid homology groups?

Candidate maps associated to one-handles, in a sufficiently stabilized setting, appear in the unoriented skein exact sequence.

**Spectrum-valued refinement.**

Problem 17.1.12. Is there a space $X_{\vec{L}}$ that can be associated to an oriented link $\vec{L}$, that is functorial under oriented saddle moves, and whose singular homology coincides with $\widehat{GH}(\vec{L})$?

Since the Maslov grading can take negative values, we need to have a variant of spaces that have homology in negative dimension. Such a generalized version of a space exists in algebraic topology: it is called a *spectrum*, see for example [**228**].

In [**206**], Sarkar constructed spaces that correspond to certain quotient complexes of $\widetilde{GH}(\mathbb{G})$. Sarkar conjectures that these could be fit together in a natural way to construct the spectrum asked for in Problem 17.1.12. More generally, one might hope to find a spectrum $X_K^-$ with an $S^1$-action, whose $S^1$-equivariant cohomology is $GH^-(K)$. A further challenge would be to find a filtration on a spectrum, generalizing the filtered quasi-isomorphism type from Chapter 13.

Note that for Seiberg-Witten theory, and $Y$ a rational homology three-sphere, Manolescu [**130**] constructed an $S^1$-spectrum whose $S^1$-equivariant cohomology is monopole Floer homology. This construction uses analysis of the Seiberg-Witten monopole equations; see also [**129**].

In a different direction, Lipshitz and Sarkar [**122**] constructed a spectrum associated to Khovanov homology.

## 17.2. Open problems in knot Floer homology

**Knot Floer homology and the fundamental group.** It would be very interesting to find a concrete relationship between the fundamental group of the complement of a knot and its knot Floer homology. One possible relationship is provided by a conjecture of Kronheimer and Mrowka [**111**], stating that the dimension of knot Floer homology (with coefficients in a field of characteristic zero) is equal to the dimension of instanton knot Floer homology [**53**]. Note that Floer's instanton homology is related to certain $SO(3)$ representations of the fundamental group of the knot complement. For other connections between Heegaard Floer homology and the fundamental group, see [**15**].

**The Fox-Milnor condition.** Many of the properties of knot Floer homology are lifts or generalizations of various familiar properties of the Alexander polynomial. Conspicuously missing from this list is the Fox-Milnor condition: if $K$ is a slice knot, then there is a polynomial $f$ in $t$ with the property that $\Delta_K(t) = f(t)\cdot f(t^{-1})$. One might think that this generalizes to the statement that if $K$ is a slice knot, then $\widehat{\mathrm{CFK}}(K) \cong C \otimes C^*$ for some chain complex $C$, where $C^*$ denotes the dual complex of $C$. This would, in turn, imply that the total rank of the knot Floer homology of a slice knot is a perfect square. In fact, this is not the case. For example, the Kinoshita-Terasaka knot of Figure 2.7 is slice, but its total homology, which can be computed using grid diagrams, has rank 33 (see Equation (4.33)). This leaves open a vague question:

Problem 17.2.1. What can be said about the structure of knot Floer homology for smoothly slice knots?

One might also hope to derive clues about potentially differentiating slice and ribbon knots (cf. Remark 2.6.3). This leads to the following (similarly vague) problem:

Problem 17.2.2. What can be said about the structure of knot Floer homology for ribbon knots?

In a slightly different direction, a knot $K$ is called *doubly slice* if there is an unknotted embedding of $S^2$ in $S^4$ whose intersection with an equatorial $S^3$ is $K$.

Problem 17.2.3. What can be said about the structure of knot Floer homology for a doubly slice knot?

**Counting more holomorphic curves.** Knot Floer homology is defined as a version of Lagrangian Floer homology in the $g$-fold symmetric product. As such, it counts holomorphic disks in this symplectic manifold.

Problem 17.2.4. Can moduli spaces of curves with genus $g > 0$ (and boundaries in $\mathbb{T}_\alpha$ and $\mathbb{T}_\beta$) be used to construct stronger knot invariants than knot Floer homology?

In [**120**], Lipshitz reformulates Heegaard Floer homology, so that the holomorphic curves counted in the differential correspond to embedded curves in $[0,1] \times \mathbb{R} \times \Sigma$. Lipshitz also formulates a version that counts curves with double-points, and includes a power series variable that records the number of double-points.

For grid diagrams, Lipshitz rephrases this in concrete terms, as described in Section 5.5. It remains an open problem to see if the double-point enhancement gives more information:

Problem 17.2.5. For every knot $K$, is the double-point enhanced grid homology isomorphic to $GH^-(K)[v]$ (in the notation of Definition 5.2.15)?

For more on this proposed homology theory, see [**120, 121**].

**Mutations.** First, recall the operation of *(Conway) mutation*: suppose that $K$ is a knot with a projection with a distinguished disk whose boundary circle meets the projection in four points, that we think of as equally spaced around the boundary circle. Let $K'$ be the new knot obtained by cutting out the disk, rotating it 180° in the plane, and then regluing it. It is known that the Alexander polynomial is mutation invariant, that is, if $K'$ is a mutant of $K$ then $\Delta_{K'}(t) = \Delta_K(t)$.

Knot Floer homology is not mutation invariant: the Conway and the Kinoshita-Terasaka knots (shown in Figure 2.7) are mutants, but the knot Floer homologies of these two knots are different. (See Exercises 4.8.6 and 4.8.7.) More conceptually, the genera of the knots are different, so by Theorem 1.3.2 their knot Floer homologies cannot be isomorphic as bigraded groups. The total dimensions of the knot Floer homologies, however, are the same. In fact, if we collapse the Maslov grading $M$ and Alexander grading $A$ on knot Floer homology to a single grading $\delta = M - A$, the $\delta$-graded grid homology groups of the Kinoshita-Terasaka and the Conway knots are the same. More generally, Baldwin and Levine [**6**] conjecture an affirmative answer to the following question:

PROBLEM 17.2.6. Is the $\delta$-graded knot Floer homology invariant under mutation?

Related questions can be asked for Khovanov homology; see [**14, 226**]. An analogous problem can be considered for genus 2 mutations; see [**149**].

**Linking and link Floer homology.** The linking number places restrictions on link Floer homology. For example, if $L$ is a link with two components, and $\vec{L}$ is any orientation on $L$, the $\delta$-graded link Floer homology of $\vec{L}$, and the linking number of the two components, determine the link Floer homology $\widehat{\mathrm{HFL}}(L)$ of $L$, endowed with any of its four possible orientations. (See for example Proposition 10.2.1.)

There are higher order obstructions to linking, due to Milnor [**142**], which can be reexpressed in terms of Massey products [**138, 189**].

For example, let $\vec{L} = \vec{L}_1 \cup \vec{L}_2 \cup \vec{L}_3$ be an oriented link with three components, and suppose that the linking numbers of any two components of $\vec{L}$ vanishes. (An example to keep in mind here is the Borromean rings.) Then, there are Seifert surfaces $F_i$ for $\vec{L}_i$ with $F_i \cap \vec{L}_j = \emptyset$ for $i \neq j$. The triple Milnor invariant is obtained as a signed number of triple points in $F_1 \cap F_2 \cap F_3$; see [**26**].

PROBLEM 17.2.7. Do the Milnor invariants place algebraic restrictions on the structure of link Floer homology?

**Torsion in knot Floer homology**. Consider knot Floer homology with integer coefficients.

PROBLEM 17.2.8. Is there a knot $K$ with the property that the abelian group $\widehat{\mathrm{HFK}}(K;\mathbb{Z})$ has torsion?

**Concordance invariants.** The invariant $\tau(K)$ can be computed once one calculates $GH^-(\mathbb{G})$. It is natural to wonder if $\tau(K)$ is easier to compute than knot Floer homology. For example:

PROBLEM 17.2.9. Is there a direct way to compute the parity of $\tau(K)$ for a knot?

Of course, such a computation would lead to a computation of $\tau$, just as one can compute the signature of a knot $K$ from the Alexander polynomials of all the knots in an unknotting sequence; see Remark 2.3.12.

Using integer coefficients, we defined $\tau(K,\mathbb{Q})$ and, for each prime $p$, an invariant $\tau(K;\mathbb{Z}/p\mathbb{Z})$ in Section 15.6.

PROBLEM 17.2.10. Exhibit a knot $K$ and two primes $p$ and $q$, for which $\tau(K;\mathbb{Z}/p\mathbb{Z}) \neq \tau(K;\mathbb{Z}/q\mathbb{Z})$; or a knot $K$ and a prime $p$ for which $\tau(K;\mathbb{Z}/p\mathbb{Z}) \neq \tau(K;\mathbb{Q})$.

Note that Problem 17.2.8 is independent of Problem 17.2.10. (See Example 15.6.2.)

As a point of comparison, Khovanov homology can also be used to construct an invariant $s(K)$ similar to $\tau(K)$. Just as $\tau$ has a collection of variations, indexed by prime numbers $p$, there is also a corresponding collection of $s$ invariants. The fact that the $\mathbb{Q}$-version and the $\mathbb{Z}/2\mathbb{Z}$-version of these $s$ invariants can be different has been verified by C. Seed, using his program Knotkit. (For the 14-crossing knot $K = K14n19265$, $s$ with coefficients in $\mathbb{Z}/2\mathbb{Z}$ is different from $s$ with coefficients in $\mathbb{Q}$.) For more questions along these lines for Khovanov homology, see Section 6 of [**123**].

We formulate an optimistic variant of Problem 17.2.10 in terms of the *smooth concordance group of knots*, the group $\mathcal{C}$ of equivalence classes of knots, where $K_1 \sim K_2$ if $K_1\#m(-K_2)$ is a slice knot. (Addition in this group is defined by taking connected sum.) It follows from a Künneth principle that $\tau(K,\mathbb{Z}/p\mathbb{Z})$ is additive under connected sums; since it vanishes for slice knots (Theorem 15.6.1), it follows that for each prime $p$, the map $K \mapsto \tau(K;\mathbb{Z}/p\mathbb{Z})$ induces a homomorphism $\tau_{\mathbb{Z}/p\mathbb{Z}}\colon \mathcal{C} \to \mathbb{Z}$ from the smooth concordance group to the integers. Similarly, $K \mapsto \tau(K;\mathbb{Q})$ induces a homomorphism $\tau_{\mathbb{Q}}$ from the smooth concordance group to the integers.

PROBLEM 17.2.11. Is the infinite collection of homomorphisms $\tau_{\mathbb{Z}/p\mathbb{Z}}$, indexed by primes $p$, together with $\tau_{\mathbb{Q}}$ linearly independent, as homomorphisms from the smooth concordance group to the integers?

Knot Floer homology in fact can be used to construct infinitely many linearly independent homomorphisms from the concordance group $\mathcal{C}$ to $\mathbb{Z}$. The first such construction is due to Hom [**88**]. We will describe a different method from [**165**] which rests on a simple modification of the construction of $\tau$.

As a preliminary step, take a rational number $t \in [0,2]$, and consider the module $GC^t(\mathbb{G})$ over the polynomial algebra $\mathbb{F}[v^t]$ generated freely by grid states. Equip the module $GC^t(\mathbb{G})$ with a grading induced by $\mathrm{gr}_t(v^{tm}\mathbf{x}) = M(\mathbf{x}) - tA(\mathbf{x}) - tm$. For a rectangle $r \in \mathrm{Rect}(\mathbf{x},\mathbf{y})$, let $\mathbb{X}(r)$ denote the number of $X$-markings in $r$, and let $\mathbb{O}(r)$ denote the number of $O$-markings in $r$. Consider the $\mathbb{F}[v^t]$-module endomorphism specified by

$$\partial_t \mathbf{x} = \sum_{\mathbf{y}\in\mathbf{S}} \sum_{\{r\in \mathrm{Rect}^\circ(\mathbf{x},\mathbf{y})\}} \#\left(\frac{\mathcal{M}(\phi)}{\mathbb{R}}\right) v^{t\mathbb{X}(r)+(2-t)\mathbb{O}(r)}\mathbf{y}. \tag{17.1}$$

Obviously, multiplication by $v$ drops $\mathrm{gr}_t$ by one; it is also fairly easy to see that the endomorphism $\partial_t$ is a differential that drops the grading $\mathrm{gr}_t$ by $1$.

Although the homology of $GC^t(\mathbb{G})$ is not a knot invariant (because of stabilizations; i.e. like $\widetilde{GH}(\mathbb{G})$, there is an extra factor of a two-dimensional vector space, taken to the $(n-1)^{st}$ tensor power, where $n$ is the grid number of the diagram $\mathbb{G}$), we can define $\Upsilon_K(t)$ to be the maximal $\mathrm{gr}_t$ of any $\mathrm{gr}_t$-homogeneous, non-torsion class in $H(GC^t(\mathbb{G}))$. According to [**165**], for each rational number $t \in [0,2]$, that quantity is a knot invariant. The function $\Upsilon_K(t)$ can be naturally extended to a piecewise linear, continuous function on $[0,2]$; and indeed, $\Upsilon$ gives a homomorphism from the smooth concordance group of knots to the vector space of real-valued, piecewise linear, continuous functions on $[0,2]$. Thus, $\Upsilon$ gives plenty of room to detect infinitely many linearly independent knots.

Using sign assignments as in Chapter 15, the construction of $\Upsilon$ can be adapted to coefficients in $\mathbb{Z}$, and hence specialized once again to $\mathbb{Z}/p\mathbb{Z}$ and $\mathbb{Q}$. There are natural analogues of Problem 17.2.10, and more optimistically, Problem 17.2.11 for the resulting functions on $[0,2]$, where $\Upsilon_K(t;\mathbb{Z}/p\mathbb{Z})$ and $\Upsilon_K(t;\mathbb{Q})$ play the roles of the integers $\tau(K;\mathbb{Z}/p\mathbb{Z})$ and $\tau(K;\mathbb{Q})$.

**Transverse invariants.** The transverse invariant of a link gives an invariant in grid homology. As in Section 14.3, viewing grid homology as the associated graded object for the filtered knot invariant, the transverse invariant inherits extra structures.

Recall the language of Definition 14.4.1: the transverse invariant is said to be a cycle to order $n$ if there is a chain $x \in \mathcal{GC}^-(\mathbb{G})$ with the following properties:

- if $a = \frac{\mathrm{sl}(\mathcal{T})+1}{2}$, then $x \in \mathcal{F}_a\mathcal{GC}^-(\mathbb{G})$;
- the projection of $x$ to $GC^-(\mathbb{G}, \frac{\mathrm{sl}(\mathcal{T})+1}{2})$ is a cycle, and it represents $\theta(\mathcal{T}) \in GH^-(\mathbb{G}, \frac{\mathrm{sl}(\mathcal{T})+1}{2})$;
- $\partial x \in \mathcal{F}_{a-n}\mathcal{GC}^-(\mathbb{G})$.

PROBLEM 17.2.12. Given $n \geq 1$, is there a transverse knot $\mathcal{T}$ whose invariant $\theta(\mathcal{T})$ can be represented by a cycle to order $n$ but not $n+1$?

An example with $n = 1$ is given in Proposition 14.4.6.

Given $k$, knot types with $k$ distinct transverse representatives with the same self-linking number are found in [**48**]. Different examples would be supplied by an affirmation of the following:

PROBLEM 17.2.13. Given any $n > 2$, is there an $n$-tuple of transverse knots $\mathcal{T}_1, \dots, \mathcal{T}_n$ that are smoothly isotopic, and with the same self-linking number, so that $\theta(\mathcal{T}_i)$ can be represented by a cycle to order $i$ but not $i+1$?

### Module realization in knot Floer homology.

PROBLEM 17.2.14. Characterize the graded $\mathbb{F}[U]$-modules that arise as knot Floer homology groups of knots.

PROBLEM 17.2.15. Which graded $\mathbb{F}[U]$-modules arise as knot Floer homology groups of more than one knot?

Note that the unknot is the only knot that has $\widehat{\mathrm{HFK}}$ of rank one [**172**]. A theorem of Ghiggini [**71**] (see also Theorem 1.3.3) implies that the trefoil knots and the figure-eight knot are uniquely characterized by their knot homologies. On the other hand, infinitely many knots with the same knot Floer homology modules were described in Section **??**; see also [**84**].

The obvious generalization of these problems is the following:

PROBLEM 17.2.16. Characterize the multi-graded $\mathbb{F}[U_1, \dots, U_\ell]$-modules that arise as link Floer homology groups of links.

A simpler question can be asked: what polytopes arise as grid homology polytopes? This is equivalent to the question of characterizing Thurston polytopes of links in $\mathbb{R}^3$.

**Axiomatic characterizations of Floer homology.** Let $W$ be the two-dimensional bigraded vector space with one generator in bigrading $(0,0)$ and another in bigrading $(-1,-1)$, and $J$ be the four-dimensional bigraded vector space with one generator in bigrading $(0,1)$, one in $(-2,-1)$, and two generators in bigrading $(-1,0)$.

DEFINITION 17.2.17. Let $\mathcal{H}(\vec{L})$ be an oriented link invariant, which has the form of a bigraded module over $\mathbb{F}[U]$. We say that $\mathcal{H}$ satisfies the ***oriented skein exact sequence*** if for each oriented skein triple $(\vec{L}_+, \vec{L}_-, \vec{L}_0)$, there are exact triangles of bigraded $\mathbb{F}[U]$-modules (with grading shifts indicated on the arrows):

$$\begin{tikzcd} \mathcal{H}(\vec{L}_+) \arrow[rr] & & \mathcal{H}(\vec{L}_-) \arrow[dl, "{(-1,0)}"] \\ & \mathcal{H}(\vec{L}_0) \arrow[ul] & \end{tikzcd}$$

if the two strands at the distinguished crossing of $\vec{L}_+$ belong to the same component; and

$$\begin{tikzcd} \mathcal{H}(\vec{L}_+) \arrow[rr] & & \mathcal{H}(\vec{L}_-) \arrow[dl, "{(-1,0)}"] \\ & \mathcal{H}(\vec{L}_0) \otimes J \arrow[ul] & \end{tikzcd}$$

if the two strands at the distinguished crossing of $\vec{L}_+$ belong to different components.

PROBLEM 17.2.18. Are there any bigraded link invariants $\mathcal{H}$, other than collapsed grid homology, that satisfy the following two properties:

- with $\mathcal{U}_n$ denoting the $n$-component unlink, $\mathcal{H}(\mathcal{U}_n) \cong \mathbb{F}[U] \otimes W^{\otimes n-1}$, and
- $\mathcal{H}$ satisfies the oriented skein sequence?

Analogous questions can be asked for the simply blocked grid homology, and coefficients in $\mathbb{Z}$ in place of $\mathbb{F}$.

Note that Khovanov and Khovanov-Rozansky have constructed other homology theories for knots [**103, 104, 105**] that satisfy similar skein exact sequences; compare also [**131, 212**]. There are various conjectures relating these invariants to knot Floer homology. There is a conjectured spectral sequence from reduced Khovanov homology to $\widehat{\mathrm{HFK}}$, see [**194**]; and from reduced HOMFLY homology to $\widehat{\mathrm{HFK}}$, see [**36**].

# Bibliography


[1] J. Alexander. Topological invariants of knots and links. *Trans. Amer. Math. Soc.*, 30(2):275–306, 1928.

[2] M. Aschenbrenner, S. Friedl, and H. Wilton. 3-manifold groups. EMS Series of Lectures in Mathematics, to appear.

[3] M. Atiyah and I. Macdonald. *Introduction to commutative algebra*. Addison-Wesley Publishing Co., Reading, Mass.-London-Don Mills, Ont., 1969.

[4] J. Baldwin. Comultiplication in link Floer homology and transversely nonsimple links. *Algebr. Geom. Topol.*, 10(3):1417–1436, 2010.

[5] J. Baldwin and W. Gillam. Computations of Heegaard Floer knot homology. *J. Knot Theory Ramifications*, 21(8):1250075, 65, 2012.

[6] J. Baldwin and A. Levine. A combinatorial spanning tree model for knot Floer homology. *Adv. Math.*, 231(3-4):1886–1939, 2012.

[7] J. Baldwin, D. Vela-Vick, and V. Vértesi. On the equivalence of Legendrian and transverse invariants in knot Floer homology. *Geom. Topol.*, 17(2):925–974, 2013.

[8] D. Bar-Natan. On Khovanov's categorification of the Jones polynomial. *Algebraic and Geometric Topology*, 2:337–370, 2002.

[9] D. Bar-Natan, J. Fulman, and L. Kauffman. An elementary proof that all spanning surfaces of a link are tube-equivalent. *J. Knot Theory Ramifications*, 7(7):873–879, 1998.

[10] D. Bennequin. Entrelacements et équations de Pfaff. In *Third Schnepfenried geometry conference, Vol. 1 (Schnepfenried, 1982)*, volume 107 of *Astérisque*, pages 87–161. 1983.

[11] J. Birman. *Braids, links, and mapping class groups*. Princeton University Press, Princeton, N.J.; University of Tokyo Press, Tokyo, 1974. Annals of Mathematics Studies, No. 82.

[12] J. Birman and M. Hirsch. A new algorithm for recognizing the unknot. *Geom. Topol.*, 2:175–220 (electronic), 1998.

[13] J. Birman and W. Menasco. Stabilization in the braid groups. II. Transversal simplicity of knots. *Geom. Topol.*, 10:1425–1452 (electronic), 2006.

[14] J. Bloom. Odd Khovanov homology is mutation invariant. *Math. Res. Lett.*, 17(1):1–10, 2010.

[15] S. Boyer, C. Gordon, and L. Watson. On L-spaces and left-orderable fundamental groups. *Math. Ann.*, 356(4):1213–1245, 2013.

[16] P. Braam and S. Donaldson. Floer's work on instanton homology, knots, and surgery. In H. Hofer, C. Taubes, A. Weinstein, and E. Zehnder, editors, *The Floer Memorial Volume*, number 133 in Progress in Mathematics, pages 195–256. Birkhäuser, 1995.

[17] H. Brunn. Über verknotete Kurven. *Verhandlungen des Internationalen Math. Kongresses (Zurich 1897)*, pages 256–259, 1898.

[18] G. Burde and H. Zieschang. *Knots*, volume 5 of *de Gruyter Studies in Mathematics*. Walter de Gruyter & Co., Berlin, second edition, 2003.

[19] D. Calegari. *Foliations and the geometry of 3-manifolds*. Oxford Mathematical Monographs. Oxford University Press, Oxford, 2007.

[20] A. Candel and L. Conlon. *Foliations. I*, volume 23 of *Graduate Studies in Mathematics*. American Mathematical Society, Providence, RI, 2000.

[21] A. Candel and L. Conlon. *Foliations. II*, volume 60 of *Graduate Studies in Mathematics*. American Mathematical Society, Providence, RI, 2003.

[22] J. Cerf. *Sur les difféomorphismes de la sphère de dimension trois* $(\Gamma_4 = 0)$. Lecture Notes in Mathematics, No. 53. Springer-Verlag, Berlin-New York, 1968.

[23] Yu. Chekanov. Differential algebra of Legendrian links. *Invent. Math.*, 150(3):441–483, 2002.

[24] D. Choi and K. Ko. Parametrizations of 1-bridge torus knots. *J. Knot Theory Ramifications*, 12(4):463–491, 2003.

[25] W. Chongchitmate and L. Ng. An atlas of Legendrian knots. *Exp. Math.*, 22(1):26–37, 2013.

[26] T. Cochran. Derivatives of links: Milnor's concordance invariants and Massey's products. *Mem. Amer. Math. Soc.*, 84(427):x+73, 1990.

[27] P. Cromwell. Embedding knots and links in an open book. I. Basic properties. *Topology Appl.*, 64(1):37–58, 1995.

[28] P. Cromwell. *Knots and links*. Cambridge University Press, Cambridge, 2004.

[29] M. Curtis. *Matrix groups*. Universitext. Springer-Verlag, New York, second edition, 1984.

[30] S. De Michelis and M. Freedman. Uncountably many exotic $\mathbf{R}^4$'s in standard 4-space. *J. Differential Geom.*, 35(1):219–254, 1992.

[31] F. Ding and H. Geiges. The diffeotopy group of $S^1 \times S^2$ via contact topology. *Compos. Math.*, 146(4):1096–1112, 2010.

[32] H. Doll. A generalized bridge number for links in 3-manifolds. *Math. Ann.*, pages 701–717, 1992.

[33] S. Donaldson. An application of gauge theory to four-dimensional topology. *J. Differential Geom.*, 18(2):279–315, 1983.

[34] S. Donaldson. Polynomial invariants for smooth four-manifolds. *Topology*, 29(3):257–315, 1990.

[35] S. Donaldson and P. Kronheimer. *The Geometry of Four-Manifolds*. Oxford Mathematical Monographs. Oxford University Press, 1990.

[36] N. Dunfield, S. Gukov, and J. Rasmussen. The superpolynomial for knot homologies. *Experiment. Math.*, 15(2):129–159, 2006.

[37] I. Dynnikov. Arc-presentations of links: monotonic simplification. *Fund. Math.*, 190:29–76, 2006.

[38] Ya. Eliashberg. Classification of overtwisted contact structures on 3-manifolds. *Invent. Math.*, 98(3):623–637, 1989.

[39] Ya. Eliashberg and M. Fraser. Topologically trivial Legendrian knots. *J. Symplectic Geom.*, 7(2):77–127, 2009.

[40] Ya. Eliashberg, A. Givental, and H. Hofer. Introduction to symplectic field theory. *Geom. Funct. Anal.*, Special Volume(Part II):560–673, 2000. GAFA 2000 (Tel Aviv, 1999).

[41] Ya. Eliashberg and M. Gromov. Convex symplectic manifolds. In *Several complex variables and complex geometry, Part 2 (Santa Cruz, CA, 1989)*, volume 52 of *Proc. Sympos. Pure Math.*, pages 135–162. Amer. Math. Soc., Providence, RI, 1991.

[42] Ya. Eliashberg and W. Thurston. *Confoliations*, volume 13 of *University Lecture Series*. AMS, Providence, RI, 1998.

[43] J. Epstein, D. Fuchs, and M. Meyer. Chekanov-Eliashberg invariants and transverse approximations of Legendrian knots. *Pacific J. Math.*, 201(1):89–106, 2001.

[44] J. Etnyre. Transversal torus knots. *Geom. Topol.*, 3:253–268 (electronic), 1999.

[45] J. Etnyre. *Legendrian and Transversal Knots*, pages 105–185. Elsevier B. V., Amsterdam, 2005.

[46] J. Etnyre and K. Honda. Knots and contact geometry. I. Torus knots and the figure eight knot. *J. Symplectic Geom.*, 1(1):63–120, 2001.

[47] J. Etnyre and K. Honda. Cabling and transverse simplicity. *Ann. of Math.*, 162(3):1305–1333, 2005.

[48] J. Etnyre, L. Ng, and V. Vértesi. Legendrian and transverse twist knots. *J. Eur. Math. Soc. (JEMS)*, 15(3):969–995, 2013.

[49] A. Floer. An instanton-invariant for 3-manifolds. *Comm. Math. Phys.*, 119:215–240, 1988.

[50] A. Floer. Morse theory for Lagrangian intersections. *J. Differential Geometry*, 28:513–547, 1988.

[51] A. Floer. A relative Morse index for the symplectic action. *Comm. Pure Appl. Math.*, 41(4):393–407, 1988.

[52] A. Floer. The unregularized gradient flow of the symplectic action. *Comm. Pure Appl. Math.*, 41(6):775–813, 1988.

[53] A. Floer. Instanton homology, surgery, and knots. In *Geometry of low-dimensional manifolds, 1 (Durham, 1989)*, volume 150 of *London Math. Soc. Lecture Note Ser.*, pages 97–114. Cambridge Univ. Press, Cambridge, 1990.

[54] A. Floer. Instanton homology and Dehn surgery. In H. Hofer, C. H. Taubes, A. Weinstein, and E. Zehnder, editors, *The Floer Memorial Volume*, number 133 in Progress in Mathematics, pages 77–97. Birkhäuser, 1995.

[55] A. Floer, H. Hofer, and D. Salamon. Transversality in elliptic Morse theory for the symplectic action. *Duke Math. J*, 80(1):251–29, 1995.

[56] R. Fox. A quick trip through knot theory. In *Topology of 3-manifolds and related topics (Proc. The Univ. of Georgia Institute, 1961)*, pages 120–167. Prentice-Hall, 1962.

[57] R. Fox. Some problems in knot theory. In *Topology of 3-manifolds and related topics (Proc. The Univ. of Georgia Institute, 1961)*, pages 168–176. Prentice-Hall, N.J., 1962.

[58] R. Fox and J. Milnor. Singularities of 2-spheres in 4-space and cobordism of knots. *Osaka J. Math.*, 3:257–267, 1966.

[59] M. Freedman. A surgery sequence in dimension four; the relations with knot concordance. *Invent. Math.*, 68(2):195–226, 1982.

[60] M. Freedman and F. Quinn. *Topology of 4-manifolds*, volume 39 of *Princeton Mathematical Series*. Princeton University Press, Princeton, NJ, 1990.

[61] K. Frøyshov. The Seiberg-Witten equations and four-manifolds with boundary. *Math. Res. Lett*, 3:373–390, 1996.

[62] K. Fukaya, Y-G. Oh, K. Ono, and H. Ohta. *Lagrangian intersection Floer theory—anomaly and obstruction*. Kyoto University, 2000.

[63] D. Gabai. Foliations and the topology of 3-manifolds. *J. Differential Geom.*, 18(3):445–503, 1983.

[64] D. Gabai. The Murasugi sum is a natural geometric operation. II. In *Combinatorial methods in topology and algebraic geometry (Rochester, N.Y., 1982)*, volume 44 of *Contemp. Math.*, pages 93–100. Amer. Math. Soc., Providence, RI, 1985.

[65] D. Gabai. Genera of the arborescent links. *Mem. Amer. Math. Soc.*, 59(339):i–viii and 1–98, 1986.

[66] E. Gallais. Sign refinement for combinatorial link Floer homology. *Algebr. Geom. Topol.*, 8(3):1581–1592, 2008.

[67] S. Garoufalidis and P. Teichner. On knots with trivial Alexander polynomial. *J. Differential Geom.*, 67(1):167–193, 2004.

[68] H. Geiges. *An introduction to contact topology*, volume 109 of *Cambridge Studies in Advanced Mathematics*. Cambridge University Press, Cambridge, 2008.

[69] H. Geiges. A contact geometric proof of the Whitney-Graustein theorem. *Enseign. Math. (2)*, 55(1-2):93–102, 2009.

[70] S. Gelfand and Yu. Manin. *Methods of homological algebra*. Springer Monographs in Mathematics. Springer-Verlag, Berlin, second edition, 2003.

[71] P. Ghiggini. Knot Floer homology detects genus-one fibred knots. *Amer. J. Math.*, 130(5):1151–1169, 2008.

[72] P. Ghiggini, P. Lisca, and A. Stipsicz. Tight contact structures on some small Seifert fibered 3-manifolds. *Amer. J. Math.*, 129(5):1403–1447, 2007.

[73] E. Giroux. Convexité en topologie de contact. *Comment. Math. Helv.*, 66(4):637–677, 1991.

[74] E. Giroux. Géométrie de contact: de la dimension trois vers les dimensions supérieures. In *Proceedings of the International Congress of Mathematicians, Vol. II (Beijing, 2002)*, pages 405–414. Higher Ed. Press, Beijing, 2002.

[75] M. Golubitsky and V. Guillemin. *Stable mappings and their singularities*. Springer-Verlag, New York-Heidelberg, 1973. Graduate Texts in Mathematics, Vol. 14.

[76] R. Gompf. Three exotic $\mathbf{R}^4$'s and other anomalies. *J. Differential Geom.*, 18(2):317–328, 1983.

[77] R. Gompf and A. Stipsicz. *4-manifolds and Kirby calculus*, volume 20 of *Graduate Studies in Mathematics*. American Mathematical Society, 1999.

[78] C. Gordon and R. Litherland. On the signature of a link. *Invent. Math.*, 47(1):53–69, 1978.

[79] C. Gordon and J. Luecke. Knots with unknotting number 1 and essential Conway spheres. *Algebr. Geom. Topol.*, 6:2051–2116, 2006.

[80] J. Greene. The lens space realization problem. *Ann. of Math. (2)*, 177(2):449–511, 2013.

[81] M. Gromov. Pseudoholomorphic curves in symplectic manifolds. *Invent. Math.*, 82(2):307–347, 1985.

[82] P. Hall. On representatives of subsets. *J. London Math. Soc.*, 1(10):26–30, 1935.

[83] A. Hatcher. *Algberaic Topology*. Cambridge University Press, 2001.

[84] M. Hedden and L. Watson. On the geography and botany of knot Floer homology. arXiv:1404.6913.

[85] M. Hedden and L. Watson. Does Khovanov homology detect the unknot? *Amer. J. Math.*, 132(5):1339–1345, 2010.

[86] J. Hillman. *Algebraic invariants of links*, volume 32 of *Series on Knots and Everything*. World Scientific Publishing Co., Inc., River Edge, NJ, 2002.

[87] M. Hirsch. *Differential topology*, volume 33 of *Graduate Texts in Mathematics*. Springer-Verlag, New York, 1994. Corrected reprint of the 1976 original.

[88] J. Hom. An infinite-rank summand of topologically slice knots. *Geom. Topol.*, 19(2):1063–1110, 2015.

[89] J. Hom and Z. Wu. Four-ball genus bounds and a refinement of the Ozsvath-Szabo tau-invariant. arxiv:1401.1565.

[90] K. Honda. On the classification of tight contact structures. I. *Geom. Topol.*, 4:309–368, 2000.

[91] M. Hutchings. Embedded contact homology and its applications. In *Proceedings of the International Congress of Mathematicians. Volume II*, pages 1022–1041, New Delhi, 2010.

[92] N. Jacobson. *Basic algebra. I.* W. H. Freeman and Company, New York, second edition, 1985.

[93] V. Jones. Hecke algebra representations of braid groups and link polynomials. *Ann. of Math. (2)*, 126(2):335–388, 1987.

[94] V. Jones. The Jones polynomial. http://math.berkeley.edu/ vfr/jones.pdf, 2005.

[95] A. Juhász. Cobordisms of sutured manifolds. arXiv:0910.4382.

[96] A. Juhász. Holomorphic discs and sutured manifolds. *Algebr. Geom. Topol.*, 6:1429–1457, 2006.

[97] A. Juhász. The sutured Floer homology polytope. *Geom. Topol.*, 14(3):1303–1354, 2010.

[98] A. Juhász and D. Thurston. Naturality and mapping class groups in Heegaard Floer homology. arXiv:1210.4996.

[99] T. Kanenobu. Infinitely many knots with the same polynomial invariant. *Proc. Amer. Math. Soc.*, 97(1):158–162, 1986.

[100] A. Kawauchi. *A survey of knot theory*. Birkhäuser Verlag, Basel, 1996. Translated and revised from the 1990 Japanese original by the author.

[101] A. Kawauchi, T. Shibuya, and S. Suzuki. Descriptions on surfaces in four-space. I. Normal forms. *Math. Sem. Notes Kobe Univ.*, 10(1):75–125, 1982.

[102] T. Khandhawit and L. Ng. A family of transversely nonsimple knots. *Algebr. Geom. Topol.*, 10(1):293–314, 2010.

[103] M. Khovanov. A categorification of the Jones polynomial. *Duke Math. J.*, 101(3):359–426, 2000.

[104] M. Khovanov and L. Rozansky. Matrix factorizations and link homology. *Fund. Math.*, 199(1):1–91, 2008.

[105] M. Khovanov and L. Rozansky. Matrix factorizations and link homology. II. *Geom. Topol.*, 12(3):1387–1425, 2008.

[106] P. Kronheimer and T. Mrowka. Gauge theory for embedded surfaces. I. *Topology*, 32(4):773–826, 1993.

[107] P. Kronheimer and T. Mrowka. The genus of embedded surfaces in the projective plane. *Math. Res. Lett.*, 1(6):797–808, 1994.

[108] P. Kronheimer and T. Mrowka. Monopoles and contact structures. *Invent. Math.*, 130(2):209–255, 1997.

[109] P. Kronheimer and T. Mrowka. Witten's conjecture and Property P. *Geom. Topol.*, 8:295–310 (electronic), 2004.

[110] P. Kronheimer and T. Mrowka. *Monopoles and three-manifolds*, volume 10 of *New Mathematical Monographs*. Cambridge University Press, Cambridge, 2007.

[111] P. Kronheimer and T. Mrowka. Knots, sutures, and excision. *J. Differential Geom.*, 84(2):301–364, 2010.

[112] P. Kronheimer and T. Mrowka. Khovanov homology is an unknot-detector. *Publ. Math. Inst. Hautes Études Sci.*, 113:97–208, 2011.

[113] P. Kronheimer and T. Mrowka. Knot homology groups from instantons. *J. Topol.*, 4(4):835–918, 2011.

[114] P. Kronheimer, T. Mrowka, P. Ozsváth, and Z. Szabó. Monopoles and lens space surgeries. *Ann. of Math. (2)*, 165(2):457–546, 2007.

[115] C. Kutluhan, Y-J. Lee, and C. Taubes. HF=HM I: Heegaard Floer homology and Seiberg–Witten Floer homology. arXiv:1007.1979.

[116] A. Lecuona. On the slice-ribbon conjecture for Montesinos knots. *Trans. Amer. Math. Soc.*, 364(1):233–285, 2012.

[117] E.-S. Lee. An endomorphism of the Khovanov invariant. *Adv. Math.*, 197(2):554–586, 2005.

[118] J. Licata. The Thurston polytope for four-stranded pretzel links. *Algebr. Geom. Topol.*, 8(1):211–243, 2008.

[119] R. Lickorish. *An introduction to knot theory*, volume 175 of *Graduate Texts in Mathematics*. Springer-Verlag, 1997.

[120] R. Lipshitz. A cylindrical reformulation of Heegaard Floer homology. *Geom. Topol.*, 10:955–1097 (electronic), 2006.

[121] R. Lipshitz. Heegaard Floer homology, double points and nice diagrams. In *New perspectives and challenges in symplectic field theory*, volume 49 of *CRM Proc. Lecture Notes*, pages 327–342. Amer. Math. Soc., Providence, RI, 2009.

[122] R. Lipshitz and S. Sarkar. A Khovanov stable homotopy type. *J. Amer. Math. Soc.*, 27(4):983–1042, 2014.

[123] R. Lipshitz and S. Sarkar. A refinement of Rasmussen's $S$-invariant. *Duke Math. J.*, 163(5):923–952, 2014.

[124] P. Lisca. Lens spaces, rational balls and the ribbon conjecture. *Geom. Topol.*, 11:429–472, 2007.

[125] P. Lisca and G. Matić. Tight contact structures and Seiberg-Witten invariants. *Invent. Math.*, 129(3):509–525, 1997.

[126] P. Lisca, P. Ozsváth, A. Stipsicz, and Z. Szabó. Heegaard Floer invariants of Legendrian knots in contact three-manifolds. *J. Eur. Math. Soc. (JEMS)*, 11(6):1307–1363, 2009.

[127] H. Lyon. Torus knots in the complements of links and surfaces. *Michigan Math. J.*, 27(1):39–46, 1980.

[128] I. MacDonald. Symmetric products of an algebraic curve. *Topology*, 1:319–343, 1962.

[129] C. Manolescu. Pin(2)-equivariant Seiberg-Witten Floer homology and the Triangulation Conjecture. arXiv:1303.2354.

[130] C. Manolescu. Seiberg-Witten-Floer stable homotopy type of three-manifolds with $b_1 = 0$. *Geom. Topol.*, 7:889–932 (electronic), 2003.

[131] C. Manolescu. Nilpotent slices, Hilbert schemes, and the Jones polynomial. *Duke Math. J.*, 132(2):311–369, 2006.

[132] C. Manolescu. An unoriented skein exact triangle for knot Floer homology. *Math. Res. Lett.*, 14(5):839–852, 2007.

[133] C. Manolescu and P. Ozsváth. Heegaard Floer homology and integer surgeries on links. arXiv:1011.1317.

[134] C. Manolescu and P. Ozsváth. On the Khovanov and knot Floer homologies of quasi-alternating links. In *Proceedings of Gökova Geometry-Topology Conference 2007*, pages 60–81. Gökova Geometry/Topology Conference (GGT), Gökova, 2008.

[135] C. Manolescu, P. Ozsváth, and S. Sarkar. A combinatorial description of knot Floer homology. *Ann. of Math. (2)*, 169(2):633–660, 2009.

[136] C. Manolescu, P. Ozsváth, Z. Szabó, and D. Thurston. On combinatorial link Floer homology. *Geom. Topol.*, 11:2339–2412, 2007.

[137] W. Massey. *Algebraic topology: an introduction.* Springer-Verlag, New York-Heidelberg, 1977. Reprint of the 1967 edition, Graduate Texts in Mathematics, Vol. 56.

[138] W. Massey. Higher order linking numbers. *J. Knot Theory Ramifications*, 7(3):393–414, 1998.

[139] J. McCleary. *User's guide to spectral sequences*, volume 12 of *Mathematics Lecture Series.* Publish or Perish Inc., Wilmington, DE, 1985.

[140] C. McMullen. The Alexander polynomial of a 3-manifold and the Thurston norm on cohomology. *Ann. Sci. de l'Ecole Norm. Sup.*, 35(2):153–171, 2002.

[141] W. Menasco and H. Matsuda. An addendum on iterated torus knots (appendix). math.GT/0610566.

[142] J. Milnor. Isotopy of links. Algebraic geometry and topology. In *A symposium in honor of S. Lefschetz*, pages 280–306. Princeton University Press, Princeton, N. J., 1957.

[143] J. Milnor. *Morse theory.* Based on lecture notes by M. Spivak and R. Wells. Annals of Mathematics Studies, No. 51. Princeton University Press, Princeton, N.J., 1963.

[144] J. Milnor. *Lectures on the $h$-cobordism theorem*. Princeton University Press, 1965. Notes by L. Siebenmann and J. Sondow.

[145] J. Milnor. *Singular points of complex hypersurfaces*. Annals of Mathematics Studies, No. 61. Princeton University Press, Princeton, N.J., 1968.

[146] K. Mohnke. Legendrian links of topological unknots. In *Topology, geometry, and algebra: interactions and new directions (Stanford, CA, 1999)*, volume 279 of *Contemp. Math.*, pages 209–211. Amer. Math. Soc., Providence, RI, 2001.

[147] E. Moise. Affine structures in 3-manifolds. V. The triangulation theorem and Hauptvermutung. *Ann. of Math. (2)*, 56:96–114, 1952.

[148] J. Montesinos. Three-manifolds as 3-fold branched covers of $S^3$. *Quart. J. Math. Oxford Ser. (2)*, 27(105):85–94, 1976.

[149] A. Moore and L. Starkston. Genus-two mutant knots with the same dimension in knot Floer and Khovanov homologies. *Algebr. Geom. Topol.*, 15(1):43–63, 2015.

[150] J. Morgan. *The Seiberg-Witten Equations and Applications to the Topology of Smooth Four-Manifold*. Number 44 in Mathematical Notes. Princeton University Press, 1996.

[151] J. Morgan, Z. Szabó, and C. Taubes. A product formula for Seiberg-Witten invariants and the generalized Thom conjecture. *J. Differential Geometry*, 44:706–788, 1996.

[152] J. Munkres. *Elementary differential topology*, volume 1961 of *Lectures given at Massachusetts Institute of Technology, Fall*. Princeton University Press, Princeton, N.J., 1966.

[153] K. Murasugi. On the genus of the alternating knot. I, II. *J. Math. Soc. Japan*, 10:94–105, 235–248, 1958.

[154] K. Murasugi. On a certain numerical invariant of link types. *Trans. Amer. Math. Soc.*, 117:387–422, 1965.

[155] K. Murasugi. On the signature of links. *Topology*, 9:283–298, 1970.

[156] K. Murasugi. *Knot theory & its applications*. Modern Birkhäuser Classics. Birkhäuser Boston Inc., Boston, MA, 2008. Translated from the 1993 Japanese original by Bohdan Kurpita, Reprint of the 1996 translation [MR1391727].

[157] L. Ng. Combinatorial knot contact homology and transverse knots. *Adv. Math.*, 227(6):2189–2219, 2011.

[158] L. Ng, P. Ozsváth, and D. Thurston. Transverse knots distinguished by knot Floer homology. *J. Symplectic Geom.*, 6(4):461–490, 2008.

[159] L. Ng and D. Thurston. Grid diagrams, braids, and contact geometry. In *Proceedings of Gökova Geometry-Topology Conference 2008*, pages 120–136. Gökova Geometry/Topology Conference (GGT), Gökova, 2009.

[160] Y. Ni. A note on knot Floer homology of links. *Geom. Topol.*, 10:695–713, 2006.

[161] Y. Ni. Knot Floer homology detects fibred knots. *Invent. Math.*, 170(3):577–608, 2007.

[162] Y-G. Oh. Fredholm theory of holomorphic discs under the perturbation of boundary conditions. *Math. Z*, 222(3):505–520, 1996.

[163] B. Owens. Unknotting information from Heegaard Floer homology. *Adv. Math.*, 217(5):2353–2376, 2008.

[164] P. Ozsváth and A. Stipsicz. Contact surgeries and the transverse invariant in knot Floer homology. *J. Inst. Math. Jussieu*, 9(3):601–632, 2010.

[165] P. Ozsváth, A. Stipsicz, and Z. Szabó. Concordance homomorphisms from knot Floer homology. arXiv:1407.1795.

[166] P. Ozsváth, A. Stipsicz, and Z. Szabó. Floer homology and singular knots. *J. Topol.*, 2(2):380–404, 2009.

[167] P. Ozsváth, A. Stipsicz, and Z. Szabó. Combinatorial Heegaard Floer homology and sign assignments. *Topology Appl.*, 166:32–65, 2014.

[168] P. Ozsváth and Z. Szabó. On the skein exact squence for knot Floer homology. arXiv:0707.1165.

[169] P. Ozsváth and Z. Szabó. Absolutely graded Floer homologies and intersection forms for four-manifolds with boundary. *Advances in Mathematics*, 173(2):179–261, 2003.

[170] P. Ozsváth and Z. Szabó. Heegaard Floer homology and alternating knots. *Geom. Topol.*, 7:225–254 (electronic), 2003.

[171] P. Ozsváth and Z. Szabó. Knot Floer homology and the four-ball genus. *Geom. Topol.*, 7:615–639, 2003.

[172] P. Ozsváth and Z. Szabó. Holomorphic disks and genus bounds. *Geom. Topol.*, 8:311–334, 2004.

[173] P. Ozsváth and Z. Szabó. Holomorphic disks and knot invariants. *Adv. Math.*, 186(1):58–116, 2004.

[174] P. Ozsváth and Z. Szabó. Holomorphic disks and three-manifold invariants: properties and applications. *Ann. of Math. (2)*, 159(3):1159–1245, 2004.

[175] P. Ozsváth and Z. Szabó. Holomorphic disks and topological invariants for closed three-manifolds. *Ann. of Math. (2)*, 159(3):1027–1158, 2004.

[176] P. Ozsváth and Z. Szabó. Heegaard Floer homology and contact structures. *Duke Math. J.*, 129(1):39–61, 2005.

[177] P. Ozsváth and Z. Szabó. Knots with unknotting number one and Heegaard Floer homology. *Topology*, 44(4):705–745, 2005.

[178] P. Ozsváth and Z. Szabó. On knot Floer homology and lens space surgeries. *Topology*, 44(6):1281–1300, 2005.

[179] P. Ozsváth and Z. Szabó. On the Heegaard Floer homology of branched double covers. *Adv. Math.*, 194(1):1–33, 2005.

[180] P. Ozsváth and Z. Szabó. Heegaard diagrams and Floer homology. In *International Congress of Mathematicians. Vol. II*, pages 1083–1099. Eur. Math. Soc., Zürich, 2006.

[181] P. Ozsváth and Z. Szabó. Holomorphic disks, link invariants and the multi-variable Alexander polynomial. *Algebr. Geom. Topol.*, 8(2):615–692, 2008.

[182] P. Ozsváth and Z. Szabó. Knot Floer homology and integer surgeries. *Algebr. Geom. Topol.*, 8(1):101–153, 2008.

[183] P. Ozsváth and Z. Szabó. Link Floer homology and the Thurston norm. *J. Amer. Math. Soc.*, 21(3):671–709, 2008.

[184] P. Ozsváth and Z. Szabó. A cube of resolutions for knot Floer homology. *J. Topol.*, 2(4):865–910, 2009.

[185] P. Ozsváth and Z. Szabó. Knot Floer homology and rational surgeries. *Algebr. Geom. Topol.*, 11(1):1–68, 2011.

[186] P. Ozsváth, Z. Szabó, and D. Thurston. Legendrian knots, transverse knots and combinatorial Floer homology. *Geom. Topol.*, 12(2):941–980, 2008.

[187] T. Perutz. Hamiltonian handleslides for Heegaard Floer homology. In *Proceedings of Gökova Geometry-Topology Conference 2007*, pages 15–35. Gökova Geometry/Topology Conference (GGT), Gökova, 2008.

[188] O. Plamenevskaya. Bounds for the Thurston-Bennequin number from Floer homology. *Algebr. Geom. Topol.*, 4:399–406, 2004.

[189] R. Porter. Milnor's $\bar{\mu}$-invariants and Massey products. *Trans. Amer. Math. Soc.*, 257(1):39–71, 1980.

[190] J. Przytycki. From Goeritz matrices to quasi-alternating links. In *The mathematics of knots*, volume 1 of *Contrib. Math. Comput. Sci.*, pages 257–316. Springer, Heidelberg, 2011.

[191] J. Rasmussen. Floer homology of surgeries on two-bridge knots. *Algebr. Geom. Topol.*, 2:757–789 (electronic), 2002.

[192] J. Rasmussen. *Floer homology and knot complements.* PhD thesis, Harvard University, 2003.

[193] J. Rasmussen. Lens space surgeries and a conjecture of Goda and Teragaito. *Geom. Topol.*, 8:1013–1031, 2004.

[194] J. Rasmussen. Knot polynomials and knot homologies. In *Geometry and topology of manifolds*, volume 47 of *Fields Inst. Commun.*, pages 261–280. Amer. Math. Soc., Providence, RI, 2005.

[195] J. Rasmussen. Khovanov homology and the slice genus. *Invent. Math.*, 182(2):419–447, 2010.

[196] K. Reidemeister. Zur dreidimensionalen Topologie. *Abh. Math. Sem. Univ. Hamburg*, 9(1):189–194, 1933.

[197] K. Reidemeister. *Knotentheorie.* Springer-Verlag, Berlin, 1974. Reprint.

[198] J. Robbin and D. Salamon. The spectral flow and the Maslov index. *Bull. London Math. Soc.*, 27(1):1–33, 1995.

[199] D. Rolfsen. *Knots and links*, volume 7 of *Mathematics Lecture Series.* Publish or Perish Inc., Houston, TX, 1990. Corrected reprint of the 1976 original.

[200] D. Roseman. Elementary moves for higher dimensional knots. *Fund. Math.*, 184:291–310, 2004.

[201] J. Rotman. *An introduction to homological algebra.* Universitext. Springer, New York, second edition, 2009.

[202] C. Rourke and B. Sanderson. *Introduction to piecewise-linear topology.* Springer-Verlag, New York-Heidelberg, 1972. Ergebnisse der Mathematik und ihrer Grenzgebiete, Band 69.

[203] L. Rudolph. An obstruction to sliceness via contact geometry and "classical" gauge theory. *Invent. Math.*, 119(1):155–163, 1995.

[204] S. Sarkar. Moving basepoints and the induced automorphisms of link Floer homology. arXiv:1109.2168.

[205] S. Sarkar. Grid diagrams and the Ozsváth-Szabó tau-invariant. *Math. Res. Lett.*, 18(6):1239–1257, 2011.

[206] S. Sarkar. Grid diagrams and shellability. *Homology Homotopy Appl.*, 14(2):77–90, 2012.

[207] S. Sarkar and J. Wang. An algorithm for computing some Heegaard Floer homologies. *Ann. of Math. (2)*, 171(2):1213–1236, 2010.

[208] M. Scharlemann. Heegaard splittings of 3-manifolds. In *Low dimensional topology*, volume 3 of *New Stud. Adv. Math.*, pages 25–39. Int. Press, Somerville, MA, 2003.

[209] N. Seiberg and E. Witten. Electric-magnetic duality, monopole condensation, and confinement in $N = 2$ supersymmetric Yang-Mills theory. *Nuclear Phys. B*, 426(1):19–52, 1994.

[210] N. Seiberg and E. Witten. Monopoles, duality and chiral symmetry breaking in $N = 2$ supersymmetric QCD. *Nuclear Phys. B*, 431(3):484–550, 1994.

[211] P. Seidel. *Fukaya categories and Picard-Lefschetz theory.* Zurich Lectures in Advanced Mathematics. European Mathematical Society (EMS), Zürich, 2008.

[212] P. Seidel and I. Smith. A link invariant from the symplectic geometry of nilpotent slices. *Duke Math. J.*, 134(3):453–514, 2006.

[213] J. Singer. Three-dimensional manifolds and their Heegaard diagrams. *Trans. Amer. Math. Soc.*, 35(1):88–111, 1933.

[214] J. Stallings. On fibering certain 3-manifolds. In *Topology of 3-manifolds and related topics (Proc. The Univ. of Georgia Institute, 1961)*, pages 95–100. Prentice-Hall, 1962.

[215] J. Świątkowski. On the isotopy of Legendrian knots. *Ann. Global Anal. Geom.*, 10(3):195–207, 1992.

[216] C. Taubes. The Seiberg-Witten and Gromov invariants. *Math. Res. Lett.*, 2(2):221–238, 1995.

[217] C. Taubes. *Metrics, connections and gluing theorems.* Number 89 in CBMS Regional Conference Series in Mathematics. AMS, 1996.

[218] W. Thurston. A norm for the homology of 3-manifolds. *Mem. Amer. Math. Soc.*, 59(339):i–vi and 99–130, 1986.

[219] G. Torres. On the Alexander polynomial. *Ann. of Math. (2)*, 57:57–89, 1953.

[220] B. Trace. On the Reidemeister moves of a classical knot. *Proc. Amer. Math. Soc.*, 89(4):722–724, 1983.

[221] P. Traczyk. A new proof of Markov's braid theorem. In *Knot theory (Warsaw, 1995)*, volume 42 of *Banach Center Publ.*, pages 409–419. Polish Acad. Sci., Warsaw, 1998.

[222] V. Turaev. *Torsions of 3-dimensional manifolds*, volume 208 of *Progress in Mathematics.* Birkhäuser Verlag, Basel, 2002.

[223] P. Turner. Five lectures on Khovanov Homology. arXiv:math/0606464.

[224] V. Vértesi. Transversely nonsimple knots. *Algebr. Geom. Topol.*, 8(3):1481–1498, 2008.

[225] L. Watson. Knots with identical Khovanov homology. *Algebr. Geom. Topol.*, 7:1389–1407, 2007.

[226] S. Wehrli. Mutation invariance of Khovanov homology over $\mathbb{F}_2$. *Quantum Topol.*, 1(2):111–128, 2010.

[227] C. Weibel. *An introduction to homological algebra*, volume 38 of *Cambridge Studies in Advanced Mathematics.* Cambridge University Press, Cambridge, 1994.

[228] G. Whitehead. Generalized homology theories. *Trans. Amer. Math. Soc.*, 102:227–283, 1962.

[229] H. Whitney. The general type of singularity of a set of $2n-1$ smooth functions of $n$ variables. *Duke Math. J.*, 10:161–172, 1943.

[230] H. Whitney. On singularities of mappings of euclidean spaces. I. Mappings of the plane into the plane. *Ann. of Math. (2)*, 62:374–410, 1955.

[231] E. Witten. Monopoles and four-manifolds. *Math. Res. Lett.*, 1(6):769–796, 1994.

[232] C.-M. Wong. Grid diagrams and Manolescu's unoriented skein exact triangle for knot Floer homology. arXiv:1305.2562.

# Index